UNIVERSITY OF BIRMINGHAM

EFFECT OF CARBON ALLOCATION, LAND USE CHANGE, AND OZONE POLLUTION ON GLOBAL CROP YIELDS OF MAJOR CEREALS: A MODELLING APPROACH

by

HECTOR ANDRES CAMARGO ALVAREZ

A thesis submitted to the University of Birmingham for the degree of

DOCTOR OF PHILOSOPHY

School of Geography, Earth & Environmental Sciences (GEES)

College of Life and Environmental Sciences (LES)

University of Birmingham

April 2023

ABSTRACT

Agriculture is currently facing environmental challenges like climate change, air pollution, and land degradation, affecting agricultural productivity and threatening global food security. Besides, the increase in per capita food consumption among medium and high-income population, plus the expected increase in global population to around 9 billion by 2050, will lead to an unprecedented demand for food sustainably produced. To reach this aim, a holistic understanding of agroecosystems and their complexities is required. The Global Gridded Crop Models (GGCMs) have been developed to fullfill this requirement. Therefore, studies about the food systems require accurate crop models with explicit simulations of the productive processes and interactions with the environment.

This thesis aims to contribute to this broad effort to improve the performance of GGCMs by improving the representations of crop growth, stress response and yield with the Lund-Postdam-Jena General Ecosystem Simulator (LPJ-GUESS) model. The improvement focused on three aspects: (1) carbon assimilation and allocation processes, (2) the impact of past land cover change, and (3) the effect of ground-level O_3 pollution on crop yields. The thesis evaluated how these factors affect simulated crop production and how the model can assess crop production under different environmental and management conditions at different spatial and temporal scales. Each of the three aspects also represents different types of uncertainty that the model has to address and are finally reflected in the model outputs, such as parameter uncertainty, input uncertainty and structural uncertainty.

LPJ-GUESS was improved, enhancing its capability to replicate yields, crop productivity processes, and the harmful effects on yield and harvest index simulated by the ozone module. These improvements have significant implications for developing more comprehensive and precise crop simulations that account for the complex interactions between crop production, environmental and management factors, and ozone. These advancements contribute to potentially more accurate global and large-scale yield simulations to better understand the impacts of climate change and terrestrial biogeochemical cycles on food production.

Overall, this thesis represents an improvement in the representation of productive crop processes and will increase the consistency of results in strategic research performed with LPJ-GUESS on the global food system. This is critical for researchers and policymakers to meet the current challenges of agriculture in feeding an increasing population in an environmentally and socially sustainable way.

ACKNOWLEDGEMENTS

First, I would like to express my gratitude to the University of Birmingham and the Global Challenges scheme for funding and providing all the resources needed to complete this research. I also want to acknowledge the LPJ-GUESS team at Lund University, who collaborated on this research and contributed their knowledge and experience, and who received me as an equal during my time there in Lund.

I thank Thomas Pugh for being my supervisor but mainly for being my friend all this time, Rob Elliott for his patience and support over the past four years, and Stefan Olin for his advice and guidance in working with LPJ-GUESS. I am grateful for their time in my research and their valuable feedback that helped me achieve the best possible result.

I also want to thank my co-authors Xuhui Wang, Chenzhi Wang, Deepak Ray, and Håkan Pleijel, for their contributions and willingness to share critical data for the thesis, as well as for taking the time to explain and answer questions. Similarly, I am grateful to those who were not co-authors but helped significantly and guided my work, such as Malin Broberg, Adrian Gustafson, and Phillip Papastefanou.

I want to express my gratitude to my parents, Martha Alvarez and Germán Camargo, my siblings Yury Camargo and Jorge Camargo, my nephew Juan Solorzano and my girlfriend Nadia Valverdi for always supporting me during my PhD journey and providing emotional support, especially during the challenging times of the pandemic.

Additionally, I want to thank the amazing people I met in Birmingham and Lund, such as Raquel Arias Font, Joseph Wayman, Dimitris Bousiotis, Carlos Gomez-Ortiz, and Kimberly Montañez.

Finally, I want to acknowledge the healthcare workers from the NHS and elsewhere for their dedication and efforts on the front line during the pandemic and, of course, I must express my gratitude to Aston Villa for making my time in Birmingham so enjoyable.

STUDENT'S CONTRIBUTION

This thesis was the result of collaborative research, specific contributions of the student are shown below.

CHAPER ONE: INTRODUCTION, was completed by the student.

CHAPTER TWO: MODELLING CROP YIELD AND HARVEST INDEX: THE ROLE OF CARBON ASSIMILATION AND ALLOCATION PARAMETERS

Authorship: Hector Camargo, Robert J R Elliott, Stefan Olin, Xuhui Wang, Chenzhi Wang, Deepak K. Ray, Thomas A. M. Pugh

Status: Published 27 December 2022 in *Modelling Earth Systems and Environment*

Students' contribution: All the compilation of data was performed by the student, except the compilation of harvest index data from Chinese papers which was performed by Xuhui Wang and Chenzhi Wang. The gridded yield reference data was supplied by Deepak K. Ray, as well as support to analyse it. Model development was carried out by the student and Stefan Olin. The simulations, data analysis and manuscript preparation was completed by the student. Continuous support and guidance in LPJ-GUESS development and analysis was carried out by Stefan Olin, Thomas Pugh and Rob Elliott.

CHAPTER THREE: INFLUENCE OF LAND COVER CHANGE ON HISTORICAL YIELD OF WHEAT, MAIZE AND RICE SIMULATED WITH LPJ-GUESS

Authorship: Hector Camargo, Robert J R Elliott, Stefan Olin, Thomas A. M. Pugh

Status: To be submitted. This work was presented at the Fall meeting of the American Geophysics Union in Chicago (12-16 December 2022)

Students' contribution: Model development, simulations, data analysis and manuscript preparation was completed by the student. Continuous support and and advices in LPJ-GUESS development and analysis was carried out by Stefan Olin, Thomas Pugh and Rob Elliott.

CHAPTER FOUR: GROUND-LEVEL OZONE POLLUTION EFFECT IN GLOBAL CROP MODELLING: THE CASE OF WHEAT

Authorship: Hector Camargo, Robert J R Elliott, Stefan Olin, H. Pleijel, Thomas A. M. Pugh

Status: To be submitted

Students' contribution: Simulations, data analysis and manuscript preparation was completed by the student. Model development was completed by the student and Stefan olin and experimental data of wheat exposure to ozone was supplied by Håkan Pleijel. Continuous support and guidance in LPJ-GUESS development and analysis was carried out by Håkan Pleijel, Stefan Olin, Thomas Pugh and Rob Elliott.

CHAPTER FIVE: CONCLUSIONS, was completed by the student.

TABLE OF CONTENTS

LIST OF FIGURES

LIST OF TABLES

CHAPTER ONE: INTRODUCTION

Agricultural production is essential for the socioeconomic development of human civilisation and is the main source for feeding the global population (Jackson et al. 2019). Agriculture also has been responsible for generating a 4% of the world GDP during the last decade (Mbow et al. 2019; The World Bank 2023). However, environmental challenges like climate change, air pollution, as well as land degradation, mainly caused by inappropriate agricultural practices and unsustainable management, affect agricultural productivity and threaten global food security (McGrath et al. 2015; Kanianska 2016; Ray et al. 2019). Furthermore, societal projections are not very promising; higher food consumption per capita among the population with medium and high incomes (Vermeulen et al. 2012), plus the expected global population projected at around 9 billion by 2050, will lead to an unprecedented demand for food (Godfray et al. 2010; United Nations 2019). So, ensuring sustainable food security while facing all the constraints is the most critical challenge for agriculture during this century.

During the last century, the increase in agricultural production has corresponded with rising demand for food and during the "green revolution" in the mid-20th century, an enormous jump in productivity occurred (Godfray et al. 2010). The productivity increase was associated with the expansion of managed land and the management intensification in existing agricultural systems, intensification includes fertilisation, irrigation, pesticide control, high-yield cultivar technology and mechanisation (Lindeskog et al. 2013; Lu and Tian 2017; Jackson et al. 2019). Changes in cropland area and input intensity have dramatically altered the environmental footprint of agriculture. Intensification has caused an unprecedented constrain of finite resources used in agriculture (Godfray et al. 2010). It has caused land degradation, with around

12 million hectares of arable land abandoned annually because of yield collapse (Godfray et al. 2010; Kanianska 2016). Furthermore, it has caused an increase in emissions of non-CO_2 greenhouse gases, such as N_2O, from inefficiencies in nitrogen and manure application (Bustamante et al. 2014; IPCC 2017; Lu and Tian 2017).

Between 9 – 14% of total greenhouse emissions are attributable to in-farm agricultural and livestock activities and 5-14% to land use and land use change (Mbow et al. 2019). Land use change emission has been estimated in several studies between 145.5 to 225 Pg C since 1850 (Lindeskog et al. 2013; Olin et al. 2015a; Pugh et al. 2015; Houghton and Nassikas 2017). Additionally, the emission of nitrogen oxides (NO_x; NO + NO_2) has also been reported from intensive nitrogen fertilisation in crops (Almaraz et al. 2018). NO_x is a precursor of tropospheric ozone (O_3), which has damaging effects on human health and is responsible for the decrease in yields of several species (Ashmore 2005).

In order to balance the goal of feeding the population with the need for sustainable production, it may be necessary to implement planning and regulation policies for land use, production management, and other factors affecting agriculture. To achieve this goal, it is necessary to have a comprehensive understanding of the feedback mechanisms between agroecosystems and key environmental factors such as climate, nutrient cycling, carbon sequestration, water management, and pollution control. Such understanding can be obtained through relevant research (Vermeulen et al. 2012; Bustamante et al. 2014; Alexander et al. 2018). However, the complexity and large scale of the global food system, in addition to the impossibility of controlled

experimentation, make it essential to use models as tools for studying the dynamics between crops, biosphere and climate (Prentice et al. 1989).

To fulfil this demand, global terrestrial biogeochemistry and biogeography models and, more recently, dynamic global vegetation models (DGVM) are used to simulate vegetation functions, structure, competition and mortality as the central role in the interaction between climate and earth systems as well as the anthropogenic changes in the biosphere (Prentice et al. 1989; Cramer et al. 1999, 2001). A similar group of these models specifically applied to agriculture, known as the Global Gridded Crop Models (GGCMs), has been developed. Despite only emerging as a model class in the late 2000s, GGCMs have become one of the core tools underlying global food security assessments (Rosenzweig et al. 2013; Elliott et al. 2015b; Folberth et al. 2016) due to their increasing maturity as technology demonstrated in community evaluation and benchmarking efforts (Müller et al. 2017).

The GGCMs have accelerated the increase of studies about agricultural productivity on a regional and global scale worldwide. However, large differences have been found between different GGCMs (Elliott et al. 2015b; Müller et al. 2017). This uncertainty is caused by several reasons, including the differences in model structures and assumptions, inputs and processes (Müller et al. 2019). Broadly, GGCMs fit into two structures, those that have been developed for field-scale and upscaled to global (Jones et al. 2003; Balkovič et al. 2013; Elliott et al. 2014) and those that have been derived from process-based dynamic global vegetation models (Bondeau et al. 2007; Boote et al. 2013). Field-scale models tend to empirically link driving environmental variables directly to plant growth and production, generally calibrated with field experiments. In contrast, ecosystem models incorporate explicit

parameterisations of processes such as crop photosynthesis and respiration, modelling the plant growth process (Rosenzweig et al. 2014).

Different GGCMs are subject to many limitations, extrapolating parameters and assumptions from field-scale models to regional or global models is a challenge. While in ecosystem models capturing the diversity of many different crop species and cultivars used globally, or the high variability in management practices at a global scale is a limitation (Boote et al. 2013; Müller et al. 2017), as well as the losses caused by pests, inefficient irrigation, and soil degradation (Rosenzweig et al. 2014).

However, the most important limitations of crop models are the lack of high-quality standard input data, including growing season dates, soil properties, irrigation areas, fertilisation rates and timing. Similarly, the availability of reference high-quality data of other model outputs different than yield, such as harvest index, leaf area or NPP, is very limited (Portmann et al. 2010; Rosenzweig et al. 2013; Müller et al. 2017).

Recently, the Agricultural Model Intercomparison and Improvement Project (AgMIP) was developed to improve the characterisation of world food security under climate change by comparing several types of GGCMs and assessing the biophysical and economic effects on crop yield. AgMIP aims to create a framework of a coordinated set of historical data for model calibration and improvement, the characterisation of uncertainties to get better projections of future agricultural production and economic impacts, as well as vulnerability analyses and adaptation strategies.

The AgMIP framework offers a reference for development and evaluation and a protocol to continue the improvement of GGCMs to represent the global agricultural system. AgMIP considered 21 models in phase 1 (Elliott et al. 2015b), and 14 were

included in the intercomparison evaluating the relationship between productivity and environmental impacts (Müller et al. 2017). Eigth of the models used in the intercomparison were fiel-scale models with processes extrapolated to larger scales like DSSAT, the 5 models composing the EPIC group and WOFOST, while the other six models were ecosystem-based models with the development of cropland modules, like PEGASUS, ORCHIDEE, LPJmL and LPJ-GUESS (Müller et al. 2017). From the latter group, LPJ-GUESS is one of the models with a mechanistic cropland module widely used for global crop evaluation (Olin et al. 2015a; Bodin et al. 2016; Müller et al. 2019). Additionally, LPJ-GUESS counts with a nitrogen dynamics module that allows the inclusion of fertilisation as a factor of study (Olin, Schurgers, et al. 2015; Lindeskog et al. 2013) and it allows the mechanistic implementation and simulation of the tropospheric ozone effect on plants based on ozone flux into the plant due to its prognostic nature which diminishes the need for empirical relationships.

Therefore, this thesis aims to contribute to this broad effort to improve the performance of GGCMs by improving the representations of crop growth, stress response and yield with the Lund-Postdam-Jena General Ecosystem Simulator (LPJ-GUESS) model.

1.1. The Lund-Postdam-Jena General Ecosystem Simulator (LPJ-GUESS)

The Lund-Postdam-Jena General Ecosystem Simulator (LPJ-GUESS) is a process-based dynamic vegetation model that simulates vegetation response to climate, atmospheric carbon dioxide levels ([CO_2]) and nitrogen dynamics. LPJ-GUESS, like many global ecosystems models, was originally developed to simulate natural vegetation but subsequently implemented a land use functionality to simulate

cropland and pastures, in addition to a nitrogen dynamics module to account for nitrogen limitation and nitrogen fertilisation in yields (Olin, Schurgers, et al. 2015; Lindeskog et al. 2013). However, it does not include yet dynamics for other nutrients like phosphorus and potassium which represents a limitation to simulate realistic yields. The crop module of version 4.1 of LPJ-GUESS simulates yield based on daily or monthly climate data, atmospheric CO_2 mixing ratio, management practices, soil physical properties and atmospheric nitrogen deposition. Model processes include photosynthesis and carbon assimilation, respiration, water uptake, evapotranspiration and carbon allocation. In addition, it includes management options such as irrigation, tillage effects on soil respiration rate and inter-growing season grass cover (Olin et al. 2015b).

LPJ-GUESS has performed well in simulating recent-historical yield and crop productivity under varying conditions for wheat and maize at global and regional scales (Olin et al. 2015a; Bodin et al. 2016; Müller et al. 2019). However, several parameters relevant to carbon assimilation and the allocation scheme are weakly constrained and poorly characterised. Furthermore, the lack of global-scale compilations of reference data of HI have made challenging the evaluation of productivity processes (Boote et al. 2013; Iizumi et al. 2014; Ringeval et al. 2021). Calibration of the most suitable parameters describing these processes and evaluating both simulated yield and HI with LPJ-GUESS can increase the accuracy of the simulates variables and, in turn, the analyses based on them.

Likewise, it is important to consider the land use history for a more accurate representation of food systems. Legacies from past land cover can have long-lasting impacts on soil health, nutrient availability (Guo and Gifford 2002), and overall crop

productivity. The global cropland area has increased dramatically from 300 million hectares to around 1600 million hectares since 1700 (Goldewijk and Ramankutty 2004; Jackson et al. 2019). Therefore, by incorporating historical land use data into crop yield simulations, models can account for these long-term effects and more accurately represent current crop productivity levels. This is particularly important when simulating yields globally due to the high temporal and spatial variability of the past land use cover and its impact.

1.2. Ozone damage

Tropospheric O_3 is a harmful air pollutant that affects and threatens food production and ecosystem health. O_3 is responsible for 5 to 16% of the global temperature change and is the second major air pollutant after the particulate matter. Human health is threatened by O_3 too; around 700 000 deaths were estimated to be directly attributed to O_3 pollution per year (Ainsworth et al. 2012a). Ozone indirectly affects food security by reducing the yields of many crops (Ainsworth et al. 2012a). The damaging effects of O_3 in plants were discovered in the 1950s and now is recognised as the most damaging rural air pollutant (Ashmore 2005; Ainsworth et al. 2012b; Pleijel and Uddling 2012).

An increase in tropospheric O_3 has been observed over the past century, produced by the photolysis of NO_2 into NO and a low-energy oxygen atom, which subsequently combines with O_2 to form O_3. NO_2 is emitted directly into the atmosphere by combustion, or produced by NO oxidation, which is also a product of combustion. This reaction is part of the oxidation of organic compounds initiated by reactive species like OH and is faster at high temperatures. This link between O_3 pollution, light and temperature means maximum concentrations of O_3 typically occur after

noontime, with a decrease after late afternoon and especially during summer (Beig et al. 2007; Lin et al. 2020).

Background O_3 mixing ratio has more than tripled to 35-40 ppb in some regions from pre-industrial levels of around 10 ppb (Ainsworth 2017). However, in some regions like North America and Europe, during the last decades, the peaks of O_3 have decreased due to reductions in precursor emissions. Conversely, in Asia, emissions of O_3 precursors have increased, causing even O_3 mixing ratios of 50 ppb in rural and suburban locations during the growing season, threatening the food supply both for local communities and globally, considering the importance of this region in cereal production (Emberson et al. 2009; Garthwaite et al. 2009).

Ozone can affect crop productivity in different ways, damaging the appearance of the product and decreasing its value, which occurs when there is transient exposure to high levels of O_3 but can also reduce the yield in the absence of visible injury under chronic exposure to relatively low O_3 levels. The effect of O_3 on NPP is controlled by the stomatal conductance that modulates the rate of penetration of O_3 into the leaf. Once inside the leaf, O_3 reacts to produce reactive oxygen species (ROS) like hydrogen peroxide, superoxide radicals, hydroxyl radicals and NO, activating the apoplast ROS quenching capacity. ROS can decrease the activity of the enzyme Rubisco but also causes a similar response to pathogenic stress, enabling ethylene, salicylic acid and jasmonic acid to express defence and programmed cell death, leading to early senescence (Ashmore 2005; Sitch et al. 2007; Ainsworth et al. 2012b).

Ozone can cause a reduction of CO_2 intake to the leaf by regulating stomatal conductance, thereby affecting the photosynthesis rate. Additionally, it can increase the allocation of resources to repair and detoxify affected tissues, also affecting yields (Ashmore 2005; Sitch et al. 2007; Ainsworth et al. 2012b). Interaction between CO_2 and O_3 can have opposite effects since future elevated CO_2 concentration may lead to a decrease of stomatal conductance, diminishing the O_3 intake as well as the damaging effects on plants, but some reports have demonstrated that despite this effect, O_3 can still offset the potential effects of elevated CO_2 by 18-34% (Sitch et al. 2007; Ainsworth et al. 2012b).

The increasing importance of O_3 in crop production has accelerated research about the effect of O_3 on agricultural production and yield. However, including O_3-induced stress in GGCMs and other crop models remains limited, with only a few models, such as WOFOST, DSSAT and LPJmL (Cappelli et al. 2016; Guarin et al. 2019b, Schauberger et al, 2019). The incorporation of O_3 impact in crop modelling stands to substantially improve both the geographical and temporal representation of crop productivity and yield, as well as increase the ability of crop modellers to explore the impact of different future scenarios for air pollution. This, in turn, can increase the reliability and flexibility of the food system analyses and assessments conducted using GGCMs like LPJ-GUESS.

1.3. Hypotheses, aims and objectives

In this thesis, the central hypothesis is that a substantial enhancement in the accuracy of crop growth and production simulated with the LPJ-GUESS ecosystem model at global and regional scales can be achieved through the improvement of the model parameterisation of carbon processes and of the structure by implementing

the representation of the ozone damage module in crops, but also by the understanding of the response to land use history and environmental input data.

This thesis aims to enhance the capacity of the LPJ-GUESS ecosystem model to represent global crop growth and productivity for future applications by the calibration of critical parameters for carbon assimilation and allocation processes, the evaluation of the effect of historical land use changes and other environmental variables on crop productivity, and the implementation of a mechanistic module simulating the impact of ground-level ozone pollution on crop yield.

1.3.1. Objectives

- Evaluate and describe the effect of selected parameters and input datasets on simulated crop production
- Identifying the benefits and limitations and uncertainties of different model setups for future research and model applications
- Implementing the ground-level ozone module in LPJ-GUESS
- Finding caveats, opportunities and needs to direct future research and continue the model improvement

The thesis consists of three research chapters, each addressing one of the above aspects, as described below:

1.3.2. **Chapter 2**: In this chapter the hypothesis is that by the constrain of critical parameters can improve the representation of yield but also senescense, carbon allocation and harvest index.

Objective: To enhance the representation of carbon assimilation and allocation processes in global wheat and maize modelling.

Specific Objectives

1. Identify the key carbon assimilation and allocation processes in LPJ-GUESS that significantly impact crop productivity.
2. Calibrate the representation of these processes within the LPJ-GUESS model and evaluate their impact on simulated crop production.
3. Assess the performance of the improved model.

This chapter focuses on modelling crop yield and harvest index, including how photosynthesis fixes carbon and how carbon is allocated to different plant organs, such as leaves, stems, and grains. Carbon assimilation and allocation efficiency vary depending on environmental conditions, such as temperature, light intensity, and water availability. The chapter reviews the importance of carbon assimilation and allocation parameters in simulating crop production and discusses how the findings contribute to developing more accurate and reliable representations of yield and crop productivity.

1.3.3. **Chapter 3**: In this chapter, the hypothesis is that land use history affects the trend of global crop production simulated with LPJ-GUESS and is an important factor to consider in future simulations.

Objective: To understand the impact of land use change legacies on crop productivity and its interaction with other model drivers using LPJ-GUESS.

Specific Objectives

1. Analyze the impact of land use change on global crop productivity
2. Assess the importance of land use change relative to other environmental drivers

While dynamic vegetation global models, such as LPJ-GUESS, have improved the simulation of vegetation cover and carbon cycling by accounting for land use change, its implications for crop yield simulations have not been well explored at large scales. This study evaluates the global effect of historical land cover changes on crop yield estimations for wheat, maize, and rice and examines the interaction of land cover change with climatic and management drivers. The findings highlight the importance of capturing accurate historical land cover changes and comprehensive fertiliser database inputs to increase the accuracy of simulated global food production, climate change impacts, and terrestrial biogeochemical cycles, particularly in simulating yield trends.

1.3.4. **Chapter 4**: In this chapter, the hypothesis is that the deleterious ground-level ozone effect on wheat productivity can be captured by the implemented module in LPJ-GUESS.

Objective: To implement, describe and evaluate the effect of ground-level ozone pollution on wheat yields using LPJ-GUESS.

Specific Objectives

1. Incorporate the effect of ground-level ozone pollution into the LPJ-GUESS model and evaluate its impact on simulated crop production.
2. Evaluate the performance of the ozone pollution implementation on yield and harvest index of wheat.
3. Assess the interaction between ozone, CO_2 and drought on crop yields.

This study evaluates the performance of the O_3 module implemented in LPJ-GUESS and provides insights into the impact of ground-level O_3 on crop productivity. The

chapter involves calibrating the rate of damage caused by O_3 and the lower and upper limits of the period of O_3 sensitivity and evaluating the calibrated module against experimentally-observed data. The model is applied to assess the interaction between O_3, CO_2, and drought. The results show that the model reproduces the damaging effect of tropospheric O_3 on crop yield and harvest index and can be used to explore strategies to mitigate the negative impact of air pollution on crop productivity.

Overall, this thesis represents an improvement in the representation of productive crop processes and will increase the consistency of results in strategic research performed with LPJ-GUESS on the global food system. This is critical for researchers, farmers, and policymakers to meet the current challenges of agriculture in feeding an increasing population in an environmentally and socially sustainable way.

1.4. REFERENCES

Ainsworth EA (2017) Understanding and improving global crop response to ozone pollution. Plant J 90:886–897. https://doi.org/10.1111/tpj.13298

Ainsworth EA, Sitch S, Collins WJ, Emberson LD (2012a) The effects of tropospheric ozone on net primary productivity and implications for climate change. Annu Rev Plant Biol 63:637–631

Ainsworth EA, Yendrek CR, Sitch S, et al (2012b) The Effects of Tropospheric Ozone on Net Primary Productivity and Implications for Climate Change ∗. Annu Rev Plant Biol 63:637–663. https://doi.org/10.1146/annurev-arplant-042110-103829

Alexander P, Rabin S, Anthoni P, et al (2018) Adaptation of global land use and management intensity to changes in climate and atmospheric carbon dioxide. Glob Chang Biol 24:2791–2809. https://doi.org/10.1111/gcb.14110

Almaraz M, Bai E, Wang C, et al (2018) Agriculture is a major source of NOx pollution in California. Sci Adv 4:1–9. https://doi.org/10.1126/SCIADV.AAU2561

Ashmore MR (2005) Assessing the future global impacts of ozone on vegetation. Plant Cell Environ 949–964

Balkovič J, van der Velde M, Schmid E, et al (2013) Pan-European crop modelling with EPIC: Implementation, up-scaling and regional crop yield validation. Agric Syst 120:61–75. https://doi.org/10.1016/j.agsy.2013.05.008

Beig G, Gunthe S, Jadhav DB (2007) Simultaneous measurements of ozone and its precursors on a diurnal scale at a semi urban site in India. J Atmos Chem 57:239–253. https://doi.org/10.1007/s10874-007-9068-8

Bodin P, Olin S, Pugh TAM, Arneth A (2016) Accounting for interannual variability in agricultural intensification: The potential of crop selection in Sub-Saharan Africa. Agric Syst 148:159–168. https://doi.org/10.1016/j.agsy.2016.07.012

Bondeau A, Smith PC, Zaehle S, et al (2007) Modelling the role of agriculture for the 20th century global terrestrial carbon balance. Glob Chang Biol 13:679–706. https://doi.org/10.1111/j.1365-2486.2006.01305.x

Boote KJ, Jones JW, White JW, et al (2013) Putting mechanisms into crop production models. Plant, Cell Environ 36:1658–1672. https://doi.org/10.1111/pce.12119

Bustamante M, Robledo-Abad C, Harper R, et al (2014) Co-benefits, trade-offs, barriers and policies for greenhouse gas mitigation in the agriculture, forestry and other land use (AFOLU) sector. Glob Chang Biol 20:3270–3290. https://doi.org/10.1111/gcb.12591

Cappelli G, Confalonieri R, Van M, et al (2016) Modelling inclusion, testing and benchmarking of the impacts of ozone pollution on crop yields at regional level Module development and testing and benchmarking with the WOFOST generic crop model

Cramer W, Bondeau A, Woodward FI, et al (2001) Global response of terrestrial ecosystem structure and function to CO2 and climate change: results from six dynamic global vegetation models. Glob Chang Biol 7:357–373. https://doi.org/10.1046/j.1365-2486.2001.00383.x

Cramer W, Kicklighter DW, Bondeau A, et al (1999) Comparing global models of terrestrial net primary productivity (NPP): overview and key results. Glob Chang Biol 5:1–15

Elliott J, Kelly D, Chryssanthacopoulos J, et al (2014) The parallel system for integrating impact models and sectors (pSIMS). Environ Model Softw 62:509–516. https://doi.org/10.1016/j.envsoft.2014.04.008

Elliott J, Müller C, Deryng D, et al (2015) The Global Gridded Crop Model Intercomparison: Data and modeling protocols for Phase 1 (v1.0). Geosci Model Dev 8:261–277. https://doi.org/10.5194/gmd-8-261-2015

Emberson LD, Buker P, Ashmore MR, et al (2009) A comparison of North American and Asian exposure – response data for ozone effects on crop yields. Atmos Environ 43:1945–1953. https://doi.org/10.1016/j.atmosenv.2009.01.005

Folberth C, Elliott J, Müller C, et al (2016) Uncertainties in global crop model frameworks: effects of cultivar distribution, crop management and soil handling on crop yield estimates. Biogeosciences Discuss 1–30. https://doi.org/10.5194/bg-2016-527

Garthwaite R, Fowler D, Stevenson D, et al (2009) Ground level ozone in the 21st century: Trends, interactions with climate and environmental impacts. IOP Conf Ser Earth Environ Sci 6:282002. https://doi.org/10.1088/1755-1307/6/28/282002

Godfray HCJ, Beddington JR, Crute IR, et al (2010) Food security: The challenge of the feeding 9 billion people. Science (80-) 327:812–818. https://doi.org/10.1016/j.geoforum.2018.02.030

Goldewijk KK, Ramankutty N (2004) Land cover change over the last three centuries due to human activities : The availability of new global data sets. GeoJournal 61:335–344

Guarin JR, Kassie B, Mashaheet AM, et al (2019) Modeling the effects of tropospheric ozone on wheat growth and yield. Eur J Agron 105:13–23. https://doi.org/10.1016/j.eja.2019.02.004

Guo LB, Gifford RM (2002) Soil carbon stocks and land use change: A meta analysis. Glob Chang Biol 8:345–360. https://doi.org/10.1046/j.1354-1013.2002.00486.x

Houghton RA, Nassikas AA (2017) Global and regional fluxes of carbon from land use and land cover change 1850–2015. Global Biogeochem Cycles 31:456–472. https://doi.org/10.1002/2016GB005546

Iizumi T, Yokozawa M, Sakurai G, et al (2014) Historical changes in global yields: Major cereal and legume crops from 1982 to 2006. Glob Ecol Biogeogr 23:346–357. https://doi.org/10.1111/geb.12120

IPCC (2017) Climate Change and Land. an IPCC special report on climate change, desertification, land degradation, sustainable land management, food security, and greenhouse gas fluxes in terrestrial ecosystems

Jackson ND, Konar M, Debaere P, Estes L (2019) Probabilistic global maps of crop-specific areas from 1961 to 2014. Environ Res Lett 14:094023. https://doi.org/10.1088/1748-9326/ab3b93

Jones JW, Hoogenboom G, Porter CH, et al (2003) The DSSAT cropping system model

Kanianska R (2016) Agriculture and its Impact on Land-Use, Environment, and Ecosystem Services. In: Landscape Ecology - The influences of Land Use and Anthropogenic impacts of landscape Creation. pp 7–26

Lin M, Horowitz LW, Xie Y, et al (2020) Vegetation feedbacks during drought exacerbate ozone air pollution extremes in Europe. Nat Clim Chang 10:444–451. https://doi.org/10.1038/s41558-020-0743-y

Lindeskog M, Arneth A, Bondeau A, et al (2013) Implications of accounting for land use in simulations of ecosystem carbon cycling in Africa. Earth Syst Dyn 4:385–407. https://doi.org/10.5194/esd-4-385-2013

Lu C, Tian H (2017) Global nitrogen and phosphorus fertilizer use for agriculture production in the past half century: Shifted hot spots and nutrient imbalance. Earth Syst Sci Data 9:181–192. https://doi.org/10.5194/essd-9-181-2017

Mbow C, Rosenzweig C, Barioni L, et al (2019) Food Security. In: Shukla PR, Skea J, Buendia EC, et al. (eds) Climate Change and Land: an IPCC special report on climate change, desertification, land degradation, sustainable land management, food security, and greenhouse gas fluxes in terrestrial ecosystems. pp 437–550

McGrath JM, Betzelberger AM, Wang S, et al (2015) An analysis of ozone damage to historical maize and soybean yields in the United States. Proc Natl Acad Sci 112:14390–14395. https://doi.org/10.1073/pnas.1509777112

Müller C, Elliott J, Chryssanthacopoulos J, et al (2017) Global gridded crop model evaluation: benchmarking , skills , deficiencies and implications. Geosci Model Dev 10:1403–1422. https://doi.org/10.5194/gmd-10-1403-2017

Müller C, Elliott J, Kelly D, et al (2019) The Global Gridded Crop Model Intercomparison phase 1 simulation dataset. Sci Data 6:1–22. https://doi.org/10.1038/s41597-019-0023-8

Olin S, Lindeskog M, Pugh TAM, et al (2015a) Soil carbon management in large-scale earth system modelling : implications for crop yields and nitrogen. Earth Syst Dyn 6:745–768. https://doi.org/10.5194/esd-6-745-2015

Olin S, Schurgers G, Lindeskog M, et al (2015b) Modelling the response of yields and tissue C : N to changes in atmospheric CO2 and N management in the main wheat regions of western Europe. Biogeosciences 12:2489–2515. https://doi.org/10.5194/bg-12-2489-2015

Pleijel H, Uddling J (2012) Yield vs . Quality trade-offs for wheat in response to carbon dioxide and ozone. Glob Chang Biol 18:596–605. https://doi.org/10.1111/j.1365-2486.2011.2489.x

Portmann FT, Siebert S, Döll P (2010) MIRCA2000-Global monthly irrigated and rainfed crop areas around the year 2000: A new high-resolution data set for agricultural and hydrological modeling. Global Biogeochem Cycles 24:n/a-n/a. https://doi.org/10.1029/2008gb003435

Prentice IC, Webb RS, Ter-Mikhaelian MT, et al (1989) Developing A Global Vegetation Dynamics Model: Results of an IIASA Summer Workshop. Novographic, Laxenburg, Austria

Pugh TAM, Arneth A, Olin S, et al (2015) Simulated carbon emissions from land-use change are substantially enhanced by accounting for agricultural management. Environ Res Lett 10:. https://doi.org/10.1088/1748-9326/10/12/124008

Ray DK, West PC, Clark M, et al (2019) Climate change has likely already affected global food production. PLoS One 14:1–18. https://doi.org/10.1371/journal.pone.0217148

Ringeval B, Müller C, Pugh TAM, et al (2021) Potential yield simulated by global gridded crop models: Using a process-based emulator to explain their differences. Geosci Model Dev 14:1639–1656. https://doi.org/10.5194/gmd-14-1639-2021

Rosenzweig C, Elliott J, Deryng D, et al (2014) Assessing agricultural risks of climate change in the 21st century in a global gridded crop model intercomparison. Proc Natl Acad Sci 111:3268–3273. https://doi.org/10.1073/pnas.1222463110

Rosenzweig C, Jones JW, Hatfield JL, et al (2013) The Agricultural Model Intercomparison and Improvement Project (AgMIP): Protocols and pilot studies. Agric For Meteorol 170:166–182. https://doi.org/10.1016/j.agrformet.2012.09.011

Schauberger B, Rolinski S, Schapho S, Müller C (2019) Global historical soybean and wheat yield loss estimates from ozone pollution considering water and temperature as modifying effects. Agric For Meteorol 265:1–15. https://doi.org/10.1016/j.agrformet.2018.11.004

Sitch S, Cox PM, Collins WJ, Huntingford C (2007) Indirect radiative forcing of climate change through ozone effects on the land-carbon sink. Nature 448:. https://doi.org/10.1038/nature06059

The World Bank (2023) The World Bank data. In: Agric. For. fishing, value added (% GDP). https://data.worldbank.org/indicator/NV.AGR.TOTL.ZS. Accessed 22 Mar 2023

United Nations (2019) World population prospects 2019, Online Edi

Vermeulen SJ, Aggarwal PK, Ainslie A, et al (2012) Options for support to agriculture and food security under climate change. Environ Sci Policy 15:136–144. https://doi.org/10.1016/j.envsci.2011.09.003

CHAPTER TWO: MODELLING CROP YIELD AND HARVEST INDEX: THE ROLE OF CARBON ASSIMILATION AND ALLOCATION PARAMETERS

2.1. Abstract

Crop yield improvement has relied on increasing the ratio of the economic organ to the total above-ground biomass, known as the harvest index (HI). In most crop models, HI is set as a cultivar parameter; however, this empirical approach does not consider that HI depends on the environment, besides plant genotype. In LPJ-GUESS, HI is simulated mechanistically depending on daily growing conditions and the assimilated partitioning. Simulated HI can validate the proper representation of crop processes and productivity, but it also is a critical output for agricultural research due to its economic importance in the food production systems. However, some relevant parameters are not well constrained at the global scale in LPJ-GUESS. Therefore, this paper aims to evaluate the sensitivity of yield and HI of wheat and maize simulated with LPJ-GUESS to eight production-allocation related parameters and identify the most suitable parameter values for global simulations. The nitrogen demand reduction after anthesis, the minimum leaf C:N and the range of leaf C:N strongly affected carbon assimilation and yield, while the retranslocation of labile stem carbon to grains and the retranslocation rate of nitrogen (N) and C from vegetative organs to grains after anthesis mainly influenced HI. To identify the best parameter values, a global database of observed HI for wheat and maize was compiled and used as a reference to constrain simulations, and the calibration was performed for yield against reference data. Two maize cultivars, corresponding to high and low yielding, emerged from the calibration, whilst a simple split between spring and winter cultivars was kept for wheat. The calibrated version of LPJ-GUESS improved the simulation of yield and HI at the global scale for both crops, providing a

basis for future studies exploring crop production under different climate and management scenarios.

Keywords: Retranslocation, N concentration, parameter sensitivity, calibration, LPJ-GUESS.

2.2. INTRODUCTION

The world population is projected to reach about 9.7 billion by the middle of the century, according to the medium variant of the World Population Prospect (United Nations, 2019). The increased population plus a higher calorie demand per capita will develop a significant challenge to ensure increasing food demand (Godfray et al. 2010; Vermeulen et al. 2012). This challenge is further complicated by expected reductions in crop production caused by climate change and other environmental issues (Ray et al. 2019; Ortiz-Bobea et al. 2021; Soleymani 2022). Therefore, a sustainable solution requires understanding the complexity of agricultural systems and their interaction with other biogeochemical dynamics (Cramer et al. 1999; Sitch et al. 2003; Lindeskog et al. 2013). The global gridded crop models (GGCMs) have answered this requirement and in the last decades, become essential tools for the analysis, interpretation and decision-making in agro-ecosystems at regional and global extents, as well as for the simulation of crop productivity, climate impact on yields, and the effect of management practices such as irrigation and fertilisation (Prentice et al. 1989; Bondeau et al. 2007; Monfreda et al. 2008; Müller et al. 2017).

To properly fulfil the role of GGCMs, grain yield prediction needs the accurate representation of production processes such as phenology, carbon assimilation and assimilate allocation (Fletcher and Jamieson 2009; Ringeval et al. 2021). Allocation

patterns vary due to genetic and environmental factors (Qin et al. 2013; Porker et al. 2020), and allocation in harvestable organs is represented by the harvest index (HI), defined as the ratio of grain dry matter to above-ground biomass. HI describes the crop success in partitioning photosynthates to produce economic biomass, and due to its direct contribution to grain yield and its economic importance, it is an essential output to be addressed in crop modelling, besides yield.

In most crops, HI has increased through domestication and breeding (Lorenz et al. 2010), and during the last decades, rising crop productivity has mainly relied on increased HI. For example, wheat cultivars released between 1860 and 1982 showed that 80% of the improvement in yield was associated with an increase in harvest index (Sinclair 1998). For maize, differences between old and modern hybrids yields are also directly related to HI increase (Lorenz et al. 2010; Liu et al. 2020). Correspondingly, grain yield is highly sensitive to factors that affect HI, such as water stress or nutrient management, which have been shown to affect the proportion of biomass converted to grains in wheat (Dai et al. 2016; Porker et al. 2020; Soleymani 2022).

Different approaches are used for HI in the GGCMs; the LPJmL model uses a defined optimum and minimum HI as cultivar-prescribed parameters only affected by water stress (Bondeau et al. 2007; Ringeval et al. 2021). Other models like the EPIC family models (group of GGCMs composed of several site-based similar models) include potential HI as a cultivar parameter that can be modified by empirical response functions to N dynamics and drought stress during the productive phase (Balkovič et al. 2013; Olin et al. 2015a; Ringeval et al. 2021). This approach is parsimonious but does not allow the analysis of the effect of multiple factors affecting

HI and limits the potential use of crop models in simulating economic carbon allocation; one of the most critical agricultural traits (Qin et al. 2013). Besides, a correct prediction of HI supports the accurate representation of production processes and yield simulation (Fletcher and Jamieson 2009)

To solve this, LPJ-GUESS has introduced a fully prognostic HI calculation. It is calculated mechanistically as a function of the assimilated carbon, the developmental stage and based on the daily fraction of net primary production (NPP) allocated to different plant tissues and the retranslocation of carbon from other organs to grains (Olin et al. 2015b). The simulation of HI in LPJ-GUESS was introduced as part of a package of updates, including a Nitrogen (N) dynamic module that accounted for the effect of N limitation and N (Olin et al. 2015b). These implementations improved the LPJ-GUESS performance in simulating the productivity of grasslands, wheat yield in Europe, and global maize and wheat yield at the country scale (Olin et al. 2015b, a; Blanke et al. 2018).

2.2.1. LPJ-GUESS

LPJ-GUESS (Smith et al. 2014) is a process-based dynamic vegetation model that simulates vegetation response to climate, atmospheric carbon dioxide levels ([CO_2]) and N dynamics. Different plant functional types (PFT) represent several vegetation categories according to growth form, phenology, photosynthetic pathway, distributional temperature limits and N requirements (Olin et al. 2015a). The land use change and crop modules (Lindeskog et al. 2013) represent crops as PFTs differing in climatic thresholds and management-related parameters like baseline sowing and harvest dates. The model also includes management options such as irrigation,

tillage and inter-growing season grass cover (Olin et al. 2015b). The main processes simulated daily to represent crops are soil hydrology, photosynthesis, canopy conductance, respiration, phenology, plant N demand, and carbon allocation (Smith et al. 2001; Olin et al. 2015b).

Carbon allocation of daily NPP and retranslocation of nutrients after anthesis and during senescence are critical factors to simulate yield in LPJ-GUESS and, subsequently, HI. These processes depend on the crop development stage, defined daily as a number between 0 and 2 in LPJ-GUESS, depending on air temperature, vernalisation and day length. Anthesis is represented by a developmental stage of 1; values below 1 represent the vegetative phase, while above 1 represent the reproductive phase. During the vegetative phase, allocation is mainly represented by a logistic growth of roots, leaves and stems. During the reproductive phase, assimilates are allocated to grains (Olin et al. 2015b). LPJ-GUESS also considers a temporary carbon pool to supply demand on days when assimilation is below respiration cost. When the stem stops growing after anthesis, redistribution of the temporary carbon pool to storage organs starts (Penning de Vries et al. 1989; Olin et al. 2015b).

Senescence is integral to annual crop development but can also be prematurely induced in leaves by adverse conditions and stress. In LPJ-GUESS, the onset of senescence occurs when the available N in leaves declines below necessary to maintain the current leaf Area Index (LAI) (Yin et al. 2000; Smith et al. 2001; Gregersen et al. 2013; Olin et al. 2015b). The necessary N to maintain LAI depends on the N uptake and the N demand from leaves according to their C:N, which is not a fixed parameter in LPJ-GUESS. Instead, it is constrained between a minimum and a

maximum leaf C:N and the optimum leaf C:N is estimated as 3/4 of this range (Wample et al. 1991; Smith et al. 2014; Olin et al. 2015b).

LPJ-GUESS has shown acceptable performance in the simulation of recent-historical yield for wheat and maize globally (Olin et al. 2015a; Bodin et al. 2016; Müller et al. 2019). However, several parameters relevant to the allocation scheme are weakly constrained and the sensitivity of simulated yield to these parameter choices is not well characterised. Furthermore, the lack of global-scale compilations of reference data of HI (Boote et al. 2013; Iizumi et al. 2014; Ringeval et al. 2021) means that LPJ-GUESS has not been tested against simultaneous constraints for both yield and HI at the global scale. In this paper, we report on the sensitivity of yield and HI outputs from LPJ-GUESS to the variation of eight parameters related to production and allocation. We further identify the most suitable choice of parameter values to simulate yield and HI across a globally distributed range of reference sites for two cultivars of wheat (*Triticum aestivum* L.) and two cultivars of maize (*Zea Mays* L.) by comparing simulated and reference yield, as well as simulated and observed HI values. Finally, a global evaluation demonstrates the fit improvement in HI and yield with the new parameter setup.

2.3. MATERIALS AND METHODS

2.3.1. Model Setup

LPJ-GUESS v4.1, revision 10304, was used in this study. This version is based on the developments presented by Olin et al. (2015b) including the daily carbon allocation scheme and N dynamics in crops. The land cover was set for only cropland and the simulations were carried out starting in 1980 for maize, spring and winter wheat. All the crops were simulated for rainfed and irrigated conditions with tillage, N

application and inter-growing season grass turned on. The model dynamically estimated sowing and harvest dates based on climate suitability and heat unit accumulation (Lindeskog et al. 2013). All simulations were performed using a 500-year spin-up with detrended [CO_2] and climate to build up C and N pools and the AgMERRA climate forcing dataset (Ruane et al. 2015). In addition, N input was provided based on the atmospheric N deposition dataset from Lamarque et al., (2010) and the cropland N fertilisation database from AgGRID (AgMIP Gridded Crop Modelling Initiative) (Elliott et al. 2015a).

2.3.2. Parameters

The effect of eight crop LPJ-GUESS parameters was evaluated on yield, harvest index (HI), NPP, Carbon mass, LAI and N pool. A total of 17280 simulations were performed, combining all the levels from each parameter (2×3×3×3×4×4×4×5). A specific combination of parameters is referred to as a setup in the following. To evaluate sensitivity to all parameters in the crop model, including their interactions, would be computationally unfeasible. Therefore, the evaluated parameters and the range of variation were chosen based on literature revision, preeliminar simulation testing and an expert assessment of parameters likely to affect the simulated harvest index and are poorly constrained by observations. These parameters were primarily related to N status in the plant, retranslocation of C and N towards the grain, leaf thickness and light extinction (Figure 2.1).

- **Stem retranslocation (*Sret*)**

Sret represents the retranslocation of carbohydrates of easy mobilisation, mainly glucose and starch, from the stem to grains. This labile C pool represents 0.4 of the

stem carbon at flowering, and it is retranslocated to the grains close to the end of the grain-filling period with a rate of 0.1 day^{-1}. Retranslocation is induced when the total demand for sugar exceeds the supply or when the growth rate of the developing storage organ drops below a certain level (Penning de Vries et al. 1989; Olin et al. 2015b). This process is briefly considered in some models since it is not reported to be crucial to simulating yield, and stem starch residuals have not shown a significant relationship with yield in maize (Penning de Vries et al. 1989; Liang et al. 2019). Therefore, two possibilities were tested: inclusion and exclusion of *Sret*.

- **Specific leaf area (*SLA*)**

SLA is calculated in LPJ-GUESS for natural vegetation according to leaf longevity described by Reich, Walters, and Ellsworth (1992) but for crops, it is a cultivar parameter for crops, this represents a limitation since *SLA* vary according to fertilisation and water status, cultivar, plant density, and others (Amanullah and Inamullah 2016). Values of 45 and 50 m^2kgC^{-1} have been reported for maize and 35 and 40 m^2kgC^{-1} for wheat (Penning de Vries et al. 1989; Mohammadi 2007; Olin et al. 2015a). Therefore, for this study, *SLA* was set to vary between 40, 45 and 50 m^2kgC^{-1} for maize and between 30, 35 and 40 m^2kgC^{-1} for wheat.

- **Minimum C:N ratio in leaves ($C{:}N_{min}$) and C:N Range ($C{:}N_{range}$)**

Since tissue C:N varies in LPJ-GUESS according to dynamics between plant demand and supply of N (Smith et al. 2014). $C{:}N_{min}$ represents the maximum N concentration in leaves; below this value, the leftover N is translocated to the labile N pool. Thus, higher values of this parameter cause higher amounts of N translocated from leaves. $C{:}N_{range}$ is a factor that multiplied by $C{:}N_{min}$ equals maximum *C:N*. The

inappropriate constraint of N limits will overestimate the N use efficiency (Smith et al. 2014; Olin et al. 2015b). For this study, $C{:}N_{min}$ was set to vary between 12.5, 15 and 17.5, since the original crop implementation of LPJ-GUESS, based on grass reports showing a $C{:}N_{min}$ of 16 (Olin et al. 2015a) and $C{:}N_{range}$ between 2, 2.78, 3.5 and 5 based on the ratio maximum/minimum C:N values reported between 2 and 5 (Olin et al.2015a; Olin et al. 2015b).

- **Retranslocation rate by of N and C (*Nret*, *Cret*)**

During the senescence process, retranslocation of N and C stored before anthesis to grains occur, but not instantaneously. In Olin, Schurgers, et al. (2015), this process is set to occur at a rate of 0.1 day^{-1}. For this study, *Nret* and *Cret* were set to vary between different rates of 0.1, 0.2, 0.3 and 0.4 day^{-1} to complete N and C retranslocation. Quicker retranslocation implies a shorter senescence period and greater depletion of previously stored pools, increasing the ratio of dry matter between grains and other organs, a.k.a HI.

- **Nitrogen extinction coefficient (kN)**

The N extinction coefficient is directly related to the light extinction coefficient. It represents the decline in leaf N concentration from top to bottom of the canopy, typically following an exponential decrease. A higher extinction coefficient means a more drastic decrease in N concentration. N distribution is one of the most important determinants of photosynthesis rate, carbon gain, and senescence regulation in the canopy in LPJ-GUESS, affecting yield and HI (Yin et al. 2000; Olin et al. 2015b; Hikosaka et al. 2016). *kN* was set to vary between 0.175, 0.233 and 0.291 $m^2\ m^{-2}$ for maize, and 0.15, 0.2 and 0.25 for wheat. Central values of these ranges were obtained from the original model setup. The range was selected from references for

wheat calculated under different conditions during the vegetative period (Yin et al. 2003; Olin et al. 2015b).

- **Nitrogen demand reduction (Ndred)**

Ndred represents the reduction in N demand by leaves after anthesis, affecting photosynthesis, carbon gain, leaf senescence, yield, and HI. This process is not fully understood but is known to occur gradually due to root senescence resulting in a change in the N source-sink relationship (Zhao et al. 2020). Some reports show that N content at anthesis in wheat is as high as 90% of N at maturity (Mi et al. 2000). Since this parameter is not well explored and the timespan at which it occurs is unclear, a wide range of *Ndred* was set, varying between 0, 2.72, 7.39, 20.09 and 100, lower values were prefered since the actual setup is around 7.39 and the value of 100 was mainly exploratory. A value of 0 means a slow reduction equal to the original LPJ-GUESS scheme, while 100 means a drastic decrease of N demand after the anthesis.

2.3.3. Harvest Index

A systematic literature review of published peer-reviewed research was conducted in August and September 2019, employing the widely used databases *Google Scholar* and *Web of Science*. A secondary search was also performed through publications cited by those in the primary search. The search was intended to identify studies published worldwide reporting the harvest index for wheat and maize. Studies published since 1990 were targeted to avoid the inclusion of old cultivars. Although studies published before 1990 were included in a few cases, in areas where no

publications were found searching by the initial time target. The following search protocol was employed:

1) Search in English, Spanish and Portuguese for each of the four crop names, “wheat”, “maize or corn” (Spanish: Trigo and maiz; Portuguese: Trigo and milho), combined with “harvest index” (Spanish: índice de cosecha; Portuguese: índice de colheita).
2) A manual review of the results to identify papers containing relevant data and potential research to include in the database depending on the availability of the document and the inclusion of harvest index values for any of the crops included in the study at a specific location.
3) A further round of searches and manual review targeted regions where few or no studies were found in the first search: Africa and South America for all the crops and North America and Europe for rice.
4) Finally, the word “meta-analysis” was also combined with all the described search terms to get studies with previously compiled datasets.

Google Scholar is prone to excessive results, from around 150 000 records in the first type of search to about 15 000 in the latter. While the *Web of Science* produced around 1000 records in the first type of search to less than 10 in the latter, for this reason, only the first 100 results in each were considered. Therefore, an examination of the results was required to identify relevant studies. A total of 46 records were identified for maize and 50 for wheat. Additionally, 64 publications (34 for maize and 34 for wheat) reported in a harvest index meta-analysis countrywide in China were collected to complement the database. These studies were published in Chinese between 2006 and 2010. Selected records

were scrutinised to filter duplicate studies or identify different studies using the same HI data. Studies were retained if they included the compulsory target variables: location (country, city and coordinates), year of the harvest, harvest index value and type of wheat (spring or winter). Information on whether crops were irrigated, rainfed, and fertilised traditionally (by synthetic fertilisers) or alternatively (organic, ecological) was also recorded if mentioned in the study.

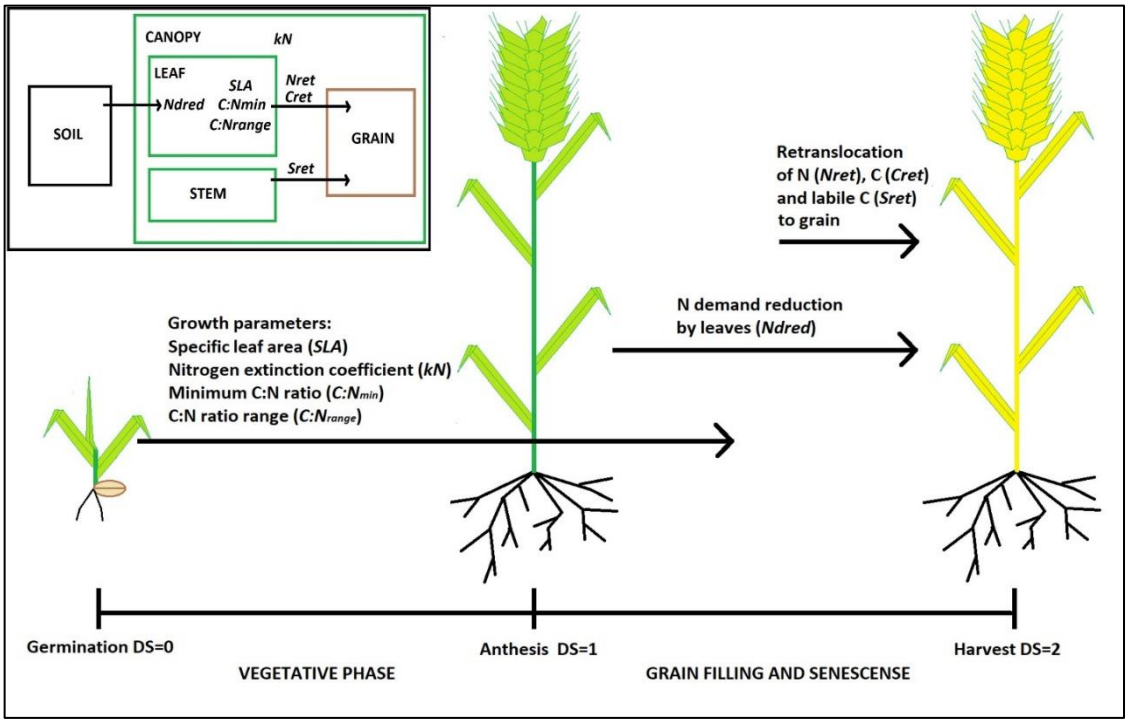

Figure 2.1. Diagram of the relationship between evaluated parameters and plant organs during different Developmental stages (DS)

When the dataset in meta-analysis studies or any compulsory variable was not included in the published document or supplementary data, the authors were contacted and requested to share the information; no response caused the rejection of the record. Detailed information about the number of records is contained in Table 2.1 and supplementary data S1. The commercial control harvest index data was chosen in studies about nutrition, plant density, or any other management practice. If

a control treatment was not explicitly included in the study, the middle levels of the treatments were selected, as well as the well-watered treatments in irrigation experiments or cultivars used as a reference (checks) in the breeding studies and ambient treatments in air concentration enrichment experiments.

Twenty locations for wheat and twenty-two for maize were selected from the compiled HI database at a 0.5° x 0.5° gridcell scale, including productive locations with high and medium-low yields and covering as many regions worldwide as possible (Table S2-1, S3). Yields from these locations were extracted from the global gridcell scaled (0.5° x 0.5° resolution) yield data reported by Ray et al. (2019), covering the period between 1970-2013. In addition, the average yield of the countries to which the selected gridcells belonged was extracted from FAO reports (Food and Agriculture Organization of the United Nations (2020). These datasets will be referred to as the “Ray” and “FAO”, respectively in this manuscript.

Table 2.1. Summary of entries by crop

Crop	Identified records	Used records	Locations	Year range	Total entries
Maize	46	44	92	1989-2017	132
Wheat	50	39	93	1974-2016	205

2.3.4. Locations and evaluation data for calibration

We preferentially calibrated against large-scale (gridcell or country) yields rather than reported site level because LPJ-GUESS is intended for application at large scale, and therefore we wished to avoid overparameterising to idiosyncrasies of particular sites or studies. Likewise, we used aggregated, rather than site-level, HI observations in the calibration (see section 2.6). Yield reference datasets at two different spatial scales were tested for parameter calibration since computational

capacity limited sampling location and, in turn, representativity to the global model performance when gridcell scale reference yield from the Ray dataset was used. In addition, the Ray dataset was estimated based on the crop statistics from about 20000 political units, so it carries some uncertainty that can affect the calibration (Ray et al. 2019). Comparison against the average reference yield of a larger political unit provides a cross-check for robustness against uncertainties caused by the Ray dataset downscaled yield.

2.3.5. Analysis of model sensitivity

Results were analysed for the years 2001-2010, taking the mean for each location over this period. According to its average simulated yields from all the setups, locations were separated into two groups. Locations with average yields above the third quartile from all the simulated yields were categorised as “High” and “Medium” when average yields were below. A “Low” category was not included since the few low-yield locations (Below the first quartile) made grouping challenging and these locations showed similar behaviour to medium-yield locations.

The mean, standard deviation from setups and location variability and the standard deviation from setups only (mean value of locations per setup) of all the output variables were calculated for all the parameter levels to inspect the variability caused by the parameter variation. Then a one factorial ANCOVA for the “High” and “Medium” groups was carried out for yield and HI, correcting the location effect by considering locations as a categorical covariate. Finally, the percentages of the sum of squares from ANCOVA (%SS) were calculated for all the main effects (parameters) and for interaction effects as the joined percentage of all the interactions where each parameter was included (Equations 2 - 1 and 2 - 2).

$$\%\mathrm{SSmain}_i = \frac{\mathrm{SSmain}_i}{\mathrm{SS}_{\mathrm{Total}}} * 100 \qquad \text{Equation 2-1}$$

$$\%\mathrm{SSinter}_i = \frac{\sum_{j=1}^{n} \mathrm{SSinter}_{i*j}}{\mathrm{SS}_{\mathrm{Total}}} * 100 \qquad \text{Equation 2-2}$$

where ***i*** represents the parameter, ***j*** *is* the interaction including the ***ith*** parameter, ***SSmain*** is the sum of squares of main effects, ***SSinter*** is the sum of squares of interaction, and $\boldsymbol{SS_{Total}}$ is the total sum of squares.

2.3.6. Parameter calibration

Only setups that simulated senescence properly were retained for the rest of the analysis, it means setups with a percentage of dead leaves at harvest for irrigated maize above 70% and above 50% for irrigated spring and winter wheat in more than half of the locations (12 for maize and 11 for wheat). These values were approximated, for maize, based on the decrease of the amount of chlorophyll in leaves during senescence reported for fertilised maize (He et al. 2004) and were set lower for wheat since the breeding programs during the last years have selected many stay-green cultivars due to its improvement in grain yield (Kipp et al. 2014). The simulated yields were masked according to the irrigated and rainfed areas reported in each location by the Spatial Production Allocation Model “SPAM” 2005 (You et al. 2014) and adjusted to fresh weight assuming a 12% net water content for wheat and 13% for maize (Müller et al. 2017). The difference between simulated yields against both reference datasets (Ray and FAO) was calculated as a fraction of the reference yield for each location in every setup. For Maize, the best setup for each location was selected by minimising the yield difference separately for FAO and Ray datasets and constraining HI to setups that produced values between the

percentiles 5th and 95th of the compiled HI database (0.30 and 0.59) to avoid atypical HI values.

In order to assess whether a single generic setup was identified for maize or whether there was variation in the best setup suggesting a variation in cultivar, a k-means algorithm was performed on the best setups set to group the locations iteratively in clusters based on simulated yield and HI (Shamim Reza 2015). The number of clusters was selected based on the within-group sum of squares method, choosing the number of clusters at which the rate of change of the sum of squares with cluster number approaches zero. Spring and winter wheat were already included in the model, and selected locations were already classified by cultivar, so no clustering was performed.

Subsequently, the 80th percentile of the yield difference (q80) was calculated for each setup separating locations by different cultivars; q80 was used to ensure that most of the locations had low yield differences instead of a central tendency statistic like mean; affected by extremely low values or median which is not sensitive to extremely high values. The average of simulated HI was also calculated per setup for each cultivar and if this value was out of the range between 0.30 and 0.59 for maize and 0.30 and 0.45 for wheat, the setup was not further included in the analysis. Wheat was higher constrained on the upper limit because the frequency distribution of the observed HI was skewed to the right compared to maize. Therefore, the setups were ranked by the low to high q80, and the best setups were those with lower q80 for each cultivar.

2.3.7. Global evaluation

The best setup and the parameter mean from the best ten setups were both selected to simulate globally, as well as the LPJ-GUESS original parameter setup (Table 2.2) defined by Olin et al. (2015b). Global simulations were performed on a 0.5° x 0.5° grid based on the same driving datasets as the sensitivity simulations (Section 2.2), and simulated yields were also masked according to “SPAM” 2005 (You et al. 2014) and adjusted to fresh weight assuming a 12% net water content for wheat and 13% for maize (Müller et al. 2017). For maize, global outputs were aggregated at a country level, and cultivars were distributed by country, minimising the difference between aggregated and FAO-reported yields. While for wheat, the cultivar distribution was taken from the recent AgMIP climate change evaluation using a crop model ensemble (Jägermeyr et al. 2021). This process was performed separately for the selection method (best or ten best mean) and reference data (Ray and FAO), producing four global simulations per crop plus the original setup simulation. A production-weighted mean absolute error (WMAE) for yield was calculated at the country and gridcell scale as in Equations 3 and 4 to compare the five global simulations and select the best setup.

$$\mathrm{WMAE} = \sum_{i=1}^{n} \mathrm{Frac\_Prod}_i * |\mathrm{Observed}_i - \mathrm{Simulated}_i| \qquad \text{Equation 2-3}$$

$$\mathrm{Frac\_Prod}_i = \frac{\mathrm{Production}_i}{\mathrm{W}_{prod}} \qquad \text{Equation 2-4}$$

where *n*, depending on the comparison scale, is either the global number of gridcells or countries where yield was simulated and reported in the Ray or FAO datasets, respectively. *Production* is the gridcell or country scale crop production. *Observed* is the reference yield at gridcell or country scale (Ray or FAO), and W_{prod} is the

aggregated world production, all reported from Ray or FAO, respectively, and averaged for 2001-2010. *Simulated* is the LPJ-GUESS simulated yield aggregated by country or for gridcell according to the scale comparison. Ray production was calculated by multiplying yield by harvested areas reported in “SPAM” 2005 (You et al. 2014). WMAE was also calculated for HI using the Equation 2 - 3 and comparing simulated HI against the compiled database at gridcell scale.

Finally, the best 50 setups per cultivar from the selected reference dataset were used to perform a descriptive analysis to show the relationship between cultivars and parameters, the distribution of parameter values and the yield difference range caused by parameters in these 50 setups.

2.4. RESULTS AND DISCUSSION

2.4.1. Sensitivity analysis

Variation of maize yield simulated in locations from “Medium” (Figure 2.2A, 2.4A) was mainly influenced by *Sret*, *C:N*$_{range}$ and *Cret*, and to a lower extent by *Nret*, *N*dred and *C:N*$_{min}$. Except for *C:N*$_{min}$, the same parameters also affected HI in this group (Figure 2.3A, 2.4B). In locations from “High”, yield was more sensitive to *Nret* and less to *C:N*$_{min}$ compared to “Medium” (Figure S2-1A, 4A). HI was more sensitive in “High” to *Nret* and similarly sensitive to the rest of the parameters as “Medium” (Figure 2.3A, S2-2A, 2.4B).

Simulated wheat yields showed high sensitivity to variation in *Sret*, *C:N*$_{range}$, *Nret*, C:N$_{min}$, and *Ndred*. *Ndred* caused more significant variation in “High” while *C:N*$_{range}$ in “Medium”(Figure 2B, S2.1B, 2.4A). *Sret, C:N*$_{range}$, *Nret* and *Ndred* caused higher variability of HI. As for yield, *Ndred* had a stronger effect than other parameters in

“High”, whilst $C:N_{range}$ did in “Medium” (Figure 2.3B, S2-2B, 2.4B). N-related parameters affected yield variation in both crops, but the effect was higher in “High” locations. This occurred because of soil N limitation in “Medium” locations (Table S2-3) which constrained yield in setups with parameter values allowing higher production compared to “High”, like 0.1 for *Nret* and 0 for *Ndred,* implying slower retranslocation and smooth N demand reduction after anthesis, therefore a more extended period of carbon assimilation (Figure S2-3).

Lower *Ndred* increases both HI and yield because N uptake after anthesis is one significant source for N in grains and allows plants to keep more foliar area and produce more assimilates. This correlation between dry weight and yield with slower post-anthesis N uptake has been previously reported for maize and wheat. Higher post-anthesis uptake occurred when available soil N increased during grain filling, increasing yield and green area index (Mi et al. 2000; Zhao et al. 2020). This indicates that N demand reduction is not a quick process, as represented by high *Ndred* values.

In wheat, yield and HI are more influenced by *Nret* than *Cret.* This occurred because the N translocation rate is directly related to leaf senescence and the photosynthetic rate depending on the ratio of nitrogen-limited LAI and the actual LAI (Yin et al. 2000; Smith et al. 2001; Gregersen et al. 2013; Olin et al. 2015b). Conversely, a higher carbon translocation indirectly causes senescence when a rapid decrease of C:N reaches a maximum N concentration. This effect was stronger in wheat, in which N*ret* effect on LAI was higher than *Cret* while LAI in maize showed a similar response between *Cret* and *Nret* (Figure S2-5), probably related to the limiting available soil N content in productive areas decreasing *Nret* sensitivity (Table S2-3). One way to

observe this is the small effect of low *Nret* (0.1) in actual leaf C:N in maize compared to wheat (Figure S2-4).

Higher wheat sensitivity to $C{:}N_{min}$, compared to maize, was notable in outputs like GPP, LAI and leaf carbon mass, which directly influence yield and HI. This is also likely due to the higher soil N content in wheat soils, which suggests that carbon assimilation in wheat is constrained by the maximum N concentration allowed in the leaves by LPJ-GUESS in more locations. Instead, this parameter was not equally critical for maize since the limited soil N content is the main factor affecting carbon assimilation in the range of conditions simulated here.

Maize was more sensitive to $C{:}N_{range}$, which regulates the minimum N concentration. Higher ranges of C:N allow lower N concentrations in leaves, decreasing photosynthetic capacity and, in turn, GPP and yield (Figure 2.2, S2-3). In addition, lower N limits favour increased LAI and vegetative growth with less N requirement, reducing HI (White et al. 2000; Hassan et al. 2007). Opposite to $C{:}N_{min}$, the limited soil N in maize soils implies that the minimum N allowed in the leaves by LPJ-GUESS constrained maize carbon assimilation in more locations than wheat. N content in soil was not standardised since that would have critically affected yield, precluding the use of sensitivity simulations for parameter calibration.

Yield and HI of both crops were highly sensitive to *Sret*, which affects grain carbon accumulation but also accumulation in vegetative organs. Consequently, it had a more significant effect and was the most critical parameter of HI. Stem dry weight loss has been widely observed after anthesis in both crops (Kiniry et al. 1992; Xue et al. 2014; Nazir et al. 2021) and is generally assumed to go to the grains, although it

lacks experimental confirmation (Penning de Vries et al. 1989; Olin et al. 2015b). Alternative hypotheses propose that remobilisation is not constant and only occurs when the growth rate of the developing storage organs drops below a certain level (Penning de Vries et al. 1989), also that labile carbon from the stem can be used to synthesise structural material and maintain the plant and roots, besides, some evidence has shown that stem retranslocation to grains is very dependent on the genotype and stress conditions (Kiniry et al. 1992; Xue et al. 2014; Nazir et al. 2021). If *Sret* was assumed to go to the grains in LPJ-GUESS, it directly affected the ratio between vegetative and harvested organs, increasing both simulated yield and HI and the likelihood of HI overestimation. In this study, *Sret* was only included or discarded, but the fraction of easily mobilised carbohydrates retranslocated to grains could be constrained depending on stress conditions, substantially reducing the uncertainty in yield and HI simulations.

Overall, simulated GPP and growth in LPJ-GUESS were mainly affected by the allowed leaf N concentration. This correlation was found previously in shrubs and grasses but is stronger in herbaceous species due to the higher allocation of nutrients in herbaceous stems compared to woody stems (Tang et al. 2018). N and carbon retranslocation and N uptake reduction after anthesis also affected GPP to a low extent due to the effect on the carbon assimilation period but had a stronger effect on yield and HI since the grains are the dominant carbon sink after anthesis. This result matches the findings in wheat and rice, where the amount of N taken up, including the post-anthesis period, has a proportional relationship with yield (Fageria 2014; Belete et al. 2018). Similarly, the stem labile retranslocation directly affects the

carbon ratio between grain and vegetative organs. For that reason, it is the most influential parameter affecting HI.

A

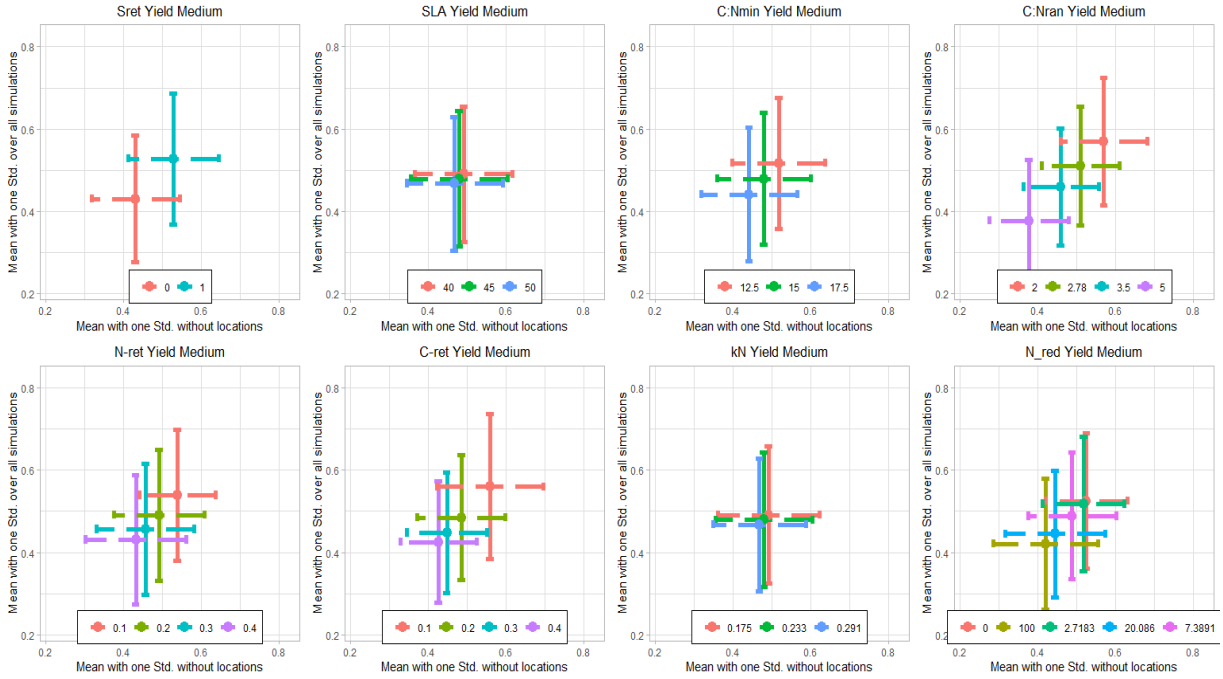

B

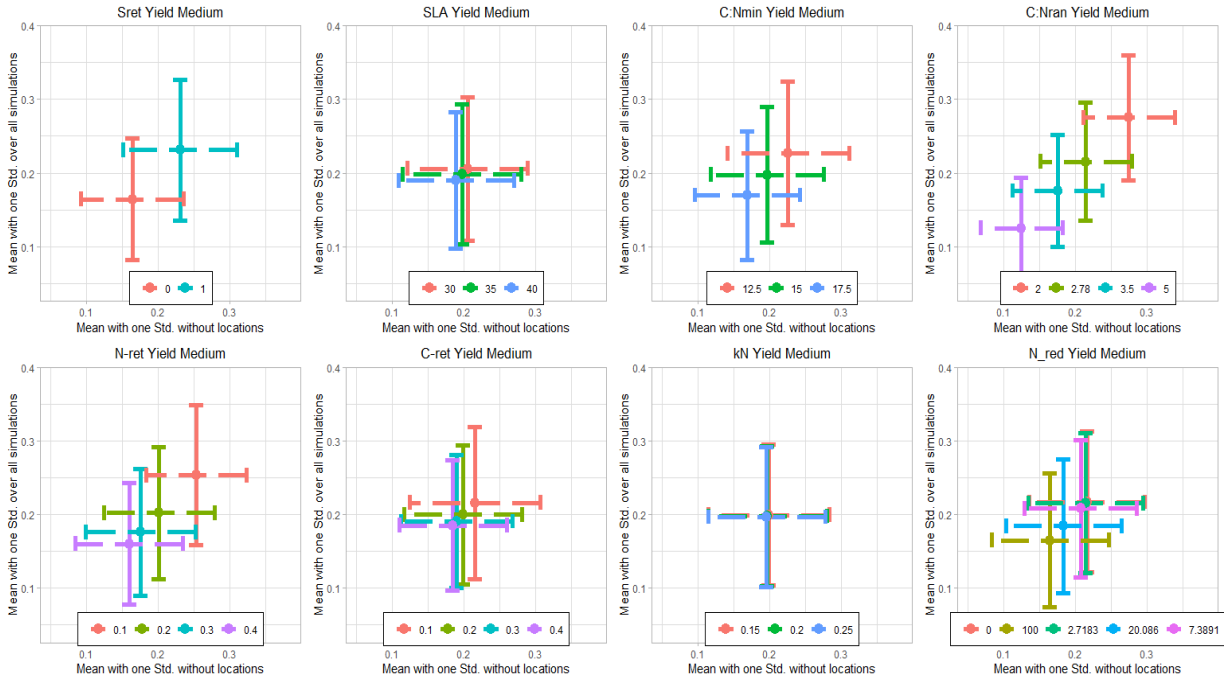

Figure 2.2. Mean values of simulated yield c for 2001-2010 for each evaluated parameter level. A. Maize medium yield locations, B. Wheat medium yield locations. Vertical bars represent the standard deviation considering all the variation from parameters and locations. Horizontal bars only consider variation from parameters. The same plot for high-yield locations can be found in Figure S2-1

A

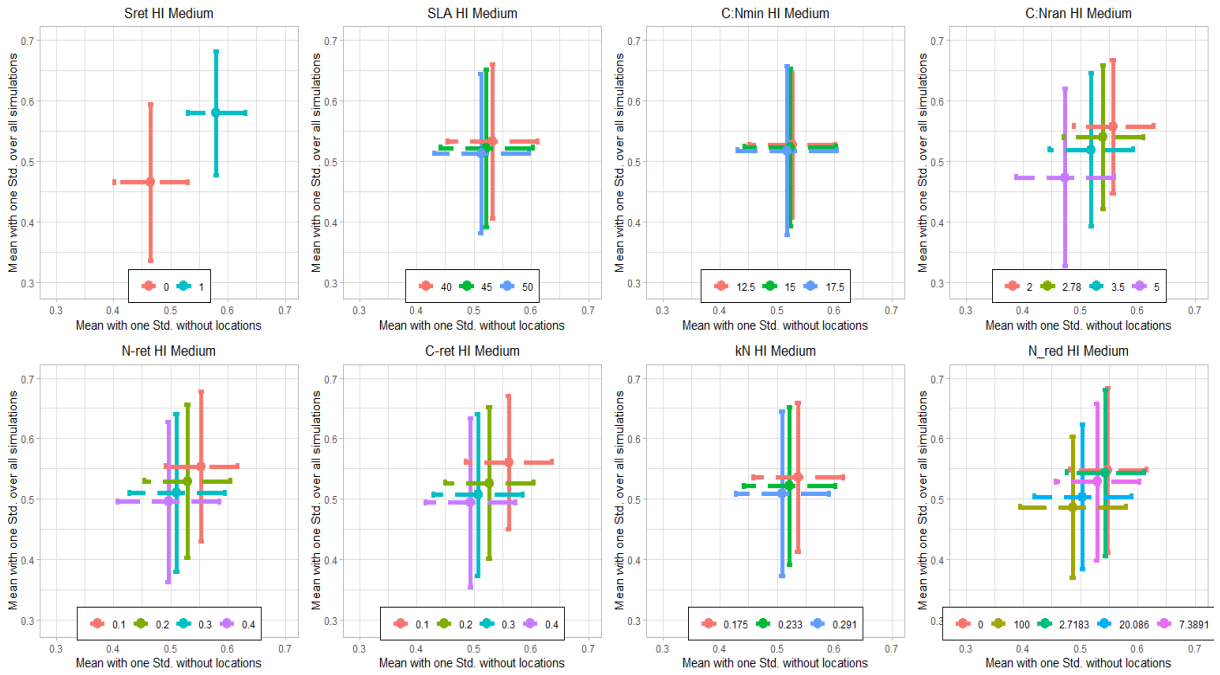

B

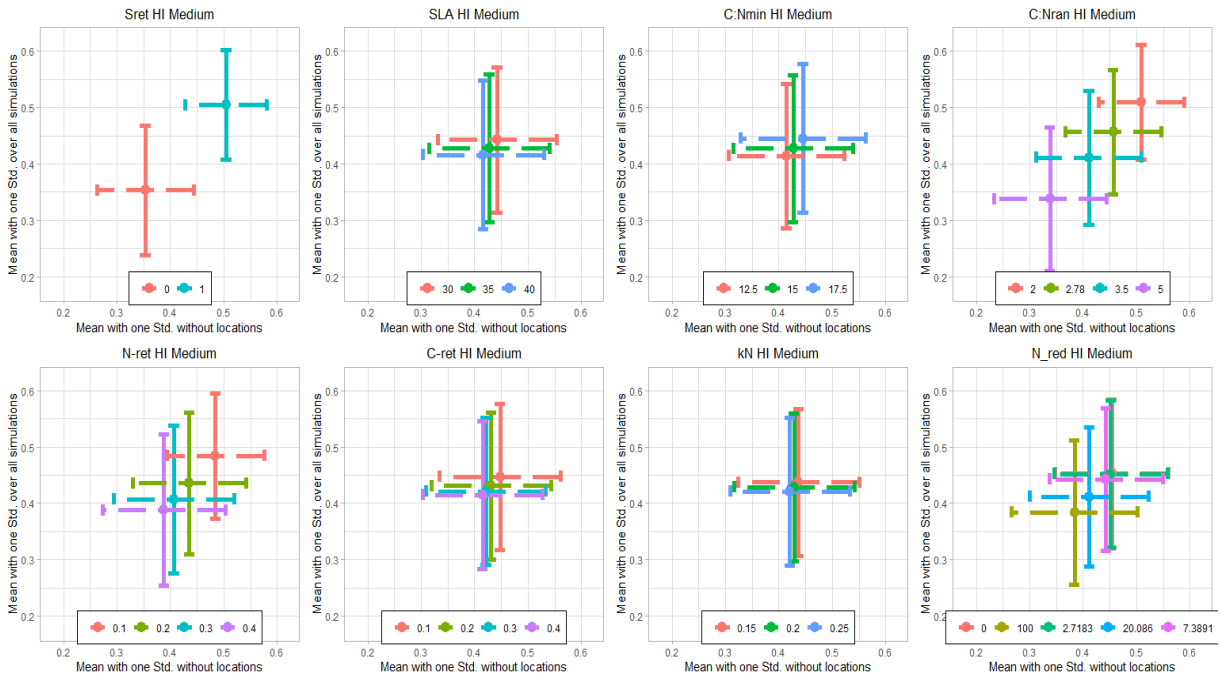

Figure 2.3. Same as Figure 2.2. But instead of simulated yield for simulated HI

A

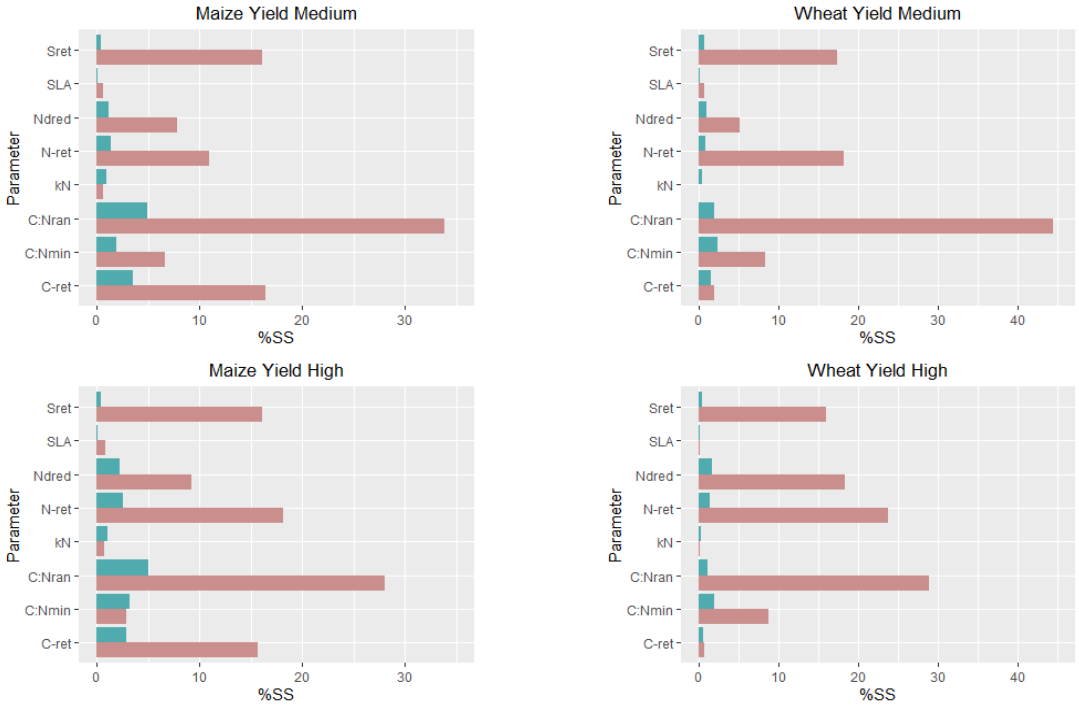

B

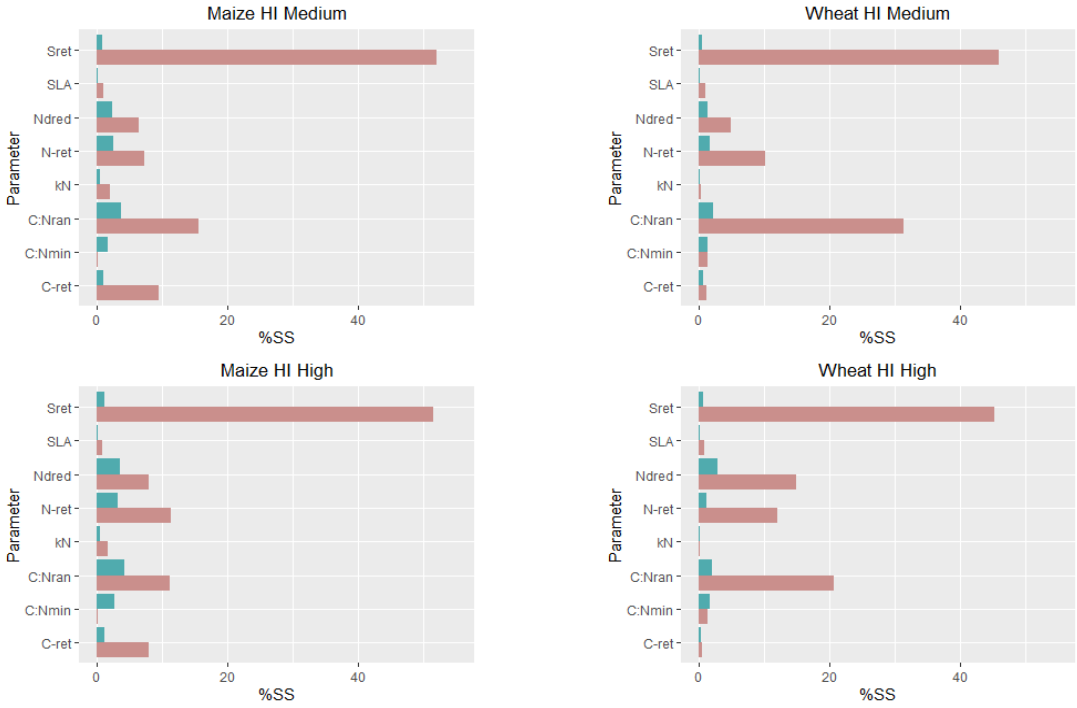

Figure 2.4. Percentage of the sum of squares for main effects (red) and added interaction effects per parameter (green): A. Simulated yield and B. Simulated HI of maize and wheat

2.4.2. Parameter calibration

The selection of the best setup for each location for maize resulted in two distinct clusters of parameters, similar for both Ray and FAO datasets. Mainly temperate regions were included in cluster 1, and sub- and tropical regions in cluster 2 (Table S2-1). The only deviations were the inclusion of China in Cluster 1 in Ray-based analysis and the inclusion of Germany and UK in cluster 2 in FAO-based analysis. Based on this result, locations with latitudes above 35 degrees (N or S), except in China, were considered to belong to cluster 1 and grow high-yielding maize. The remaining locations were in cluster 2 and grew low-yielding maize. Both clusters consisted of eleven locations. The parameterisation from cluster 1 will be referred to as high-yielding maize and cluster 2 as low-yielding maize in the following.

From the original 17280 setups, 15617 were retained after filtering by the senescence criteria for maize (not performed by cultivar since this filter was applied before clustering), 11525 for winter wheat and 8901 for spring wheat. After constraining by HI, the considered number of setups for the minimisation of yield difference decreased to 7904 for high-yielding maize, 13439 for low-yielding maize, 5435 for winter wheat and 3506 for spring wheat. The minimisation of yield difference then allowed to identify the best and the mean of the ten best setups per cultivar and crop separately by reference dataset (Table 2.2).

High-yielding maize had lower *Nret* and *Cret* values due to the slower retranslocation favouring a more extended photo assimilation period, and C:N parameters that produce higher N concentration; lower $C{:}N_{min}$ and $C{:}N_{range}$. On the other hand, wheat only showed cultivar difference in $C{:}N_{range}$ and *kN* with higher values and *Nret* with lower values for winter wheat. None of the selected setups included stem retranslocation (Sret); SLA and kN did not show a clear pattern between cultivars in both crops. Still, both parameters showed middle to high values related to lower yield and HI values. Similarly, no pattern was found in *Ndred,* but considering the wide range of this parameter, only low values were part of the best setups indicating that slow N demand reduction after anthesis, similar to the original LPJ-GUESS setup, fits better with reference yield. Evidence supports this result since both crops have shown to continue uptaking N after anthesis, depending on the soil N availability. Besides, maize has been reported to absorb more N than wheat to satisfy ear N demand (Mi et al. 2000; Fageria 2014; Zhao et al. 2020).

Global simulations using the best Ray-calibrated setups produced higher values of WMAE for both crops compared to the FAO-calibrated setups indicating a better fit at

both scales. In wheat, the mean of the best ten Ray-calibrated setups at country and gridcell scales showed higher WMAE than the original setup. At the gridcell scale, the best FAO setup behaved better, while at the country scale, the mean of the best ten FAO-calibrated setups had better behaviour. However, the latter setup better fitted HI in both crops and scales (data not shown). Therefore, the mean of the best ten FAO-calibrated setups was selected as the best LPJ-GUESS parameterisation for global simulations in both crops (Table 2.3).

The distribution of the best fifty setups per cultivar and crop using FAO as reference data (Figures 2.5, 2.6, S2-7, S2-8) only showed *Sret = 0* for both crops and cultivars, except winter wheat which had 12 setups with *Sret=1.* This means that yield and HI estimations were better adjusted without labile carbon retranslocation from the stem to grain. The most contrasting parameters between wheat cultivars, similar to the ten best setups mean, were C:N_{range}, *Nret* and *kN.* The best-fitted setups for spring wheat only had C:N_{range} of 2, while winter wheat had different values in 32 setups, showing higher sensitivity to this parameter.

Table 2.2. Selected setups according to reference dataset by crop and cultivar and original setups in LPJ-GUESS. (-Av) represents the setups based on the parameters mean of the ten best setups. Shaded rows represent the selected setup after global evaluation

Crop	Cultivar	Dataset	SLA	C:Nmin	C:Nrange	Nret	Cret	kN	Ndred
Maize	**Clust 1**	**Ray**	45	12.5	2.0	0.3	0.1	0.29	2.7
Maize	**Clust 2**	**Ray**	50	17.5	5.0	0.4	0.4	0.23	2.7
Maize	**Clust 1**	**FAO**	50	12.5	2.0	0.1	0.1	0.29	0.0
Maize	**Clust 2**	**FAO**	50	17.5	5.0	0.4	0.4	0.23	2.7
Maize	**Clust 1**	**Ray-Av**	45	12.5	2.1	0.2	0.2	0.24	2.6
Maize	**Clust 2**	**Ray-Av**	46	17.5	5.0	0.4	0.4	0.24	4.6
Maize	**Clust 1**	**FAO-Av**	50	12.5	2.0	0.2	0.1	0.24	5.8
Maize	**Clust 2**	**FAO-Av**	48	17.5	5.0	0.4	0.4	0.26	2.4
Maize	**Original**	**Original**	**45**	**15**	**5**	**0.1**	**0.1**	**0.27**	**0**
Wheat	**Spring**	**Ray**	40	12.5	2.0	0.4	0.3	0.15	7.4

Wheat	**Winter**	**Ray**	40	12.5	2.8	0.1	0.4	0.25	2.7
Wheat	**Spring**	**FAO**	40	12.5	2.0	0.4	0.2	0.15	0.0
Wheat	**Winter**	**FAO**	40	12.5	2.8	0.1	0.4	0.25	0.0
Wheat	**Spring**	**Ray-Av**	37	12.5	2.0	0.4	0.3	0.18	2.5
Wheat	**Winter**	**Ray-Av**	34	12.5	3.9	0.2	0.3	0.25	1.4
Wheat	**Spring**	**FAO-Av**	40	12.5	2.0	0.4	0.2	0.18	2.6
Wheat	**Winter**	**FAO-Av**	40	12.5	2.5	0.1	0.2	0.25	1.1
Wheat	**Original**	**Original**	**35**	**15**	**5**	**0.1**	**0.1**	**0.27**	**0**

Spring wheat had a more frequent value for *kN* of 0.15, while in winter wheat, it was 0.25, indicating that winter wheat has a more pronounced decrease of N concentration moving from the top to the bottom of the canopy. However, sensitivity to this parameter was low, so it does not affect yield or HI significantly. *Nret* had higher values in spring wheat, causing winter wheat to keep the green tissue for a more extended time, while *Cret* had a similar trend in both cultivars, showing independence between the effect of carbon and N retranslocation rate in LPJ-GUESS. Winter wheat also had low values of *Ndred*, representing slower N demand reduction after anthesis and, again, a more extended green period. This response between cultivars agrees with the reported longer growing period of winter wheat compared to spring wheat (He et al. 2019).

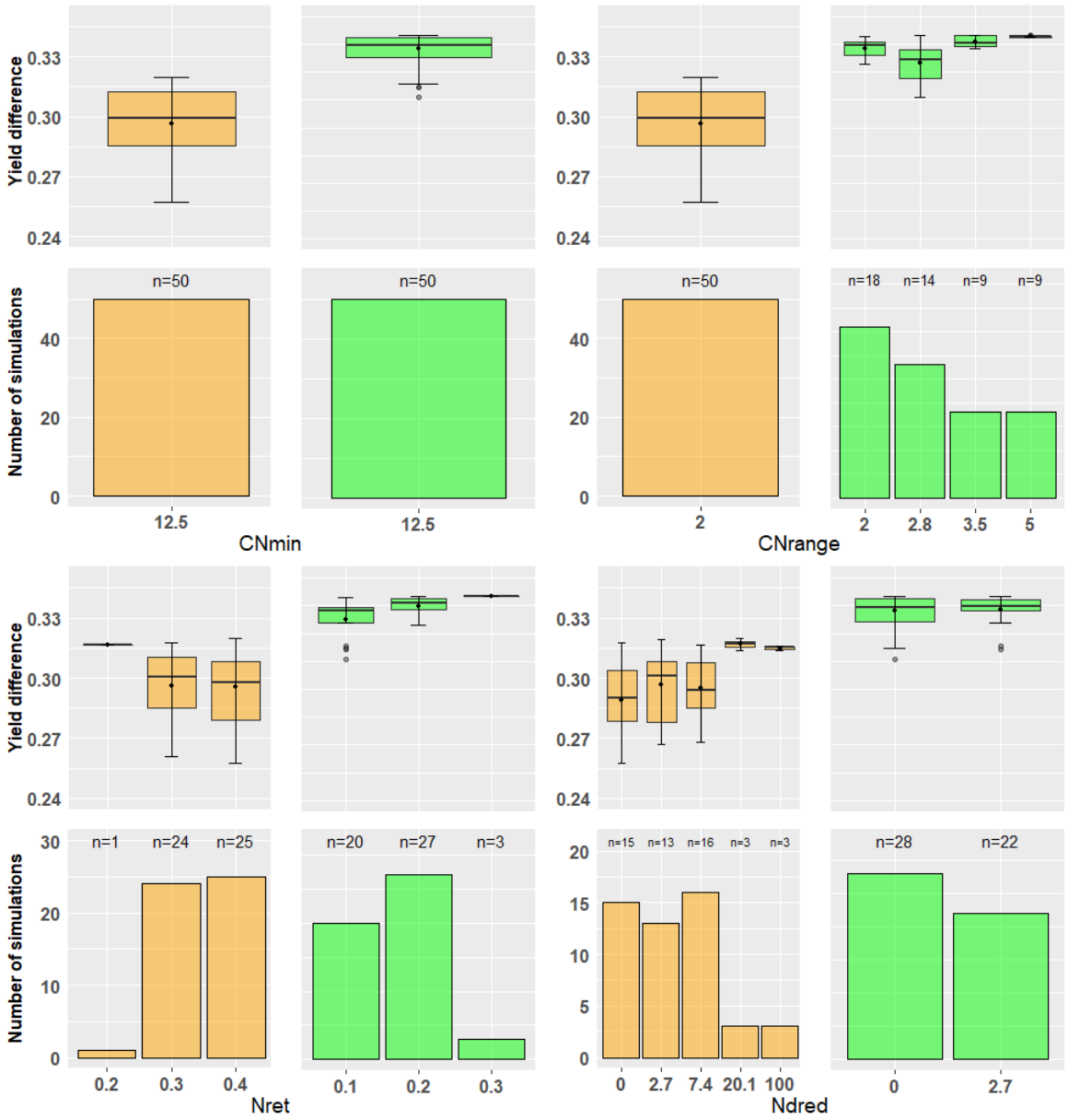

Figure 2.5. Wheat boxplots of the yield difference (FAO - simulated) as a proportion of FAO yield, distribution of the best fifty setups by parameter levels. Orange for spring wheat and green for winter wheat

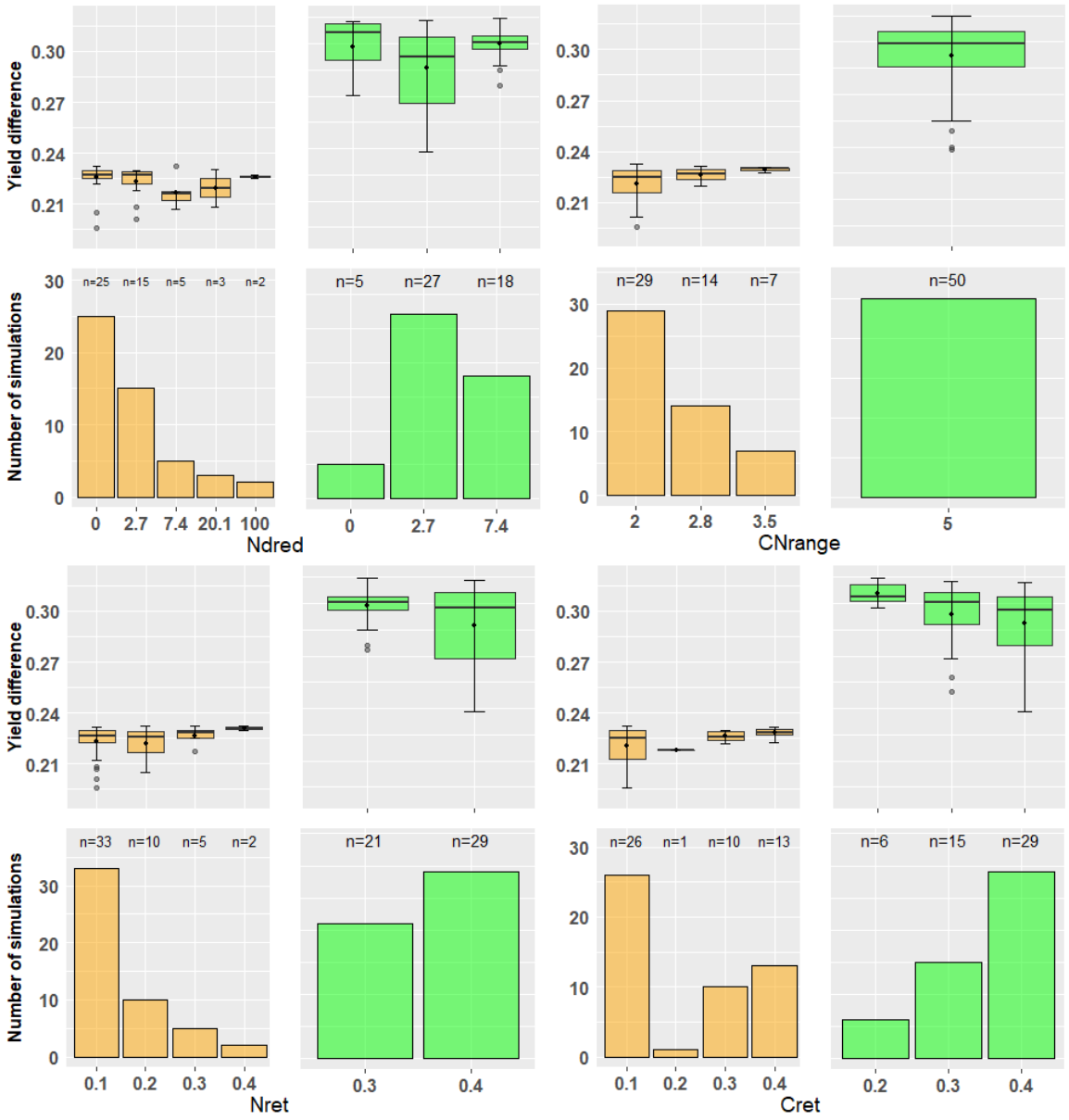

Figure 2.6. Maize boxplots of the yield difference (FAO - simulated) as a proportion of FAO yield, distribution of the best fifty setups by parameter levels. Orange for high-yielding and green for low-yielding maize

The best fifty setups for maize also showed similar responses to the mean of the ten best setups; low-yielding maize only included setups with $C{:}N_{range}$ values of 5 and high values of $C{:}N_{min}$ between 15 and 17.5 while high-yielding maize included $C{:}N_{range}$ values of 3.5, 2.8 and mostly of 2, whilst $C{:}N_{min}$ was always 12.5, indicating that high yielding maize requires lower C:N leaf and consequently higher concentrations of N. *Nret* and *Cret* had lower values for high yielding maize indicating

slower retranslocation of N and carbon to the grains. In high-yielding maize, *Ndred* distribution included the whole parameter range, but the lowest two levels, 0 and 2.7, represented 80% of the best fifty setups. SLA was not a parameter of high sensitivity, but high values of SLA are more frequent in all the best setups of all cultivars in both crops. Accordingly, the final selected setups included SLA values close to 50 for maize and 40 for wheat (Table 2.2; Figures 2.5 and 2.6).

Lower values of SLA (thicker leaves) have been reported to decrease LAI and water stress favouring NPP and harvest index in wheat and other cereals (White et al. 2000; Chen et al. 2020). LPJ-GUESS captures this effect on LAI but not in leaf carbon mass assimilation (Figure S2-5, S2-6), meaning that this parameter does not alter the photosynthetic capacity; this can also be observed in the minor GPP variation caused by SLA (Figure S2-3).

2.4.3. Global evaluation

The mean of the best ten FAO-calibrated setups was selected for global evaluation due to its low WMAE at both scales (Table 2.3). This setup produced aggregated yields by country with satisfactory goodness of fit compared to FAO reported yields averaged between 2001 and 2010 (Figure 2.7). Although there was an underestimation of wheat yield in some countries, the ordinary least squares linear regression line between simulated and observed yields by country was not significantly different to 1:1 line considering intercept and slope (R^2=0.53). In maize, the regression line had a significantly different slope and intercept to the 1:1 line (R^2=0.52), but the 95% confidence intervals of the regressions included most of the

1:1 line for both crops. The first five producers by crop were also well captured, except for Pakistan in wheat (Figure 2.7).

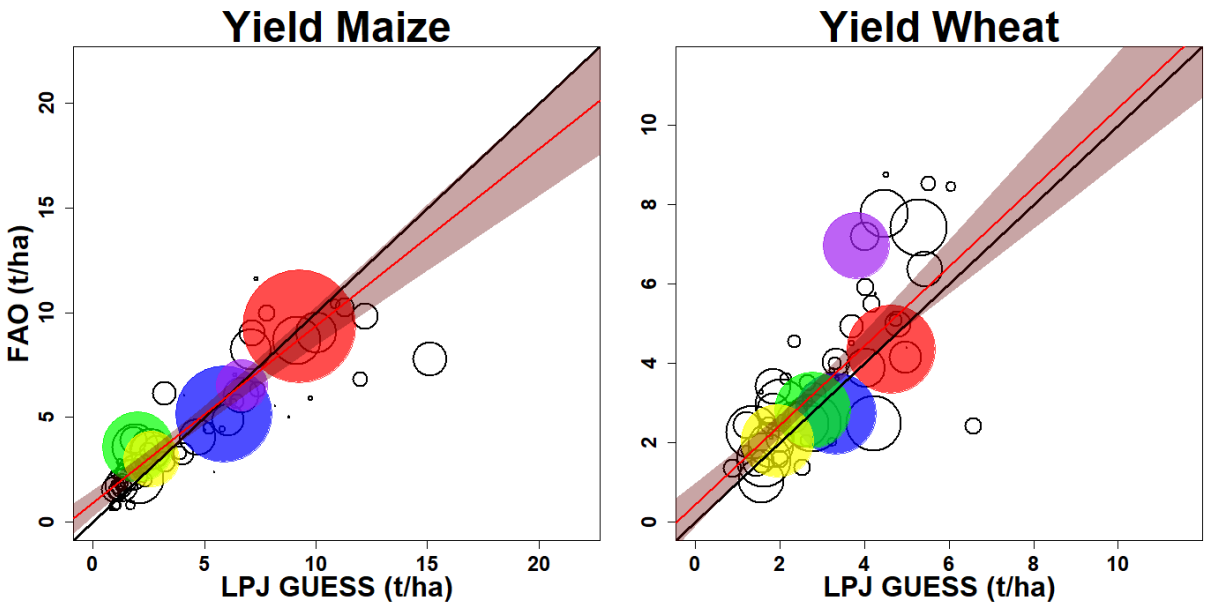

Figure 2.7. By country comparison between simulated yields with LPJ-GUESS and reported by FAO averaged values (2001-2010). Circle size is proportional to production reported by FAO during the same period. Coloured dots show the five top producers in the world. In order (for wheat and maize): Red (China, USA), Blue (India, China), Green (USA, Brazil), Yellow (Russia, Mexico) and Purple (Pakistan, Argentina). Red lines represent the adjusted linear regression between simulated and observed yields. Shaded areas show the 95% confidence interval, and black lines represent the 1:1 line

Global simulations at the gridcell level showed similar patterns to those reported in the Ray dataset, with most productive areas showing differences below 3 t ha^{-1}. The model overestimated maize yield in regions like the southeast of the USA and Argentina. However, there is a clear improvement worldwide in yield estimation compared to the original model setup, which presented a substantial overestimation for almost all the simulated countries (Olin et al. 2015a). The improvement in Africa, Asia, and South America at the gridcell scale is significant (Figure 2.8). Differences between simulated and reference yields are more evident at the gridcell than at the

country scale, suggesting an improvement in the estimation in some areas of those previously poorly simulated countries.

Table 2.3. WMAE of the selected and original setups evaluated globally at gridcell and country scale. (-Av) represents the setups based on the parameters mean of the best ten setups

	Gridcell scale		Country scale	
	Maize	**Wheat**	**Maize**	**Wheat**
Ray	1.47	1.19	0.76	0.89
Ray-Av	1.44	1.74	0.79	1.35
FAO	1.42	1.14	0.66	0.83
FAO-Av	1.43	1.15	0.63	0.8
Original	2.73	1.19	2.55	1.03

In wheat, differences between yield from new and original setups against Ray global gridded yield were similar, and no significant improvement is noticeable. Both setups show underestimation in western and eastern Europe and East and South Asia overestimation. However, the calibration process significantly improved the estimation of HI for both crops. HI was strongly overestimated in the original setup, even showing values above 0.75 in both crops in several locations (Figure 2.9). In contrast, the global distributions of HI had a similar median compared to reference data in the calibrated setup. A more subtle evaluation of HI response will require datasets which show how HI varies systematically as a function of growing conditions. Such responses were not apparent in the compiled HI database.

Additionally, the included low-yielding maize cultivar also showed lower HI than high-yielding maize in the global simulation, with a global mean HI for irrigated maize of 0.33 and 0.53, respectively. Low-yielding maize was distributed in subtropical and tropical countries (Figure S2-9). In wheat, the new cultivar distribution had more winter wheat areas in Argentina, South Africa, Australia and the USA (Jägermeyr et

al. 2021). Winter wheat showed lower HI values than spring wheat, with a global mean HI for irrigated wheat of 0.39 and 0.49, respectively.

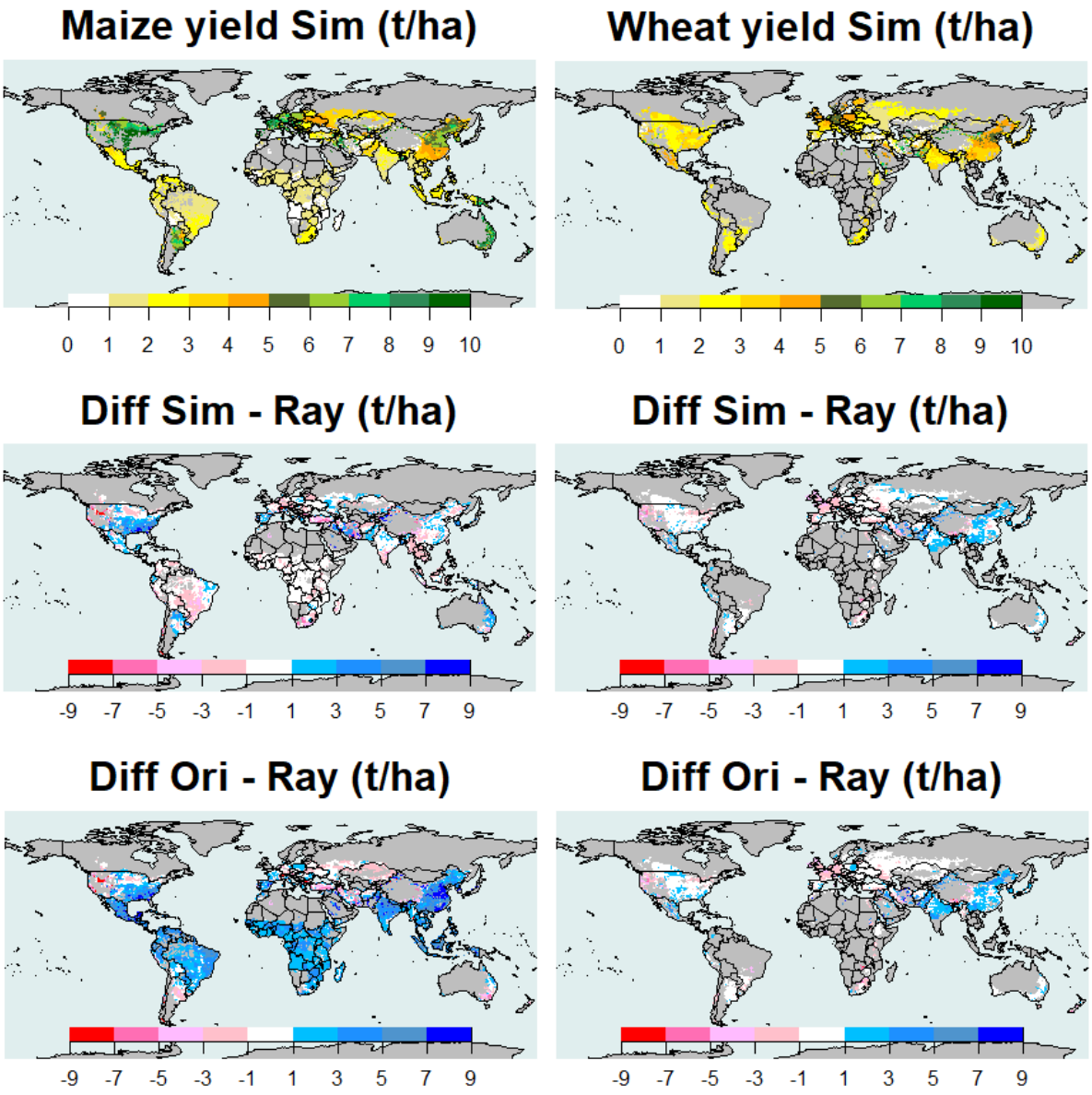

Figure 2.8. Gridded yield simulated with LPJ-GUESS using the selected setup, mean of the parameters from the best ten setups (Top). The yield difference between the selected setup and Ray reported yield (simulated-Ray) (middle), and yield difference between the original setup and Ray reported yield (original-Ray) (bottom) for maize (left) and wheat (right). Average from the decade 2001-2010

Even though the cultivar global distribution improved the representation of crops production in LPJ-GUESS, given the significant influence of some studied parameters here on HI and yield, further observations to constrain them in a variety

of cultivars would be particularly valuable to ensure that calibrated ranges generated in studies such as this one correspond closely to reality and represent genotypic differences such as tolerance to abiotic stresses, growth properties and productivity (Balkovič et al. 2013; Soleymani 2022). In the absence of such observations, especially for carbon assimilation and retranslocation rates, the values attained in the calibration performed in this study may be used as a basis for other large-scale modelling exercises.

Figure 2.9. Boxplot for HI from the compiled database and simulated HI using the original model and the newly selected setup for wheat and maize

The sensitivity and parameterisation performed here improved the estimation of global yield and harvest index of maize and wheat compared to the original setup used in LPJ-GUESS (Olin et al. 2015b), implying an improvement of the representation of crop production processes (Fletcher and Jamieson 2009). The improved version of LPJ-GUESS to simulate major crops growth and yield involves progress in the investigation of growing and management conditions at the regional and global scale (Rosenzweig et al. 2013). This is going to be particularly useful in estimating more accurately the effects of future climate change scenarios on global productivity of food systems, food security, and global economics since agriculture represents between 1 and 60% of national GDP in some countries (Rosenzweig et al. 2013; Mbow et al. 2019).

2.5. CONCLUSIONS

The sensitivity analysis showed that the main parameters affecting simulated carbon assimilation, GPP and yield were those related to N concentration, such as the leaf minimum C:N ratio and C:N ratio range. The carbon reallocation parameters, such as the retranslocation of labile carbon from stem to grain after anthesis and the retranslocation rate of N and carbon during senescence from leaf to grain, were more critical for HI. Although these parameters also affected GPP and yield to a lower extent, they directly influenced the allocation of carbon in grains and vegetative organs, causing high variation in HI. The extent to which labile carbon is retranslocated to grains was the most crucial parameter for HI simulation. It was the only parameter that had the effect of decreasing HI without significantly affecting yield.

The carbon assimilation rate and the period with active photosynthesis were highly affected by the N and carbon retranslocation rate and N demand reduction after anthesis. Lower carbon and N retranslocation rates and lower N uptake demand reduction after anthesis represent a more extended period of productive green tissue and higher assimilation with consequent implications for GPP, yield and HI. Exclusion of the labile carbon retranslocation from stem to grains produced a better fit for yield keeping HI within acceptable limits.

For maize, two cultivars were created according to yield distribution in the selected locations. Maize cultivars were contrasting in C:N ratio parameters as well as N and Carbon retranslocation rates. The high-yielding cultivar of maize had lower values of minimum and range leaf C:N ratio, Carbon and N retranslocation rates compared to low-yielding maize, indicating the need for higher leaf N concentration, a higher capacity for carbon assimilation and a more extended production period. On the other hand, wheat cultivars were only contrasting in the range of leaf C:N and N retranslocation rate, which was lower for winter wheat, indicating a longer productive and green period.

The cultivar parameterisation and global distribution developed in this study improved the global yield and HI estimation compared to the original setup used in LPJ-GUESS. The calibrated version of the LPJ-GUESS crop model forms a basis for studies investigating how changes in management and growing conditions, as well as the future climate change scenarios, affect the global crop growth and yield of maize and wheat.

2.6. REFERENCES

Amanullah, Inamullah (2016) Dry Matter Partitioning and Harvest Index Differ in Rice Genotypes with Variable Rates of Phosphorus and Zinc Nutrition. Rice Sci 23:78–87. https://doi.org/10.1016/j.rsci.2015.09.006

Balkovič J, van der Velde M, Schmid E, et al (2013) Pan-European crop modelling with EPIC: Implementation, up-scaling and regional crop yield validation. Agric Syst 120:61–75. https://doi.org/10.1016/j.agsy.2013.05.008

Belete F, Dechassa N, Molla A, Tana T (2018) Effect of nitrogen fertilizer rates on grain yield and nitrogen uptake and use efficiency of bread wheat (Triticum aestivum L.) varieties on the Vertisols of central highlands of Ethiopia. Agric Food Secur 7:1–12. https://doi.org/10.1186/s40066-018-0231-z

Blanke J, Boke-Olén N, Olin S, et al (2018) Implications of accounting for management intensity on carbon and nitrogen balances of European grasslands. PLoS One 13:. https://doi.org/10.1371/journal.pone.0201058

Bodin P, Olin S, Pugh TAM, Arneth A (2016) Accounting for interannual variability in agricultural intensification: The potential of crop selection in Sub-Saharan Africa. Agric Syst 148:159–168. https://doi.org/10.1016/j.agsy.2016.07.012

Bondeau A, Smith PC, Zaehle S, et al (2007) Modelling the role of agriculture for the 20th century global terrestrial carbon balance. Glob Chang Biol 13:679–706. https://doi.org/10.1111/j.1365-2486.2006.01305.x

Boote KJ, Jones JW, White JW, et al (2013) Putting mechanisms into crop production models. Plant, Cell Environ 36:1658–1672. https://doi.org/10.1111/pce.12119

Chen J, Engbersen N, Stefan L, et al (2020) Diversity increases yield but reduces reproductive effort in crop mixtures. 18:. https://doi.org/10.1101/2020.06.12.149187

Cramer W, Kicklighter DW, Bondeau A, et al (1999) Comparing global models of terrestrial net primary productivity (NPP): overview and key results. Glob Chang Biol 5:1–15

Dai J, Bean B, Brown B, et al (2016) Harvest index and straw yield of five classes of wheat. Biomass and Bioenergy 85:223–227. https://doi.org/10.1016/j.biombioe.2015.12.023

Elliott J, Müller C, Deryng D, et al (2015) The global gridded crop model intercomparison: data and modeling protocols for phase 1 (v1.0). Geosci Model Dev 8:261–277. https://doi.org/10.5194/gmd-8-261-2015

Fageria NK (2014) Nitrogen Harvest Index and Its Association With Crop Yields. J Plant Nutr 37:795–810. https://doi.org/10.1080/01904167.2014.881855

Fletcher AL, Jamieson PD (2009) Causes of variation in the rate of increase of wheat harvest index. F Crop Res 113:268–273. https://doi.org/10.1016/j.fcr.2009.06.002

Food and Agriculture Organization of the United Nations (2020) FAOSTAT. http://www.fao.org/faostat/en. Accessed 3 Apr 2020

Godfray HCJ, Beddington JR, Crute IR, et al (2010) Food security: The challenge of the feeding 9 billion people. Science (80-) 327:812–818. https://doi.org/10.1016/j.geoforum.2018.02.030

Gregersen PL, Culetic A, Boschian L, Krupinska K (2013) Plant senescence and crop productivity. Plant Mol Biol 82:603–622. https://doi.org/10.1007/s11103-013-0013-8

Hassan MJ, Nawab K, Ali A (2007) Response of Specific Leaf Area (SLA), Leaf Area Index (LAI) and Leaf Area Ratio (LAR) of Maize (Zea mays L .) To Plant Density , Rate and Timing of Nitrogen Application. Appl Sci 2:235–243

He D, Fang S, Liang H, et al (2019) Contrasting yield responses of winter and spring wheat to temperature rise in China. Environ Res Lett 15:. https://doi.org/10.1088/1748-9326/abc71a

He P, Zhou W, Jin J (2004) Carbon and Nitrogen Metabolism Related to Grain Formation in Two Different Senescent Types of Maize. J Plant Nutr 27:295–311. https://doi.org/10.1081/PLN-120027655

Hikosaka K, Anten NPR, Borjigidai A, et al (2016) A meta-analysis of leaf nitrogen distribution within plant canopies. Ann Bot 118:239–247. https://doi.org/10.1093/aob/mcw099

Iizumi T, Yokozawa M, Sakurai G, et al (2014) Historical changes in global yields: Major cereal and legume crops from 1982 to 2006. Glob Ecol Biogeogr 23:346–357. https://doi.org/10.1111/geb.12120

Jägermeyr J, Müller C, Ruane A, et al (2021) Climate change signal in global agriculture emerges earlier in new generation of climate and crop models. Nat Food 2:873–885. https://doi.org/https://doi.org/10.1038/s43016-021-00400-y.

Kiniry JR, Tischler CR, Rosenthal WD, Gerik TJ (1992) Nonstructural Carbohydrate Utilization by Sorghum and Maize Shaded during Grain Growth. Crop Sci 32:131–137. https://doi.org/10.2135/cropsci1992.0011183x003200010029x

Kipp S, Mistele B, Schmidhalter U (2014) Identification of stay-green and early senescence phenotypes in high-yielding winter wheat, and their relationship to grain yield and grain protein concentration using high-throughput phenotyping techniques. Funct Plant Biol 41:227–235. https://doi.org/10.1071/FP13221

Lamarque JF, Bond TC, Eyring V, et al (2010) Historical (1850-2000) gridded anthropogenic and biomass burning emissions of reactive gases and aerosols: Methodology and application. Atmos Chem Phys 10:7017–7039. https://doi.org/10.5194/acp-10-7017-2010

Liang XG, Gao Z, Zhang L, et al (2019) Seasonal and diurnal patterns of non-structural carbohydrates in source and sink tissues in field maize. BMC Plant Biol 19:1–11. https://doi.org/10.1186/s12870-019-2068-4

Lindeskog M, Arneth A, Bondeau A, et al (2013) Implications of accounting for land use in simulations of ecosystem carbon cycling in Africa. Earth Syst Dyn 4:385–407. https://doi.org/10.5194/esd-4-385-2013

Liu W, Hou P, Liu G, et al (2020) Contribution of total dry matter and harvest index to maize grain yield—A multisource data analysis. Food Energy Secur 9:1–12. https://doi.org/10.1002/fes3.256

Lorenz AJ, Gustafson TJ, Coors JG, de Leon N (2010) Breeding maize for a bioeconomy: A literature survey examining harvest index and stover yield and their relationship to grain yield. Crop Sci 50:1–12. https://doi.org/10.2135/cropsci2009.02.0086

Mbow C, Rosenzweig C, Barioni L, et al (2019) Food Security. In: Shukla PR, Skea J, Buendia EC, et al. (eds) Climate Change and Land: an IPCC special report on climate change, desertification, land degradation, sustainable land management, food security, and greenhouse gas fluxes in terrestrial ecosystems. pp 437–550

Mi G, Tang L, Zhang F, Zhang J (2000) Is nitrogen uptake after anthesis in wheat regulated by sink size? F Crop Res 68:183–190. https://doi.org/10.1016/S0378-4290(00)00119-2

Mohammadi GR (2007) Growth parameters enhancing the competitive ability of corn (Zea mays L.) against weeds. Weed Biol Manag 7:232–236. https://doi.org/10.1111/j.1445-6664.2007.00261.x

Monfreda C, Ramankutty N, Foley JA (2008) Farming the planet: 2. Geographic distribution of crop areas, yields, physiological types, and net primary production in the year 2000. Global Biogeochem Cycles 22:1–19. https://doi.org/10.1029/2007GB002947

Müller C, Elliott J, Chryssanthacopoulos J, et al (2017) Global gridded crop model evaluation: benchmarking , skills , deficiencies and implications. Geosci Model Dev 10:1403–1422. https://doi.org/10.5194/gmd-10-1403-2017

Müller C, Elliott J, Kelly D, et al (2019) The Global Gridded Crop Model Intercomparison phase 1 simulation dataset. Sci Data 6:1–22. https://doi.org/10.1038/s41597-019-0023-8

Nazir MF, Sarfraz Z, Mangi N, et al (2021) Post-anthesis mobilization of stem assimilates in wheat under induced stress. Sustain 13:1–10. https://doi.org/10.3390/su13115940

Olin S, Lindeskog M, Pugh TAM, et al (2015a) Soil carbon management in large-scale earth system modelling : implications for crop yields and nitrogen. Earth Syst Dyn 6:745–768. https://doi.org/10.5194/esd-6-745-2015

Olin S, Schurgers G, Lindeskog M, et al (2015b) Modelling the response of yields and tissue C : N to changes in atmospheric CO2 and N management in the main wheat regions of western Europe. Biogeosciences 12:2489–2515. https://doi.org/10.5194/bg-12-2489-2015

Ortiz-Bobea A, Ault TR, Carrillo CM, et al (2021) Anthropogenic climate change has slowed global agricultural productivity growth. Nat Clim Chang 11:306–312. https://doi.org/10.1038/s41558-021-01000-1

Penning de Vries F, Jansen D, ten Berge H, Bakema A (1989) Simulation of ecophysiological process of growth in several annual crops, 1st edn. Pudoc Wageningen, Wageningen

Porker K, Straight M, Hunt JR (2020) Evaluation of G × E × M Interactions to Increase Harvest Index and Yield of Early Sown Wheat. Front Plant Sci 11:1–14. https://doi.org/10.3389/fpls.2020.00994

Prentice IC, Webb RS, Ter-Mikhaelian MT, et al (1989) Developing A Global Vegetation Dynamics Model: Results of an IIASA Summer Workshop. Novographic, Laxenburg, Austria

Qin XL, Weiner J, Qi L, et al (2013) Allometric analysis of the effects of density on reproductive allocation and Harvest Index in 6 varieties of wheat (Triticum). F Crop Res 144:162–166. https://doi.org/10.1016/j.fcr.2012.12.011

Ray DK, West PC, Clark M, et al (2019) Climate change has likely already affected global food production. PLoS One 14:1–18. https://doi.org/10.1371/journal.pone.0217148

Reich P, Walters M, Ellsworth D (1992) Leaf Life-Span in Relation to Leaf , Plant , and Stand Characteristics among Diverse Ecosystems. Ecol Monogr 62:365–392

Ringeval B, Müller C, Pugh TAM, et al (2021) Potential yield simulated by global gridded crop models: Using a process-based emulator to explain their differences. Geosci Model Dev 14:1639–1656. https://doi.org/10.5194/gmd-14-1639-2021

Rosenzweig C, Jones JW, Hatfield JL, et al (2013) The Agricultural Model Intercomparison and Improvement Project (AgMIP): Protocols and pilot studies. Agric For Meteorol 170:166–182. https://doi.org/10.1016/j.agrformet.2012.09.011

Ruane AC, Goldberg R, Chryssanthacopoulos J (2015) Climate forcing datasets for agricultural modeling: Merged products for gap-filling and historical climate series estimation. Agric For Meteorol 200:233–248. https://doi.org/10.1016/j.agrformet.2014.09.016

Shamim Reza M (2015) Study of Multivariate Data Clustering Based on K-Means and Independent Component Analysis. Am J Theor Appl Stat 4:317. https://doi.org/10.11648/j.ajtas.20150405.11

Sinclair TR (1998) Historical changes in harvest index and crop nitrogen accumulation. Crop Sci 38:638–643. https://doi.org/10.2135/cropsci1998.0011183X003800030002x

Sitch S, Smith B, Prentice IC, et al (2003) Evaluation of ecosystem dynamics, plant geography and terrestrial carbon cycling in the LPJ dynamic global vegetation model. Glob Chang Biol 9:161–185. https://doi.org/10.1046/j.1365-2486.2003.00569.x

Smith B, Prentice IC, Climate MTS (2001) Representation of vegetation dynamics in the modelling of terrestrial ecosystems : comparing two contrasting approaches within European climate space. Glob Ecol Biogepgraphy 10:621–637

Smith B, Wårlind D, Arneth A, et al (2014) Implications of incorporating N cycling and N limitations on primary production in an individual-based dynamic vegetation model. Biogeosciences 11:2027–2054. https://doi.org/10.5194/bg-11-2027-2014

Soleymani A (2022) Modeling the water requirement of wheat and safflower using the ET-HS model. Model Earth Syst Environ. https://doi.org/10.1007/s40808-022-01370-1

Tang Z, Xu W, Zhou G, et al (2018) Patterns of plant carbon, nitrogen, and phosphorus concentration in relation to productivity in China's terrestrial ecosystems. Proc Natl Acad Sci U S A 115:E6095–E6096. https://doi.org/10.1073/pnas.1808126115

United Nations (2019) World population prospects 2019, Online Edi

Vermeulen SJ, Aggarwal PK, Ainslie A, et al (2012) Options for support to agriculture and food security under climate change. Environ Sci Policy 15:136–144. https://doi.org/10.1016/j.envsci.2011.09.003

Wample R, Bary A, Burr T (1991) Heat tolerance of dormant Vitis vinifera cuttings. Am J Enol Vitic 42:67–72

White MA, Thornton PE, Running SW, Nemani RR (2000) Parameterization and Sensitivity Analysis of the BIOME–BGC Terrestrial Ecosystem Model: Net Primary Production Controls. Earth Interact 4:1–85. https://doi.org/10.1175/1087-3562(2000)004<0003:pasaot>2.0.co;2

Xue Q, Rudd JC, Liu S, et al (2014) Yield determination and water-use efficiency of wheat under water-limited conditions in the U.S. Southern High Plains. Crop Sci 54:34–47. https://doi.org/10.2135/cropsci2013.02.0108

Yin X, Lantinga EA, Schapendonk AHCM, Zhong X (2003) Some quantitative relationships between leaf area index and canopy nitrogen content and distribution. Ann Bot 91:893–903. https://doi.org/10.1093/aob/mcg096

Yin X, Schapendonk AHCM, Kropff MJ, et al (2000) A generic equation for nitrogen-limited leaf area index and its application in crop growth models for predicting leaf senescence. Ann Bot 85:579–585. https://doi.org/10.1006/anbo.1999.1104

You L, Wood S, Wood-Sichra U, Wu W (2014) Generating global crop distribution maps: From census to grid. Agric Syst 127:53–60. https://doi.org/10.1016/j.agsy.2014.01.002

Zhao B, Niu X, Ata-Ul-Karim ST, et al (2020) Determination of the post-anthesis nitrogen status using ear critical nitrogen dilution curve and its implications for nitrogen management in maize and wheat. Eur J Agron 113:125967. https://doi.org/10.1016/j.eja.2019.125967

2.7. SUPPLEMENTARY MATERIAL

2.7.1. S2-1 Literature for HI compilation database

S2-1.1 Wheat Literature

Barraclough PB, Howarth JR, Jones J, et al (2010) Nitrogen efficiency of wheat: Genotypic and environmental variation and prospects for improvement. Eur J Agron 33:1–11. https://doi.org/10.1016/j.eja.2010.01.005

Barriga P (1974) Indice de Cosecha en Trigo de primavera. Agro Sur 2:17–20

Bolaños A, Britto R (1991) Heredabilldad del índice de cosecha en trigo (Triticum aestivum L.) y su relación con tres componentes de rendimiento. Agron Colomb 8:268–279

Bredemeier C, Mundstock C (2001) SEÇÃO IV - FERTILIDADE DO SOLO E NUTRIÇÃO DE PLANTAS. Rev Bras Cienc do solo 25:

Broberg MC, Feng Z, Xin Y, Pleijel H (2015) Ozone effects on wheat grain quality - A summary. Environ Pollut 197:203–213. https://doi.org/10.1016/j.envpol.2014.12.009

Carranza-Gallego G, Guzmán GI, Soto D, et al (2018) Modern wheat varieties as a driver of the degradation of Spanish rainfed mediterranean agroecosystems throughout the 20th century. Sustain 10:. https://doi.org/10.3390/su10103724

Castañeda-saucedo MC, López-castañeda C, León TBC, et al (2009) Rendimiento y calidad de la semilla de cebada y trigo en campo e invernadero. Interciencia 24:

Dai J, Bean B, Brown B, et al (2016) Harvest index and straw yield of five classes of wheat. Biomass and Bioenergy 85:223–227. https://doi.org/10.1016/j.biombioe.2015.12.023

Fan J, McConkey B, Janzen H, et al (2017) Harvest index–yield relationship for estimating crop residue in cold continental climates. F Crop Res 204:153–157. https://doi.org/10.1016/j.fcr.2017.01.014

Fangmeier A, Grüters U, Hertstein U, et al (1996) Effects of elevated CO2, nitrogen supply and tropospheric ozone on spring wheat. I. Growth and yield. Environ Pollut 91:381–390. https://doi.org/10.1016/0269-7491(95)00042-9

Fitzgerald GJ, Tausz M, O'Leary G, et al (2016) Elevated atmospheric [CO2] can dramatically increase wheat yields in semi-arid environments and buffer against heat waves. Glob Chang Biol 22:2269–2284. https://doi.org/10.1111/gcb.13263

Flintham JE, Börner A, Worland AJ, Gale MD (1997) Optimizing wheat grain yield: Effects of Rht (gibberellin-insensitive) dwarfing genes. J Agric Sci 128:11–25. https://doi.org/10.1017/S0021859696003942

Guarda G, Padovan S, Delogu G (2004) Grain yield, nitrogen-use efficiency and baking quality of old and modern Italian bread-wheat cultivars grown at different nitrogen levels. Eur J Agron 21:181–192. https://doi.org/10.1016/j.eja.2003.08.001

Hakala K (1998) Growth and yield potential of spring wheat in a simulated changed climate with increased CO2 and higher temperature. Eur J Agron 9:41–52. https://doi.org/10.1016/S1161-0301(98)00025-2

Högy P, Wieser H, Köhler P, et al (2009) Effects of elevated CO2 on grain yield and quality of wheat: Results from a 3-year free-air CO2 enrichment experiment. Plant Biol 11:60–69. https://doi.org/10.1111/j.1438-8677.2009.00230.x

Kemanian AR, Stöckle CO, Huggins DR, Viega LM (2007) A simple method to estimate harvest index in grain crops. F Crop Res 103:208–216. https://doi.org/10.1016/j.fcr.2007.06.007

Kobata T, Koç M, Barutçular C, et al (2018) Harvest index is a critical factor influencing the grain yield of diverse wheat species under rain-fed conditions in the Mediterranean zone of southeastern Turkey and northern Syria. Plant Prod Sci 21:71–82. https://doi.org/10.1080/1343943X.2018.1445534

Le Gouis J, Béghin D, Heumez E, Pluchard P (2000) Genetic differences for nitrogen uptake and nitrogen utilisation efficiencies in winter wheat. Eur J Agron 12:163–173. https://doi.org/10.1016/S1161-0301(00)00045-9

Mellado M (1997) Rendimiento de Grano y Paja e Indice de Cosecha de Trigos Hermanos (triticum aestivum L.) de Diferente Altura. Agric Tec 57:96–101

Mishra AK, Rai R, Agrawal SB (2013) Differential response of dwarf and tall tropical wheat cultivars to elevated ozone with and without carbon dioxide enrichment: Growth, yield and grain quality. F Crop Res 145:21–32. https://doi.org/10.1016/j.fcr.2013.02.007

Moreira MA, Angulo Filho R, Rudorff BFT (1999) Eficiência do uso da radiação e índice de colheita em trigo submetido a estresse hídrico em diferentes estádios de

desenvolvimento. Sci Agric 56:597–603. https://doi.org/10.1590/s0103-90161999000300012

Nedel J (1994) Progresso Genético no Rendimiento de Gráos de Cultivares de Trigo Lançadas para Cultivo Entre 1940 e 1992. Pesqui Agropecu Bras 29:1565–1570

Onyibe JE (2005) Effect of irrigation regime on growth and development of two wheat cultivars (Triticum aestivum L.) in the Nigerian Savanna. J Agric Rural Dev Trop Subtrop 106:177–192

Pleijel H, Gelang J, Sild E, et al (2000) Effects of elevated carbon dioxide, ozone and water availability on spring wheat growth and yield. Physiol Plant 108:61–70. https://doi.org/10.1034/j.1399-3054.2000.108001061.x

Qin XL, Weiner J, Qi L, et al (2013) Allometric analysis of the effects of density on reproductive allocation and Harvest Index in 6 varieties of wheat (Triticum). F Crop Res 144:162–166. https://doi.org/10.1016/j.fcr.2012.12.011

Reynolds MP, Pask AJD, Hoppitt WJE, et al (2017) Strategic crossing of biomass and harvest index—source and sink—achieves genetic gains in wheat. Euphytica 213:. https://doi.org/10.1007/s10681-017-2040-z

Roldán VC (2016) Respuesta del rendimiento en cultivares de trigo de diferente largo de ciclo a través de dos fechas de siembra en el ambiente semiárido bajo riego en Santiago del Estero

Sanchez-Garcia M, Royo C, Aparicio N, et al (2013) Genetic improvement of bread wheat yield and associated traits in Spain during the 20th century. J Agric Sci 151:105–118. https://doi.org/10.1017/S0021859612000330

Tessema T, Tanner D (1997) GRASS WEED COMPETITION AND CALCULATED ECONOMIC THRESHOLD DENSITIES IN BREAD WHEAT IN ETHIOPIA. African Crop Sci J 5:

Van Oijen M, Schapendonk AHCM, Jansen MJH, et al (1999) Do open-top chambers overestimate the effects of rising CO2 on plants? An analysis using spring wheat. Glob Chang Biol 5:411–421. https://doi.org/10.1046/j.1365-2486.1999.00233.x

Walter J, Edwards J, McDonald G, Kuchel H (2018) Photogrammetry for the estimation of wheat biomass and harvest index. F Crop Res 216:165–174. https://doi.org/10.1016/j.fcr.2017.11.024

Wang JY, Mo F, Nguluu SN, et al (2016) Exploring micro-field water-harvesting farming system in dryland wheat (Triticum aestivum L.): An innovative management for semiarid Kenya. F Crop Res 196:207–218. https://doi.org/10.1016/j.fcr.2016.07.001

Weigel HJ, Manderscheid R (2012) Crop growth responses to free air CO 2 enrichment and nitrogen fertilization: Rotating barley, ryegrass, sugar beet and wheat. Eur J Agron 43:97–107. https://doi.org/10.1016/j.eja.2012.05.011

Wnuk A, Górny AG, Bocianowski J, Kozak M (2013) Visualizing harvest index in crops. Commun Biometry Crop Sci 8:48–59

Zhang B, Li FM, Huang G, et al (2006) Yield performance of spring wheat improved by regulated deficit irrigation in an arid area. Agric Water Manag 79:28–42. https://doi.org/10.1016/j.agwat.2005.02.007

Zhang G, Sakai H, Usui Y, et al (2015) Grain growth of different rice cultivars under elevated CO2 concentrations affects yield and quality. F Crop Res 179:72–80. https://doi.org/10.1016/j.fcr.2015.04.006

Zhang H, Turner NC, Poole ML (2012) Increasing the harvest index of wheat in the high rainfall zones of southern Australia. F Crop Res 129:111–123. https://doi.org/10.1016/j.fcr.2012.02.002

S2-1.2 Maize Literature

Abebe A, Pathak H, Singh SD, et al (2016) Growth, yield and quality of maize with elevated atmospheric carbon dioxide and temperature in north-west India. Agric Ecosyst Environ 218:66–72. https://doi.org/10.1016/j.agee.2015.11.014

Aderibigbe S, Sakariyawo O, Kasali A (2017) Performance of Maize (Zea mays) Cultivars as Influenced by Grade and Aplication Rate of Organo-Mineral Fertiliser in a Transitory Rain Forest. Agrosearch 17:78–98

Akinnuoye-Adelabu DB, Modi AT (2017) Planting Dates and Harvesting Stages Influence on Maize Yield under Rain-Fed Conditions. J Agric Sci 9:43. https://doi.org/10.5539/jas.v9n9p43

Al-Naggar AMM, Shabana RA, Atta MMM, Al-Khalil TH (2015) Maize response to elevated plant density combined with lowered N-fertilizer rate is genotype-dependent. Crop J 3:96–109. https://doi.org/10.1016/j.cj.2015.01.002

Ali S, Inamullah, Arif M, et al (2019) Maize productivity as influenced by potassium under reduced irrigation regimes. Sarhad J Agric 35:171–181. https://doi.org/10.17582/journal.sja/2019/35.1.171.181

Amanullah, Inamullah (2016) Dry Matter Partitioning and Harvest Index Differ in Rice Genotypes with Variable Rates of Phosphorus and Zinc Nutrition. Rice Sci 23:78–87. https://doi.org/10.1016/j.rsci.2015.09.006

Anjum SA, Raza MM, Ullah S, et al (2019) Influence of Different Tillage Practices on Yield of Autumn Planted Maize (Zea mays L.). Pakistan J Agric Res 32:. https://doi.org/10.17582/journal.pjar/2019/32.2.293.301

Avila RG, MAGALHÃES PC, DE ALVARENGA AA, et al (2017) Drought-Tolerant Maize Genotypes Invest in Root System and Maintain High Harvest Index During Water Stress. Rev Bras Milho e Sorgo 15:450. https://doi.org/10.18512/rbms.v15i3.842

Bänziger M, Edmeades GO, Lafitte HR (1999) Selection for drought tolerance increases maize yields across a range of nitrogen levels. Crop Sci 39:1035–1040. https://doi.org/10.2135/cropsci1999.0011183X003900040012x

Bocianowski J, Nowosad K, Szulc P (2019) Soil tillage methods by years interaction for harvest index of maize (Zea mays L.) using additive main effects and multiplicative interaction model. Acta Agric Scand Sect B Soil Plant Sci 69:75–81. https://doi.org/10.1080/09064710.2018.1502343

Burzaco JP, Ciampitti IA, Vyn TJ (2014) Nitrapyrin impacts on maize yield and nitrogen use efficiency with spring-applied nitrogen: Field studies vs. meta-analysis comparison. Agron J 106:753–760. https://doi.org/10.2134/agronj2013.0043

Claverie M, Demarez V, Duchemin B, et al (2012) Maize and sunflower biomass estimation in southwest France using high spatial and temporal resolution remote sensing data. Remote Sens Environ 124:844–857. https://doi.org/10.1016/j.rse.2012.04.005

Cox WJ, Cherney JH (2018) Agronomic Comparisons of Conventional and Organic Maize during the Transition to an Organic Cropping System. Agronomy 8:. https://doi.org/10.3390/agronomy8070113

Dale AE, Drennan DSH (1997) Transplanted maize (Zea mays) for grain production in southern England. I. Effects of planting date, transplant age at planting and cultivar on grain yield. J Agric Sci 128:27–35. https://doi.org/10.1017/S0021859696003875

Di Matteo JA, Ferreyra JM, Cerrudo AA, et al (2016) Yield potential and yield stability of Argentine maize hybrids over 45 years of breeding. F Crop Res 197:107–116. https://doi.org/10.1016/j.fcr.2016.07.023

Durães FOM, Magalhães PC, Oliveira AC (2002) Índice de Colheita Genético e as Possibilidades da Genética Fisiológica para Melhoramento do Rendimento de Milho. Rev Bras Milho e Sorgo 1:33–40. https://doi.org/10.18512/1980-6477/rbms.v1n1p33-40

Echarte L, Andrade FH (2003) Harvest index stability of Argentinean maize hybrids released between 1965 and 1993. F Crop Res 82:1–12. https://doi.org/10.1016/S0378-4290(02)00232-0

Farhad W, Saleem MF, Cheema MA, Hammad HM (2009) Effect of poultry manure levels on the productivity of spring maize (Zea mays L.). J Anim Plant Sci 19:122–

125

Farré I, Faci JM (2006) Comparative response of maize (Zea mays L.) and sorghum (Sorghum bicolor L. Moench) to deficit irrigation in a Mediterranean environment. Agric Water Manag 83:135–143. https://doi.org/10.1016/j.agwat.2005.11.001

Fenalce (1974) Aspectos Tecnicos de la Produccion de Maiz en Colombia. 15–22

Ferreira VM, Magalhães PC, Ozanam F, Durães M (2000) PRODUTIVIDADE DE GENÓTIPOS DE MILHO (Zea mays L .) SOB MANEJO DIFERENCIADO DE IRRIGAÇÃO E ADUBAÇÃO 1 PRODUCTIVITY OF MAIZE (Zea Mays L .) GENOTYPES UNDER DIFFERENT IRRIGATION MANAGEMENT AND FERTILIZATION SYSTEMS

Gondwe B, Mweetwa A, Munyinda K, et al (214AD) EVALUATION OF MAIZE (Zea mays L) GENOTYPES FOR NITROGEN USE EFFICIENCY By. Zambian J Agric Sci 10:. https://doi.org/10.1038/132817a0

Hay RKM, Gilbert RA (2001) Variation in the harvest index of tropical maize: Evaluation of recent evidence from Mexico and Malawi. Ann Appl Biol 138:103–109. https://doi.org/10.1111/j.1744-7348.2001.tb00090.x

Hütsch BW, Schubert S (2018) Maize harvest index and water use efficiency can be improved by inhibition of gibberellin biosynthesis. J Agron Crop Sci 204:209–218. https://doi.org/10.1111/jac.12250

Ion V, Dicu G, Dumbravă M, et al (2015) Harvest index at maize in different growing conditions. Rom Biotechnol Lett 20:10951–10960

Javeed HMR, Zamir MSI, Nadeem M, et al (2014) Response of maize phenology and harvest index to tillage and poultry manure. Pakistan J Agric Sci 51:633–638

Khan S, Khan A, Jalal F, et al (2017) Dry Matter Partitioning and Harvest Index of Maize Crop as Influenced by Integration of Sheep Manure and Urea Fertilizer. Adv Crop Sci Technol 05: https://doi.org/10.4172/2329-8863.1000276

Larramendi R, Hernández G, Cruz O, et al (2016) CRECIMIENTO E ÍNDICE DE COSECHA DE VARIEDADES LOCALES DE MAÍZ (Zea mays L.) EN

COMUNIDADES DE LA REGIÓN FRAILESCA DE CHIAPAS, MÉXICO. Cultiv Trop 37:137–145. https://doi.org/10.13140/RG.2.1.1404.6967

Mohammed Toungos BD, Njodi M, Babayola A, Kashim H (2019) MULTILOCATIONAL TRIAL ON SAMMAZ MAIZE (Zea mays L) VARIETY ON YIELD PERFORMANCE IN THE NORTHERN GUINEA SAVANNAH ZONE, NIGERIA

Moosavi S, Mirhadi J, Khanghah A, et al (2013) Study the Effects of Kadostim Organic Fertilizer on Yield and Harvest Index Maize Cultivars in Ardabil Study the Effects of Kadostim Organic Fertilizer on Yield and Harvest Index Maize Cultivars in Ardabil. Int J Basic Sci Appl Res 2:

Nikju MB, Mobasser HR, Ganjali HR (2015) Influence of variety on biological yield, harvest index, percent of protein in Zea mays. Biol Forum 7:662–667

Noah O (2019) Fertilization of Maize and Its Impact on Yield Component of Harvest Index

Pagani A, Echeverría HE, Andrade FH, Sainz Rozas HR (2012) Effects of nitrogen and sulfur application on grain yield, nutrient accumulation, and harvest indexes in maize. J Plant Nutr 35:1080–1097. https://doi.org/10.1080/01904167.2012.671410

Pennington D (2013) Harvest Index: A predictor of corn stover yield. file:///C:/Users/hac809/Desktop/Hector/PhD/Project/Papers/HI/Maize/Pennington, 2013.html

Sabagh A El, Barutçular C, Saneoka H (2015) Assessment of Drought Tolerance Maize Hybrids at Grain Growth Stage in Mediterranean Area. 9:967–970

Tadesse A (2015) Yield Related Traits and Yield of Quality Protein Maize (Zea mays L .) affected by Nitrogen Levels to achieve maximum yield in the Central Rift Valley of Ethiopia. 5:139–148

Thapa SB, Shrestha P, Sah SK, et al (2019) Effect of different genotypes, tillage methods and plant populations on dry matter, grain yield, stover yield and harvest index of hybrid maize. Int J Glob Sci Res 6:. https://doi.org/10.26540/ijgsr.v6.i1.2019.132

Tittonell P, Vanlauwe B, Leffelaar PA, Giller KE (2005) Estimating yields of tropical maize genotypes from non-destructive, on-farm plant morphological measurements. Agric Ecosyst Environ 105:213–220. https://doi.org/10.1016/j.agee.2004.04.002

Tolk JA, Howell TA, Evett SR (1999) Effect of mulch, irrigation, and soil type on water use and yield of maize. Soil Tillage Res 50:137–147. https://doi.org/10.1016/S0167-1987(99)00011-2

Tollenaar M, Deen W, Echarte L, Liu W (2006) Effect of crowding stress on dry matter accumulation and harvest index in maize. Agron J 98:930–937. https://doi.org/10.2134/agronj2005.0336

Trachsel S, San Vicente FM, Suarez EA, et al (2016) Effects of planting density and nitrogen fertilization level on grain yield and harvest index in seven modern tropical maize hybrids (Zea mays L.). J Agric Sci 154:689–704. https://doi.org/10.1017/S0021859615000696

Wasaya A, Tahir M, Tanveer A, Yaseen M (2012) Response of maize to tillage and nitrogen management. J Anim Plant Sci 22:452–456

Zamudio-gonzález B, Tadeo-robledo M, Espinosa-calderón A, et al (2016) Índice de cosecha con macro-nutrimentos en grano de maíz * Harvest index with macro-nutrients in corn grain Resumen Introducción. 7:1077–1089

2.7.2. Additional results

Table S2-1. Maize location coordinates and reported yields and clustering according to Ray (Ray et al. 2019) and FAO (Food and Agriculture Organization of the United Nations 2020) in kg ha^{-1}. The percentage of variation takes Yield-FAO as the reference. Ray, FAO based and final clustering

Long.	Lat.	Country	Yield-Ray	Yield-FAO	Var (%)	Clus-Ray	Clus-FAO	Clus-final
-58.30	-37.75	***Argentina***	5.42	6.52	-16.8	1	1	1
-44.25	-19.13	***Brazil***	3.32	3.59	-7.6	2	2	2
108.07	34.28	***China***	5.56	5.16	7.8	1	2	2
126.79	43.15	***China***	7.97	5.16	54.5	1	2	2
126.63	47.43	***China***	6.68	5.16	29.5	1	2	2
1.17	43.45	***France***	8.24	8.69	-5.1	1	1	1
8.68	50.58	***Germany***	7.11	9.00	-21.0	1	2	1
12.63	9.23	***Guinea***	1.10	1.72	-35.9	2	2	2
3.12	10.05	***Guinea***	1.17	1.20	-2.0	2	2	2
77.20	28.62	***India***	1.20	2.08	-42.4	2	2	2
-99.12	18.67	***Mexico***	2.69	2.98	-9.7	2	2	2
-97.63	20.45	***Mexico***	1.53	2.98	-48.6	2	2	2
71.58	34.02	***Pakistan***	2.27	2.86	-20.5	2	2	2
30.27	-29.62	***South Africa***	4.36	3.50	24.7	2	2	2
-0.82	41.72	***Spain***	10.80	9.82	9.9	1	1	1
-0.91	51.47	***UK***	8.62	7.00	23.2	1	2	1
-86.99	40.47	***USA***	10.57	9.34	13.1	1	1	1
-85.53	42.25	***USA***	8.41	9.34	-9.9	1	1	1
-85.32	42.60	***USA***	8.65	9.34	-7.4	1	1	1
-86.02	42.94	***USA***	8.45	9.34	-9.6	1	1	1
-84.86	43.65	***USA***	8.02	9.34	-14.2	1	1	1
-85.11	45.00	***USA***	5.95	9.34	-36.3	1	1	1

Table S2-2. Same as S2 but for wheat

Longitud	Latitud	Country	Yield-Ray	Yield-FAO	Variation (%)
142.10	-36.75	***Australia***	0.19	0.16	24.7
142.00	-35.12	***Australia***	0.14	0.16	-10.1
-51.63	-30.83	***Brazil***	0.12	0.21	-41.8
-52.41	-28.23	***Brazil***	0.25	0.21	16.2
-72.10	-36.57	***Chile***	0.43	0.46	-5.2
108.07	34.28	***China***	0.42	0.44	-2.5
113.58	34.85	***China***	0.48	0.44	10.3
115.48	38.85	***China***	0.58	0.44	32.5
125.84	48.02	***China***	0.36	0.44	-17.8
23.50	60.82	***Finland***	0.36	0.36	-0.2
8.67	50.57	***Germany***	0.76	0.74	2.3
82.99	25.27	***India***	0.21	0.27	-23.6
-98.90	19.48	***Mexico***	0.27	0.49	-44.4
5.66	52.00	***Netherlands***	0.85	0.85	0.2
16.90	52.45	***Poland***	0.42	0.39	8.0
32.88	39.95	***Turkey***	0.23	0.23	1.0
-111.97	33.07	***USA***	0.63	0.28	125.1
-98.09	36.39	***USA***	0.20	0.28	-27.7
-120.71	45.49	***USA***	0.29	0.28	3.6
-97.66	46.33	***USA***	0.30	0.28	6.7

Table S2-3. Soil Nitrogen pool (g N/kg soil)

	Maize		**Wheat**	
	Mean	***std***	***Mean***	***std***
High	0.215	0.11	0.332	0.06
Medium	0.167	0.06	0.27	0.18

A

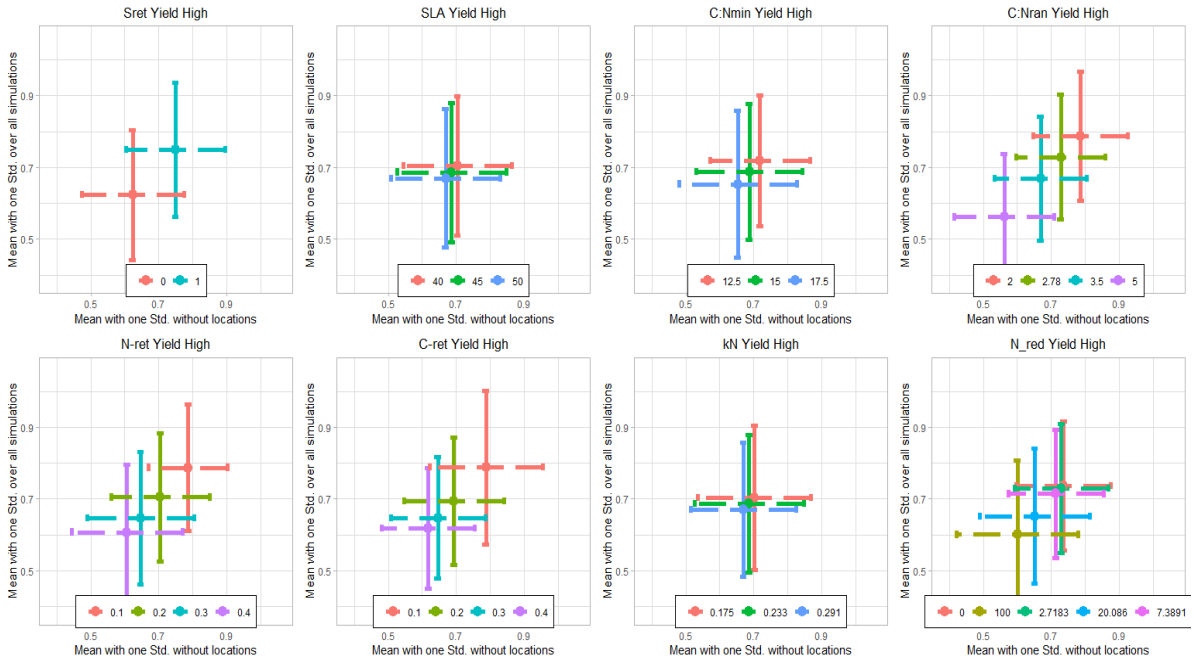

B

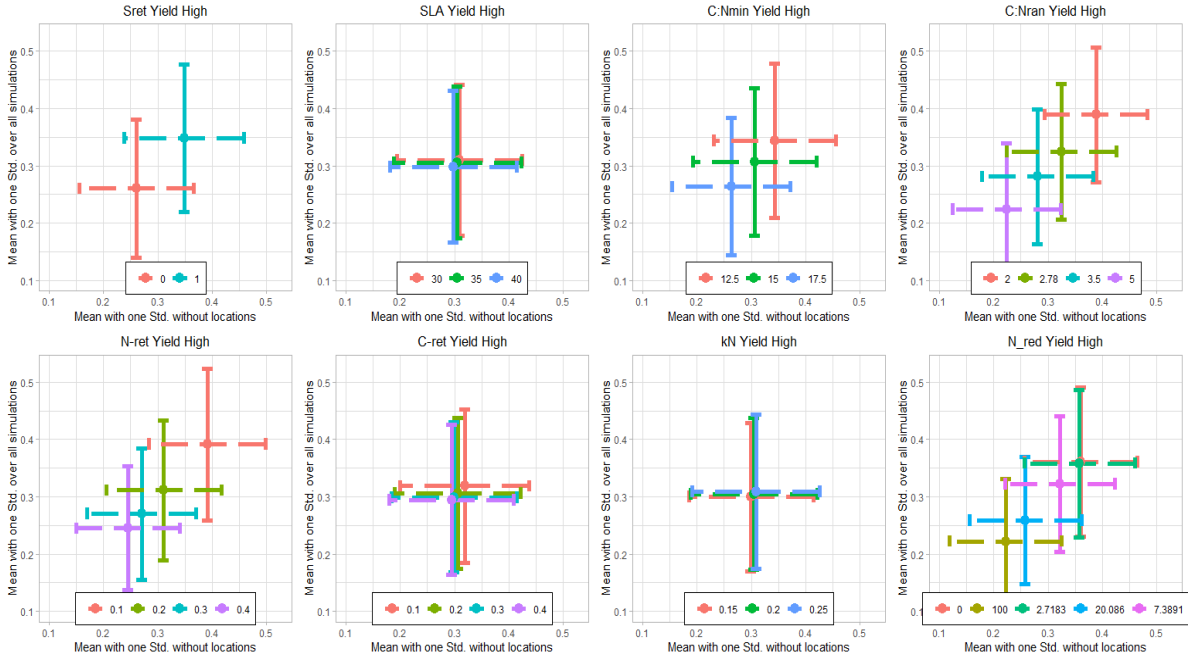

Figure S2-1. Mean values of simulated yield for the decade 2001-2010 for each evaluated parameter level. A. Maize high yield locations, B. Wheat high yield locations. Vertical bars represent the standard deviation considering all the variation from parameters and locations. Horizontal bars only consider variation from parameters

A

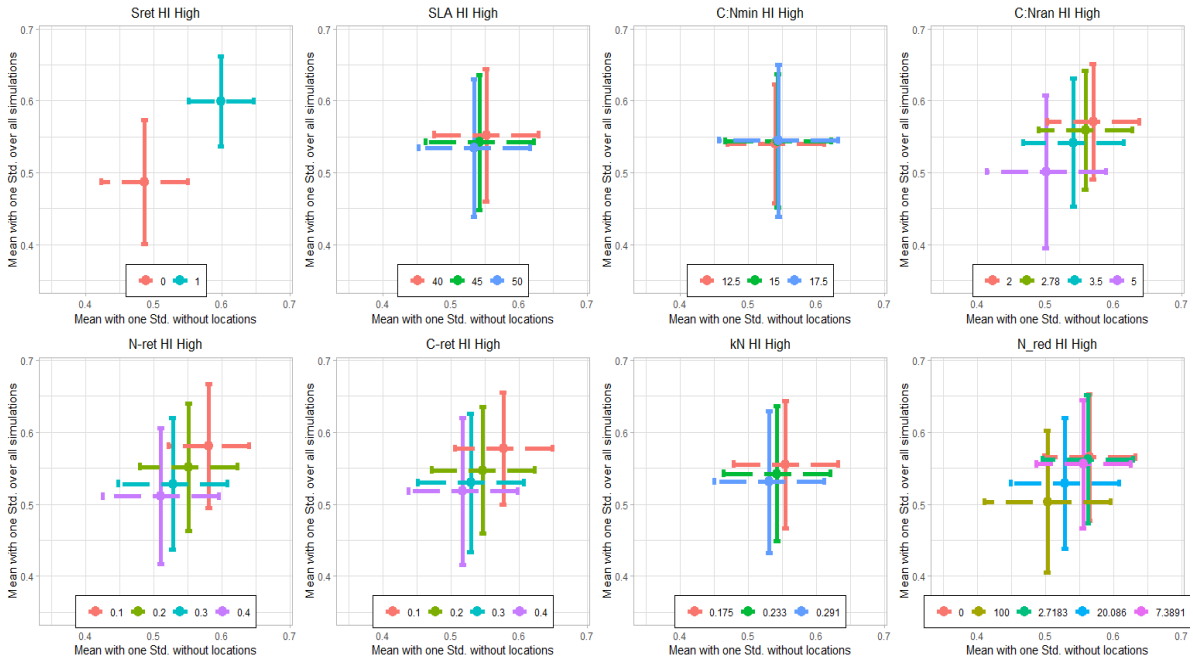

B

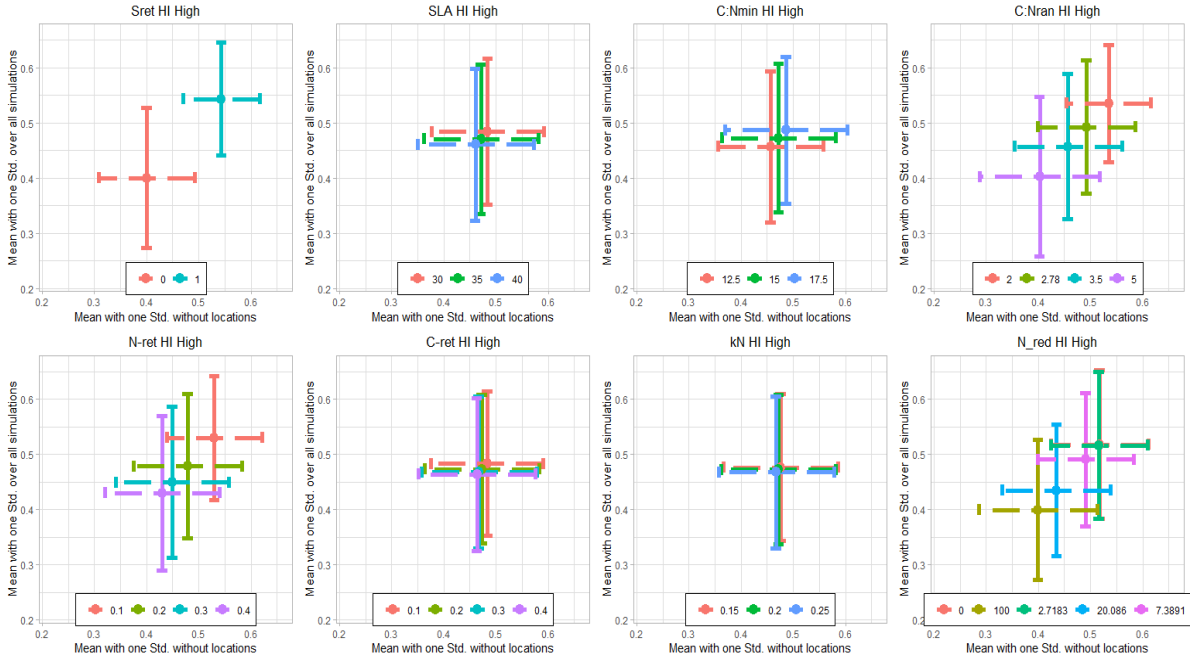

Figure S2-2. Same as Figure S2-1. But instead of simulated yield for simulated HI

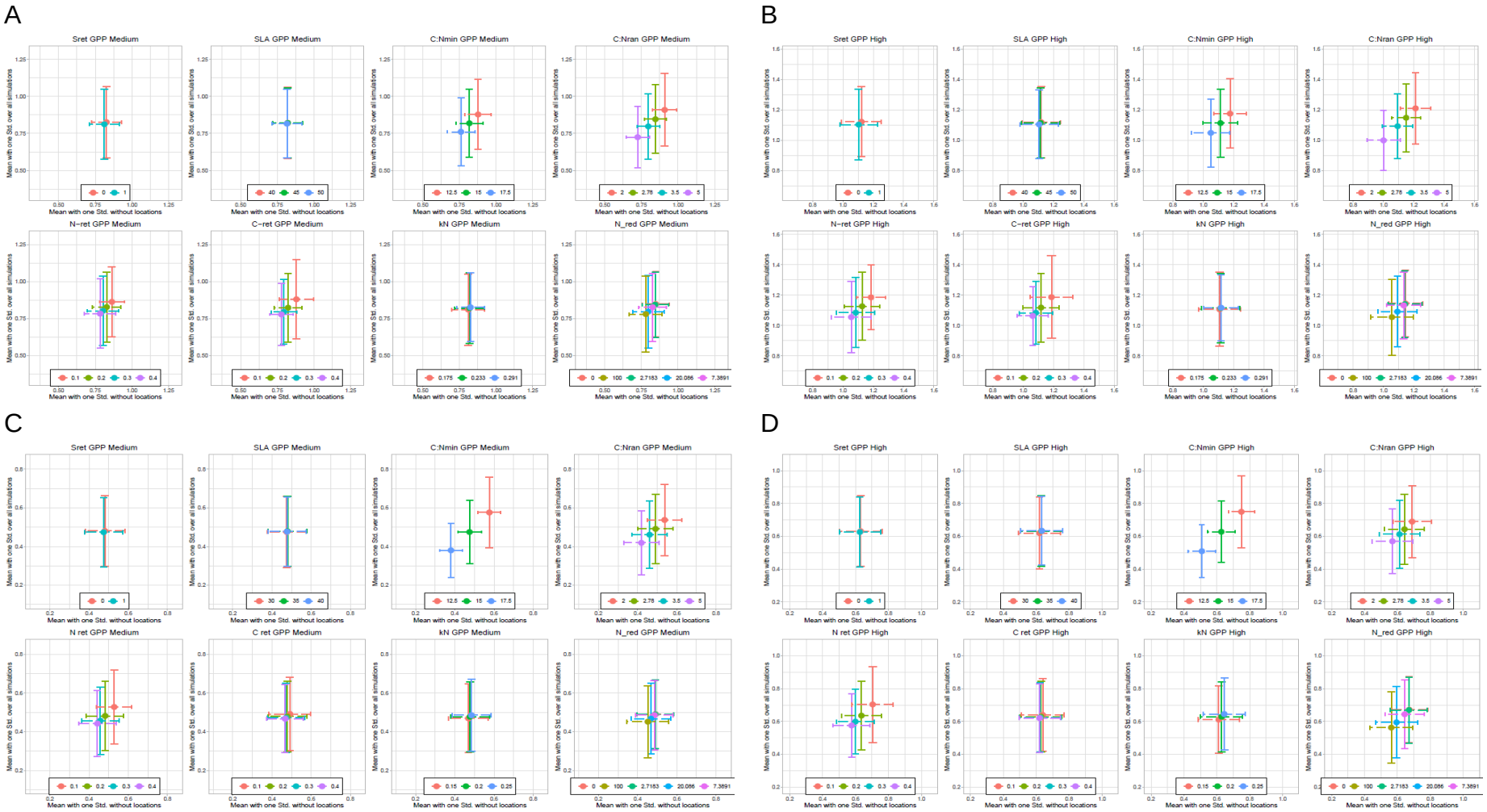

Figure S2-3. Mean values of simulated GPP for the decade 2001-2010 for each level of the evaluated parameters in “Medium” and “High” locations for maize (A and B) and wheat (C and D)

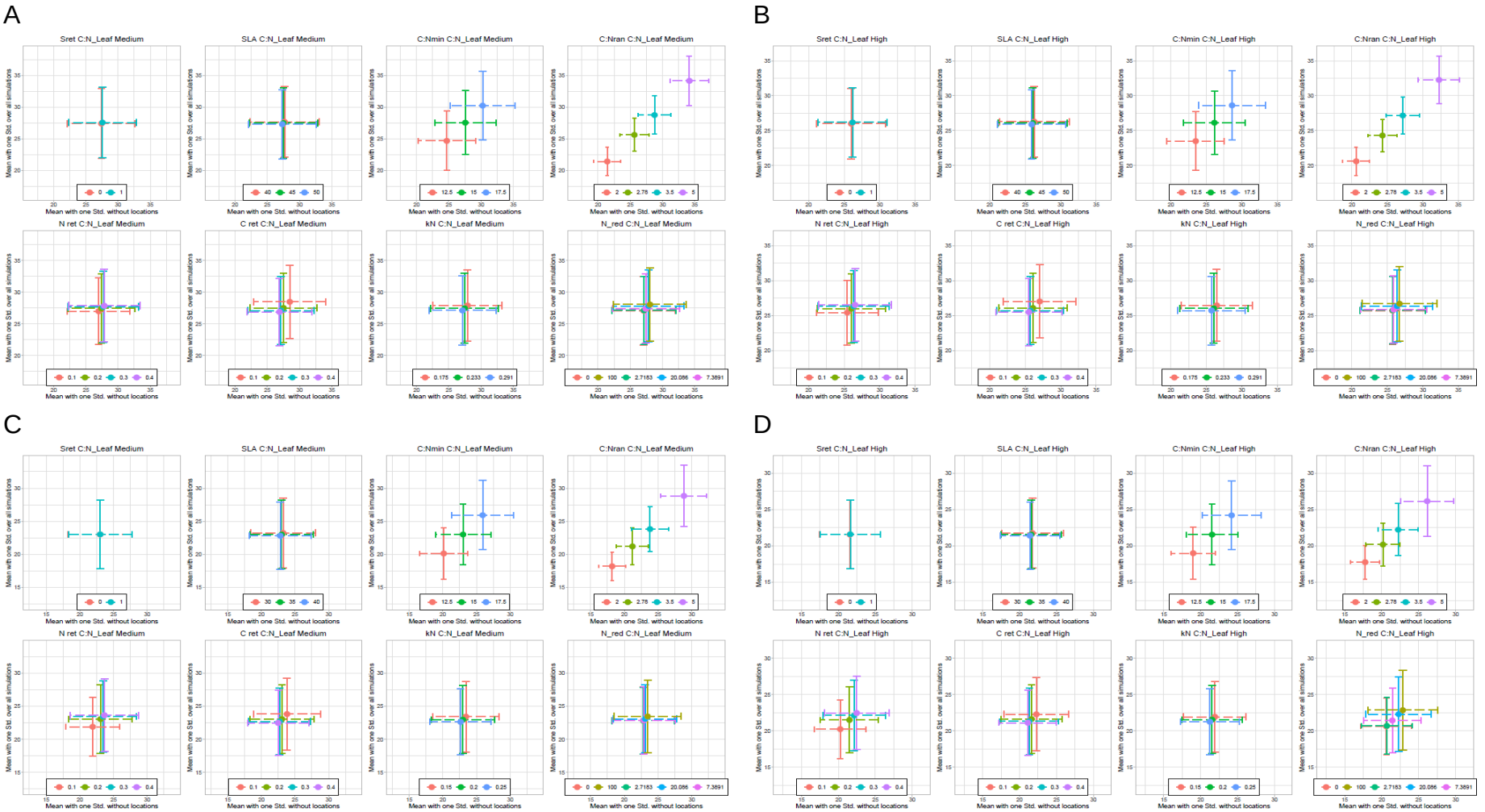

Figure S2-4. Mean values of simulated C:N ratio in leaves for the decade 2001-2010 for each level of the evaluated parameters in "Medium" and "High" locations for maize (A and B) and wheat (C and D)

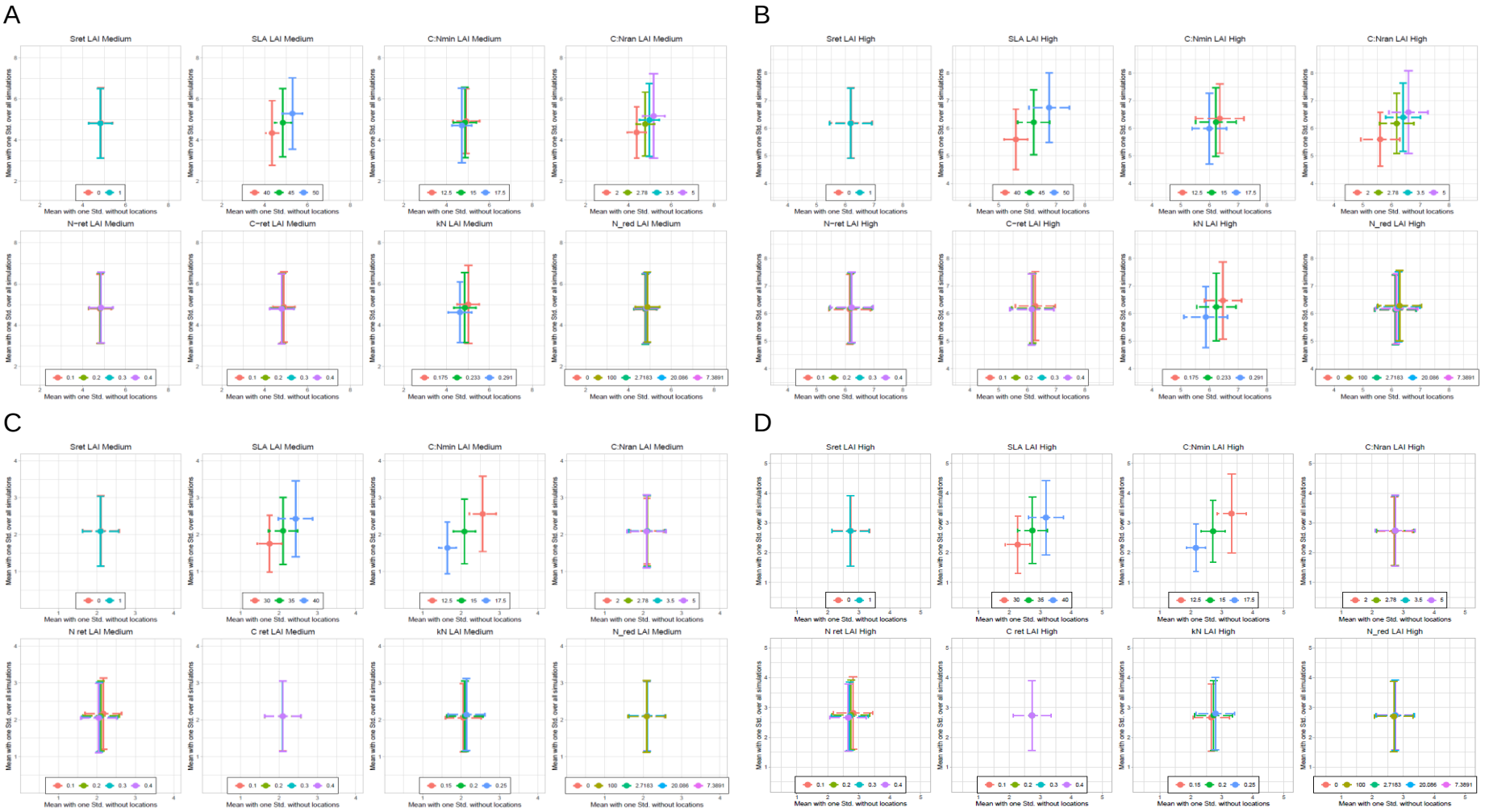

Figure S2-5. Mean values of simulated LAI for the decade 2001-2010 for each level of the evaluated parameters in “Medium” and “High” locations for maize (A and B) and wheat (C and D)

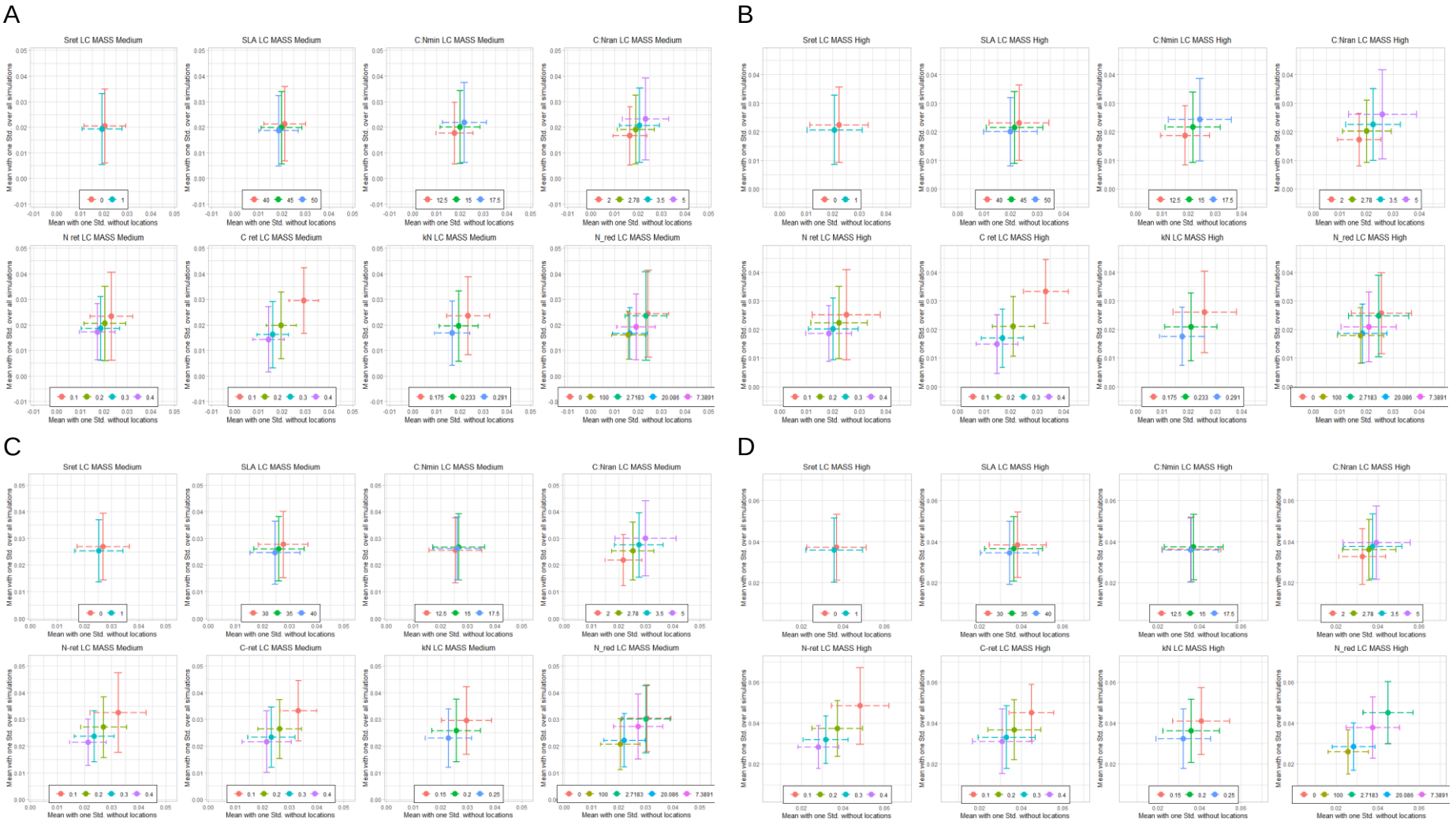

Figure S2-6. Mean values of simulated carbon mass in leaves for the decade 2001-2010 for each level of the evaluated parameters in "Medium" and "High" locations for maize (A and B) and wheat (C and D)

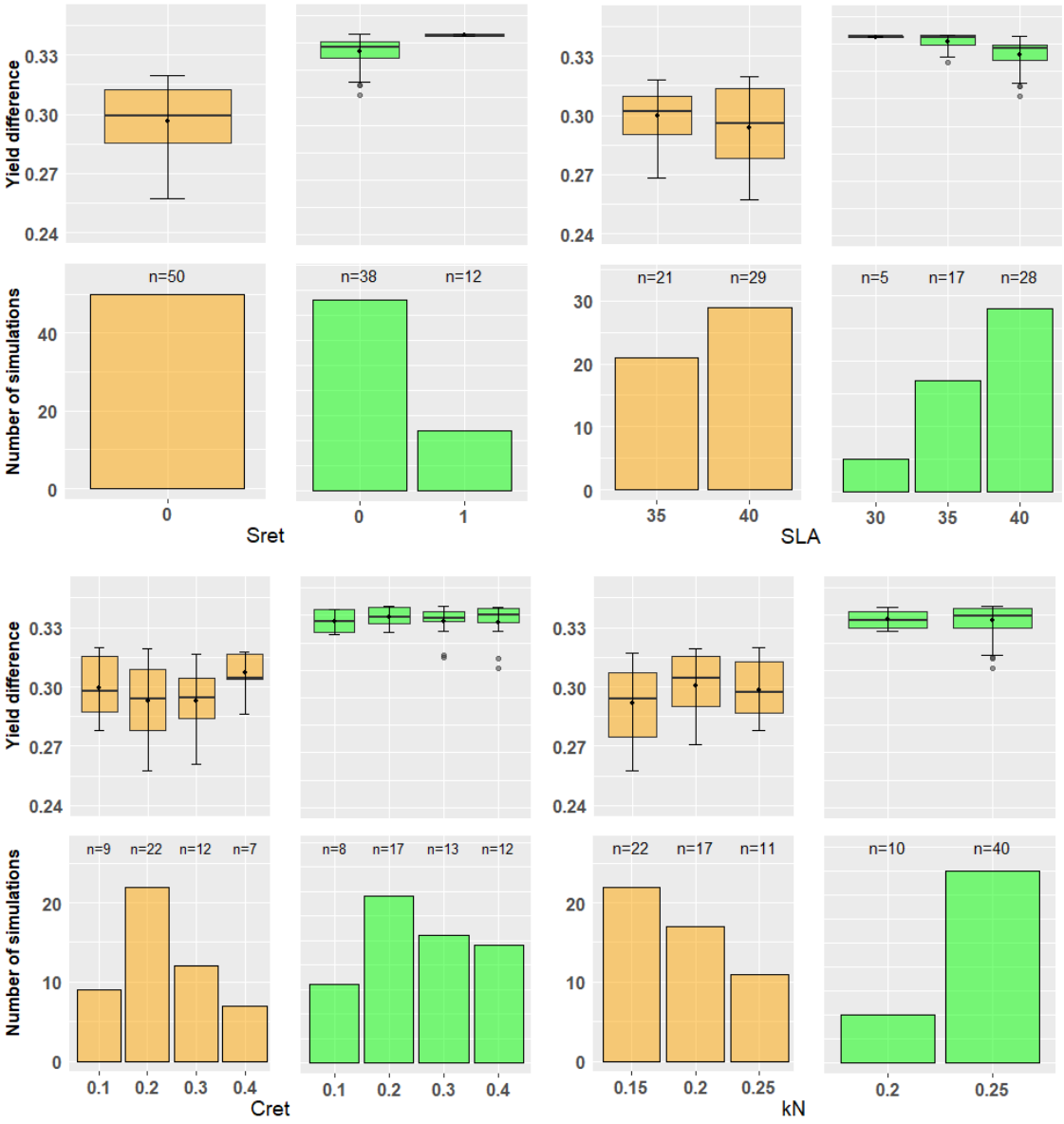

Figure S2-7. Wheat boxplots of the yield difference and distribution of the best fifty setups by parameter level considering FAO country yield as reference. Orange spring wheat and green for winter wheat

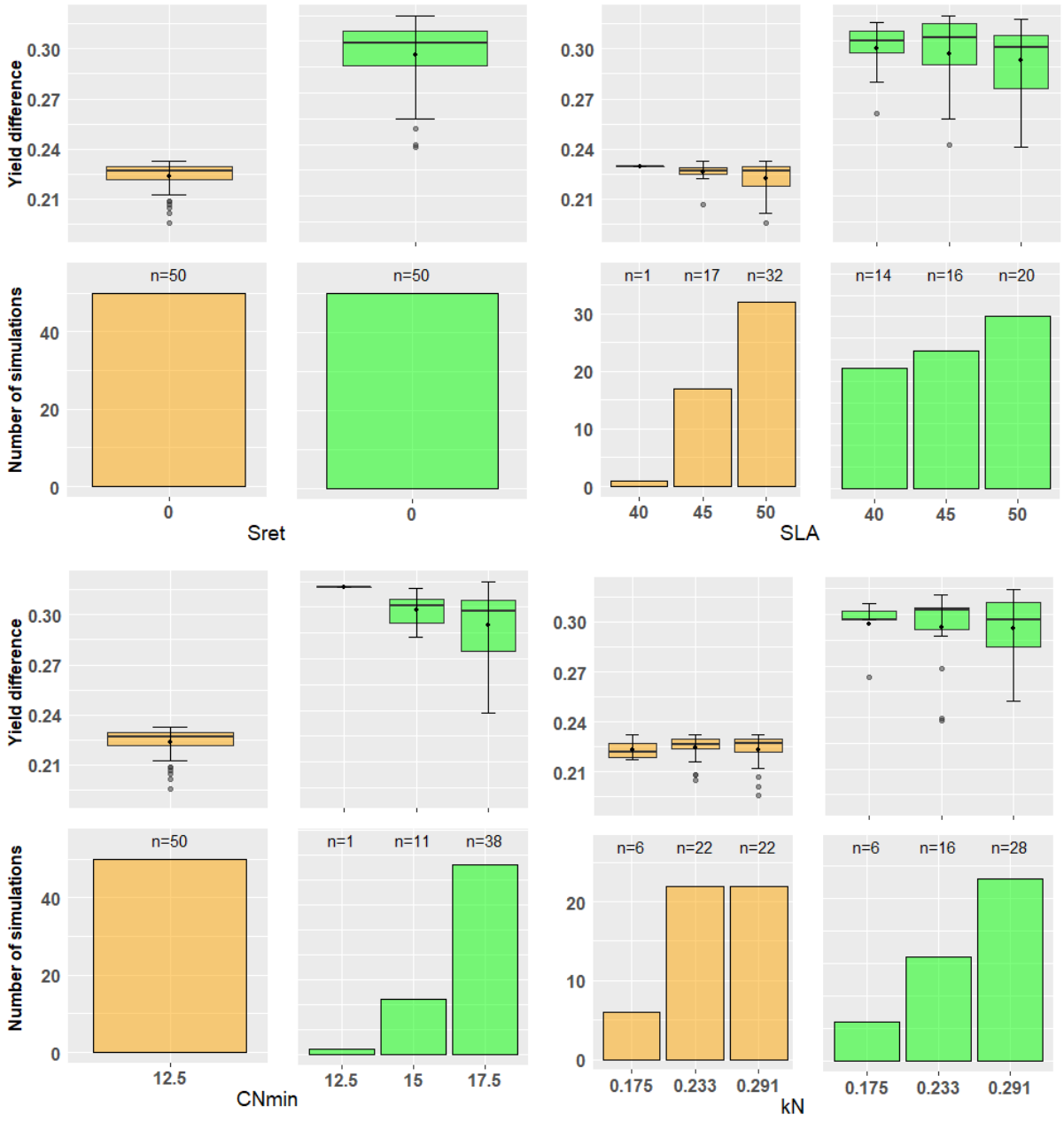

Figure S2-8. Maize boxplots of the yield difference and distribution of the best fifty setups by parameter levels considering FAO country yield as reference. Orange for high yielding and green for low yielding maize

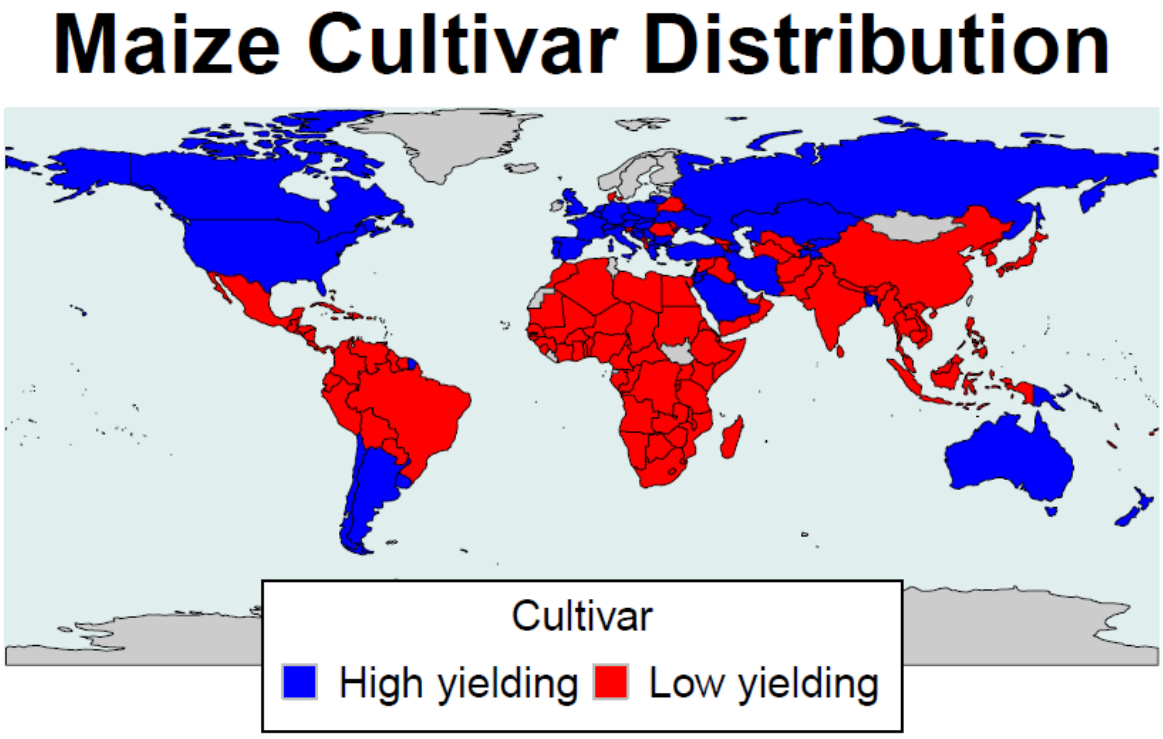

Figure S2-9. High and low yielding maize global distribution. Countries with grey colour reported less than 1000 harvested hectares in average for 2001-2010

CHAPTER THREE: INFLUENCE OF LAND COVER CHANGE ON HISTORICAL YIELD OF WHEAT, MAIZE AND RICE SIMULATED WITH LPJ-GUESS

3.1. Abstract

During the last century, global cropland area has increased by about 67% to compensate for a growing population and the subsequent increase in demand for food, fibre and energy. This pattern of continuous land cover (LC) change may has had a considerable impact on global food production. Taking LC change into account in dynamic vegetation global models, like LPJ-GUESS, has improved the simulation of vegetation cover and carbon cycling. The legacy of past LC changes substantially affects soil organic carbon and nutrient content, where nutrient availability is a key determinant of crop yield. However, the implications of past LC changes for crop yield have not been well explored in large-scale modelling. The contribution of this study is to evaluate the global effect of the history of LC changes on global crop yield estimations for wheat, maize and rice and the interaction of the history of LC changes with climatic and management drivers. A total of 56 global simulations were performed by combining three different factors. (1) Four different setups for global LC before the historical simulation: cropland, natural vegetation, conversion of natural vegetation to pasture before conversion to cropland, and a historical LC change reconstruction. (2) The individual contributions of five drivers: atmospheric CO_2, precipitation, radiation, temperature and fertilisation, plus two simulations including all driver variable and holding all drivers constant. (3) Two different climate forcings: CRU-NCEP (historical simulations from 1960 to 2010) and AgMERRA (historical simulations from 1980 to 2010). Both climate-forcing datasets showed a similar relative response in trends and interannual variability. Simulations with previous LC of natural vegetation and pastures caused higher soil nitrogen and carbon pools, increasing yields at the beginning of the historical simulations. In contrast,

simulations with continuous cropland had similar trends to the simulations using a LC change reconstruction. All the LC setups tended to simulate similar yields by the end of the historical simulation. Fertilisation was the main driver contributing to the yield trend, followed by atmospheric CO_2 in wheat and rice. Interannual variability was mainly caused by variations in fertilisation, precipitation, and to a lesser extent, temperature. The main results highlight the importance of capturing accurate historical LC changes and having comprehensive fertiliser database inputs to increase the accuracy of simulated global food production, climate change impacts and terrestrial biogeochemical cycles, particularly when simulating yield trends.

Keywords: Cropland, soil fertility, natural vegetation, pastures, CO_2 concentration, climate.

3.2. INTRODUCTION

Land cover changes combine natural and anthropogenic systems that directly influence local soil, water and air interactions, bringing regional and even global consequences (Noszczyk 2019). Since 1700, it is estimated that global cropland area has increased dramatically from 300 million ha to around 1600 million ha (Goldewijk and Ramankutty 2004; Goldewijk et al. 2017; Jackson et al. 2019). During the last century, cropland area increased by about 67%, meaning that in 2015 a large part of the ice-free earth area was covered by managed land, with 12% used for growing crops and 25% used for pasture (Goldewijk et al. 2017; IPCC 2017).

The expansion of managed land is a result of a growing human population and higher per capita consumption of food, fibre, and energy (Lindeskog et al. 2013) alongside the inability of yield improvements from agricultural technology to supply

and compensate the increased demand (Vermeulen et al. 2012; Kanianska 2016). Additionally, expansion is enhanced by other human activities such as conservation, biofuel crops and the loss of productive land (Godfray et al. 2010). Inappropriate agricultural practices and unsustainable management can contribute to soil degradation, carbon (C) and nutrient depletion, soil loss from water and wind erosion, soil compaction from intensive mechanisation, salinisation and desertification (Kanianska 2016; Krause et al. 2016). These limitations can result in yield depletion, low profitability and even the abandonment of cropland (Godfray et al. 2010).

The pattern of continuous land cover change and increasing cropland cover may dramatically alter the environmental footprint of agriculture (Goldewijk et al. 2017). Carbon emissions resulting from land cover change have been estimated in several studies as 156 Pg C between 1850-2000 (Lindeskog et al. 2013) 145.5 Pg C between 1850-2015 (Houghton and Nassikas 2017), 180 Pg C over the last 150-200 years with a current rate of around 1 Pg C yr^{-1} (Olin et al. 2015a) and 185 Pg C between 1750-2010, representing about one-third of the total anthropogenic carbon emissions (Le Quéré et al. 2014). In addition, the conversion of natural to anaerobic environments in flooded rice paddies cause around 34% of the total methane emissions, not considering biomass burning (Mosier et al. 1998; Schaefer 2019). Crop nitrogen (N) fertilisation also increases emissions of non-CO_2 greenhouse gases such as N_2O and methane (Mosier et al. 1998; Olin et al. 2015a; Lu and Tian 2017) due to over-application of fertiliser or the lack of simultaneity with the timing of crop demand, crop soils emitted around 3 Mt N_2O yr^{-1} (~0.8 Pg C-eq yr^{-1}) between 2007-2016 (IPCC 2017).

The transition from pastures, native forests, and tree plantations to cropland typically results in a decrease in soil carbon stocks. First, land clearing for agriculture releases carbon from vegetation through burning and decomposition, and later from harvested biomass removed each year. In addition, tillage and uncovered soil during cultivation enhance heterotrophic soil respiration (Guo and Gifford 2002; Krause et al. 2016). Conversely, natural vegetation favours soil organic carbon, even though it depends on several factors. For example, some species accumulate more litter or roots than other. N-fixing species may sequester more soil C stocks due to the extra N input in addition to the higher biomass production. Natural grasslands tend to have higher organic matter in soils than natural forests (Guo and Gifford 2002). Managed pastures often also have relatively high soil C stocks depending on climate and management due to their high biomass turnover rate and cooling effect on the soil (Guo and Gifford 2002; Krause et al. 2016).

Land cover change to expand cropland area is not the only factor that supports global population growth; the enormous increases in cropland productivity since the mid-1900s caused by the so-called “green revolution” allowed for higher food production growth (Godfray et al. 2010). This increase in productivity is associated with the intensification of inputs into agricultural systems, including fertilisation, irrigation, pesticides, high-yielding cultivar technologies and mechanisation (Lu and Tian 2017; Jackson et al. 2019). However, global demand for food is predicted to increase by between 70-100% in 2050 (Godfray et al. 2010; United Nations, 2019; Ray et al. 2022; Vermeulen et al. 2012) while production is increasingly limited by the availability of certain resources such as water and quality soil as well as different environmental conditions like higher atmospheric CO_2 and different climatic regimes.

Furthermore, these factors will be intensified by efforts to mitigate negative environmental effects and the push to more sustainable agriculture (Godfray et al. 2010; Ray et al. 2019).

To support the assessment of the impact of changes in land use and intensity associated with meeting increased demand, alongside adapting to climate change and mitigating negative environmental impacts, the ability to make assessments of how these changes impact regional-global scale crop production and carbon cycling is necessary (Vermeulen et al. 2012; Bustamante et al. 2014; Alexander et al. 2018). This requires the ability to model and accurately represent food production in both high- and low-intensity systems across the full range of relevant climates (Prentice et al. 1989; Monfreda et al. 2008). Global Gridded Crop Models (GGCMs) like the Lund-Postdam-Jena General Ecosystem Simulator (LPJ-GUESS) have been developed to fulfil this demand.

3.2.1. LPJ-GUESS

The dynamic vegetation model LPJ-GUESS (Smith et al. 2014) simulates the response of different plant functional types (PFT) to climate, atmospheric carbon dioxide concentration ([CO_2]) and N dynamics (Lindeskog et al. 2013; Olin et al. 2015b). LPJ-GUESS simulates yield based on daily or monthly climate data, [CO_2], prescribed management practices, soil physical properties, and atmospheric N deposition. PFTs represent several growth forms, phenology, photosynthetic pathway, distributional temperature limits and N requirements (Olin et al. 2015a). Crops in LPJ-GUESS are simulated as PFTs that differ in parameters and response to climate and management. Management options include rainfed and irrigation (inundation in the case of rice), fertilisation, tillage, and inter-growing season grass

cover (Olin et al. 2015b). The main processes simulated daily to represent crops are soil hydrology, photosynthesis, canopy conductance, respiration, phenology, plant N demand, and carbon allocation (Smith et al. 2001; Olin et al. 2015b)

Land cover dynamics and crop management were implemented in LPG-GUESS to improve the simulation of vegetation cover and carbon cycling (Lindeskog et al. 2013; Olin et al. 2015a). LPJ-GUESS simulates three distinct land cover types, natural vegetation, pastures and cropland and is able to explicitly simulate yearly shifts between them based on the grid cell net difference of land cover fractions (net LC changes) or based on the fraction of the addition of all the changes at sub-grid cell scales (gross LC changes). While gross LC changes can improve the accuracy of LC dynamics modelling, they also present technical limitations for efficiently processing the extensive information involved (Lindeskog et al. 2013; Bayer et al. 2017). Several studies have shown how relevant land cover history and dynamics at a large scale are to simulation of natural vegetation, carbon balance, and ecosystem processes (Lindeskog et al. 2013; Krause et al. 2016; Alexander et al. 2018). However, LPJ-GUESS and other GGCM studies have rarely accounted for the impact of land cover change legacies on crop yield simulation and the size of this impact has not been quantified, despite the well-known effects of agriculture on soil carbon and nutrient stocks.

This study aims to:

a. Quantify how land cover change legacy of nutrient stocks, and their interactions with other important inputs, affect simulated crop production at global and regional scales,

b. Provide recommendations for accounting for the effects of land use history in GGCM simulations to improve the models ability to represent the food production system and food security analyses.

To achieve the study aims, this study applies the LPJ-GUESS dynamic global vegetation model, which includes a detailed representation of agriculture and land use change, to evaluate the global effect of land cover change on global crop yield trends for wheat, maize and rice and its interaction with yield drivers such as climate, atmospheric CO_2, and soil fertilisation over the period 1960-2010.

3.3. METHODS

3.3.1. Model Setup

Global simulations of yield were performed using LPJ-GUESS v 4.1, revision 10304. The simulations were carried out at the global scale on a 0.5° x 0.5° grid for high- and low-yielding maize, spring and winter wheat, and rice. As previously performed for maize and wheat (Camargo-Alvarez et al. 2022), rice was calibrated for production and harvest index-related parameters (Supplementary S1). Winter and spring wheat were simulated and distributed globally according to the recent AgMIP climate change evaluation (Jägermeyr et al. 2021). For maize, high and low-yielding cultivars were simulated according to the global distribution reported for 2000-2010 by Camargo-Alvarez et al. (2022) using a similar approach to the distribution used in GEPIC and PEPIC models (Folberth et al. 2016).

Sowing and harvest dates were calculated automatically for each grid cell based on the prevailing climate, as described in Lindeskog et al. (2013), following Waha et al. (2012) and one growing season per year was simulated for each crop in each

location. Both rainfed and fully-irrigated conditions were simulated for each grid cell, except for rice, for which inundated conditions where simulated instead of irrigated.

The model dynamically estimated sowing and harvest dates based on climate suitability and heat unit accumulation (Lindeskog et al. 2013). Tillage was implemented following Pugh et al. (2015) and Olin et al. (2015b) and intercrop grass was turned off. All simulations were performed using 500 years to approach equilibrium accumulating vegetation, soil and litter carbon from bare soil, known as the spinup (Smith 2001; Wramneby et al. 2008). This period uses mean [CO2] and detrended climate from the first 30 years of the actual simulation to build up C and N pools. N input was provided based on the atmospheric N deposition dataset from Lamarque et al., (2010) and the global gridded at 0.5° x 0.5° cropland N fertilisation database from AgGRID (AgMIP GRIDded Crop Modelling Initiative) estimated for circa the year 2000 (Mueller et al. 2012; Elliott et al. 2015a). Values from this fertilisation database were rescaled between 1961 and 2010 based on the relative variations reported in the fertilisation dataset from Lu and Tian, (2017) to create a global fertilisation time series. The gridded data of texture, pH and organic matter in soils was from (Batjes 2016).

3.3.2. Experimental settings

Fifty-six global simulations were performed by combining two different factors. The first factor consisted of four different setups of land cover change (LC) at the global level during spinup and historical simulations. The second factor (DRI) consisted of seven combinations where some drivers were allowed to vary and other were kept fixed. In the case of CO_2 and fertilisation rate constant values were used. For climate, the first year of the historical simulation was repeated during the whole period.

3.3.2.1. Land cover change setups

1. Five hundred years of spinup with cropland cover and historical simulation from 1901 to 2010 for CRU-NCEP. For AgMERRA the spinup is until 1980, and then the historical simulation is undertaken (LCcrop). This is the spinup previously used for crop-focused papers (Olin et al. 2015b; Camargo-Alvarez et al. 2022).
2. Five hundred years of natural vegetation spinup and land cover change to cropland in 1960. Land cover change to cropland in 1980 for AgMERRA (LCnat).
3. Five hundred years of natural vegetation spinup and land cover change to grassland in 1920, then to cropland in 1960. Land cover change to cropland in 1980 for AgMERRA (LCnatpas).
4. Land cover history from Land Use Harmonization 2 (Hurtt et al. 2020), specifying land transitions between natural vegetation, pasture, and cropland annually starting from 1901, I.e. the best estimate of actual LC history. Land cover fractions of 1901 are used for previous years (LCLUH).

3.3.2.2. Driver combinations (DRI)

1. All drivers time varying (Allvar).
2. CO_2 is time varying, other drivers fixed (CO2var).
3. Precipitation is time varying, other drivers fixed (Precvar).
4. Radiation is time varying, other drivers fixed (Radvar).
5. Temperature is time varying, other drivers fixed (Tempvar).
6. Fertilisation is time varying, other drivers fixed (Fervar).
7. All drivers fixed (Allcons).

3.3.2.3. Forcing Climates

All the simulations were performed using CRU-NCEP and AgMERRA forcing climates. However, a direct comparison between climate datasets was not performed since the historical simulations have different spans and spinup periods. Rather the datasets are compared qualitatively. A different spinup protocol was used for CRU-NCEP, reflecting the longer climate time series available. During spinup, simulations use detrended climate data and atmospheric [CO_2] from the first historical year (Smith 2001; Olin et al. 2015a). In the case of CRU-NCEP, the first historical year is 1901 and then observed climate and [CO_2] data were used during the LC setups before 1960. In AgMERRA, the first historical year is 1981, meaning that LC setups occurred during the spinup with constant 1981 climate and [CO_2].

3.3.3. Data analysis

Harvested areas and yield estimation

Global gridded harvested areas were estimated from the Spatial Production Allocation Model “SPAM” (You et al. 2014) and the History Database of the Global Environment (HYDE version 3.2) (Goldewijk et al. 2017). Although SPAM provides separately irrigated and rainfed harvested areas by crop, it is only available for 2000, 2005 and 2010. Therefore, harvested areas for 1961, 1970, 1980 and 1990 were estimated by scaling irrigated and rainfed SPAM-2000 areas according to the relative changes in the total harvested area between the above years and 2000 reported in HYDE. Then a linear interpolation was performed between the resultant years to complete a yearly database from 1961 to 2010 at 0.5° x 0.5° resolution. Finally, harvested areas per grid cell were scaled to force the nationally aggregated estimated areas to match FAO (Food and Agriculture Organization of the United

Nations 2020) national reported areas by crop. This scaling was applied homogeneously at the country scale. Final estimations were aggregated to provide a global time series of irrigated and rainfed harvested areas of maize, wheat and rice.

The simulated yield (t DM ha^{-1}) was adjusted to fresh weight to compare with FAOstat yields. A 12% net water content was assumed for maize and wheat and 13% for rice (Müller et al. 2017). The simulated yield was multiplied by the harvested areas by grid cell to calculate the total production separated by irrigated, rainfed and inundated areas according to the case being examined. Subsequently, this grid cell-scale production was aggregated to the global scale, and yield was calculated by dividing production by the global aggregated harvested areas. This process was carried out by crop and year to obtain a time series of simulated yield following Equation 3 – 1.

$$\mathrm{GYield_t} = \frac{\sum_{i=1}^{n} \mathrm{Yield_{irr,i,t}} * \mathrm{Area_{irr,i,t}} + \sum_{i=1}^{n} \mathrm{Yield_{rf,i,t}} * \mathrm{Area_{rf,i,t}}}{\sum_{i=1}^{n} \mathrm{Area_{irr,i,t}} + \sum_{i=1}^{n} \mathrm{Area_{rf,i,t}}} \quad \text{Equation 3 - 1}$$

where *i* is the index of the grid cell to be aggregated, *t* is the year, *n* is the number of grid cells in that spatial unit, *irr* represents full irrigated conditions, and *rf* represents rainfed conditions. *GYield* is the global aggregated yield, *Yield* and *Area* (harvested area) are at the grid cell-scale.

3.3.3.1. Time series comparison

Simulated yield typically showed a sharp change in the few years following the land cover transition. Therefore, the number of years required after the land cover transition for the yield to stabilise, after which the trend of the global yield starts to increase (the inflection point), was recorded for each simulation and compared. Then, the first five years of the time series were removed to avoid long-term trends

being affected by the anomalies occurring during the first years after the conversion to cropland. Then, an analysis of covariance (ANCOVA) was performed by climate to find the effect of LC and DRI on simulated global yield through time, which was expressed as years after 1960 for CRU-NCEP simulations and 1980 for AgMERRA. This method evaluates the interaction of the different levels and time to compare slopes. Also, a regression analysis with explanatory coded indicator variables (or 'dummy') for LC levels was performed to compare linear adjusted models of LCcrop and other LCs. Similarly, regression analysis with dummy variables was used to compare the slopes of Allvar against the rest of the DRI levels.

Slopes of global time series of simulated yield from the LC_{crop} with Allvar and CRU-NCEP climate (regular setup for crop simulation) were compared to the FAO global yield time series trend. The detrended time series correlation between both datasets was also calculated. To calculate the trends at grid cell level, the equivalent process was performed: Linear regressions were adjusted to yield time series between 1961 and 2010 at 0.5° x 0.5° resolution at grid cell-scale. Slope and intercept were calculated per grid cell to evaluate the spatial trends of yield. Grid cell-level trends were only calculated for the simulation from LC_{crop}, Allvar and CRU-NCEP.

To analyse interannual variability, detrended time series were obtained as the residuals of adjusted linear models from each global time series simulation. Then, the variance and the coefficient of variation (Equation 3 - 2) were calculated from detrended data. A Levene test was carried out by climate to evaluate significant differences in interannual variability between LC levels. The Levene tests (Levene 1960) were also run to compare variances from DRI levels.

$$CV_i = \frac{\sigma_i}{\text{Mean Yield}_i} \qquad \text{Equation 3 - 2}$$

where *i* represents the time series to calculate the CV, σ is the standard deviation from the detrended time series and the mean yield is from the original time series.

3.3.4. Soil Fertility

Global simulated yield time series for all the crops were calculated and separated by high and low fertilisation areas. High fertilisation areas were selected as the grid cells in the top 20th percentile of higher fertilisation rate by crop (60 kg N ha^{-1} for wheat, 65 kg N ha^{-1} for maize and 51 kg N ha^{-1} for rice). The remaining grid cells were classified as low fertilisation areas according to the N fertilisation database from AgGRID for the year 2000 (Elliott et al. 2015a). This was performed for simulations with CRU-NCEP forcing climate and all drivers constant for the four levels of LC and the three crops. Only these levels were considered since the objective was to evaluate the effect of LC in different nutrient conditions during the first period of the simulations. Intercepts (linear adjusted yield in the year 1960) of high and low fertilisation time series were compared by LC separately using an ANCOVA and a paired t-test performed comparing both time series between 1961 and 1970.

All analyses were performed using the packages *dplyr, plyr*, *rworldmap, raster, forecast* and *ncdf4* of the software R version 3.6.2 (R Core Team 2019).

3.4. RESULTS

3.4.1. Time series comparison

The inflection point, after which there is an increasing trend in the global yield, varies substantially due to LC and DRI factors and the crop. CRU-NCEP wheat showed inflection points after 2000 in the global time series for LC_{nat} and LC_{natpas} and all the

drivers except for Allvar and Fervar. This means that yield decreased during most of the time series. LC_{crop} and $LC_{LUH,}$ on the other side, had early inflection points during the first ten years of simulation, indicating the early start of the increasing yield trends. In maize, all the LC levels showed a decreasing trend for Allcons, CO2var, Radvar and Tempvar during the whole period, never reaching an inflection point, for that reason this value was estimated as 2010, the last year of the study. While Allvar, Fervar and Precvar showed later inflection points in LC_{nat} and LC_{natpas} compared to LC_{crop} and LC_{LUH}. Rice had a similar pattern to wheat, but the inflection points occurred, in general, earlier in all LCs and drivers (Figure 3.1).

AgMERRA wheat showed inflection points early during the first five years of simulation for all drivers in LC_{crop} and LC_{LUH} except for Allcons and Radvar in LC_{LUH}, which occurred late around 2005. LC_{nat} and LC_{natpas} had inflection points later than 2000 in all drivers. In maize, a similar response to CRU-NCEP showed a decreasing trend for Allcons, CO2var, Radvar and Tempvar in all the LC levels, except for Tempvar in $LC_{crop,}$ while Allvar, Fervar and Precvar showed later inflection points in LC_{nat} and LC_{natpas} compared to LC_{crop} and LC_{LUH}. Rice had early inflection points for all the simulations except for Radvar in all the LC levels, Allcons in LC_{natpas}, and Allcons and Tempvar in LC_{nat} and LC_{natpas} (Figure 3.1).

According to the ANCOVA, significant effects of LC and DRI on global yield were found through time for the three crops using both climate datasets, but no significant interaction between LC and DRI was found through time, except for rice when CRU-NCEP was used as forcing climate (Table S3-1). Linear regressions showed that global simulated yield slopes of LC_{nat} and LC_{natpas} were significantly lower than the slopes caused by LC_{crop}, while no difference was found against trends of LC_{LUH} for all

the crops and both climates. Intercepts of LC_{crop} were significantly lower than LC_{nat} and LC_{natpas} for both climates except for rice with CRU-NCEP, which did not show differences between the intercepts of LC_{crop}, LC_{LUH} and LC_{natpas}. Intercepts of LC_{crop} and LC_{LUH} were not significantly different with AgMERRA climate in the three crops. With CRU-NCEP, wheat and maize LC_{LUH} showed significantly higher intercepts (Figures 3.2 and S3-1, Table S3-2).

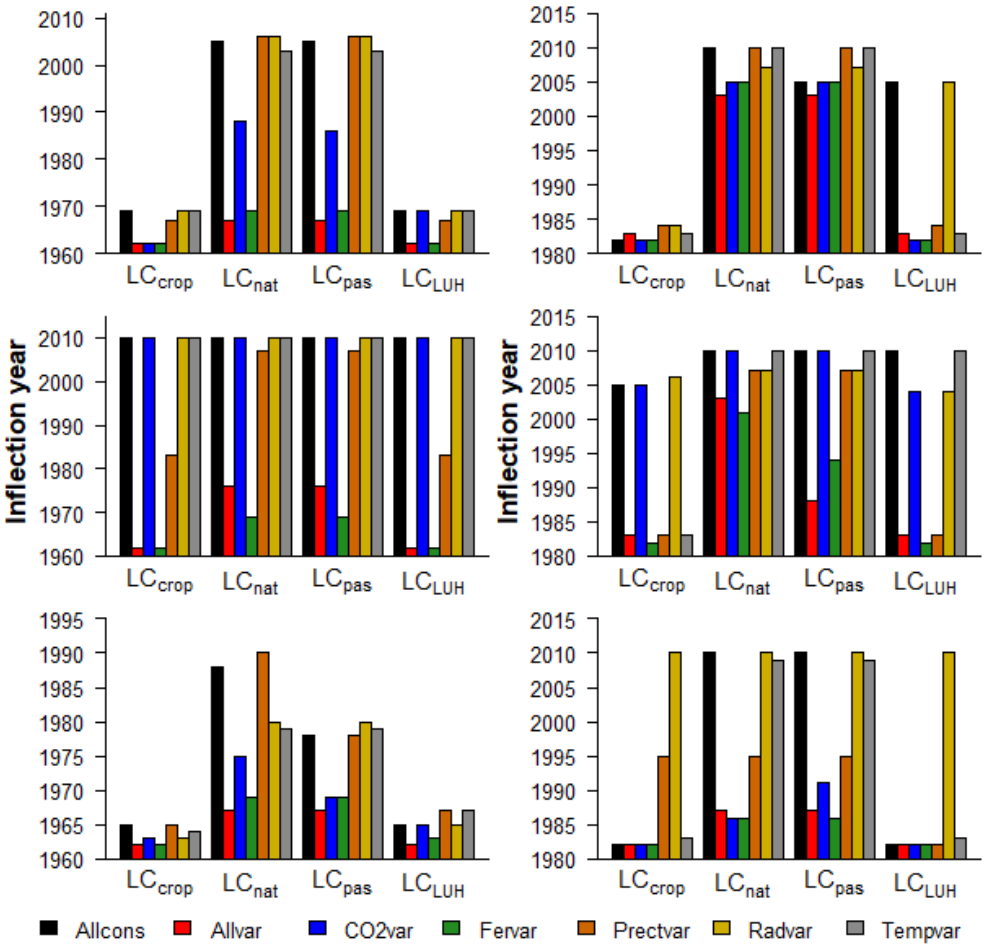

Figure 3.1. Inflection point (year), after which yield trend increases for all levels of LC and DRI. Left: CRU-NCEP simulations. Right: AgMERRA simulations Top: wheat, middle: maize, bottom: Rice

When all drivers were variable (Allvar), the slopes were significantly higher compared to individual drivers alone for the three crops and two climates. The only exemptions

are CO2var in wheat with AgMERRA climate and Fervar in maize with both climates. Besides slopes, Fervar intercepts were not significantly different to the intercepts of Allvar with both climates, confirming similar trends for both driver levels. Intercepts were typically significantly higher for Allvar and Fervar than for the other DRI combinations, mainly with CRU-NCEP, but the response was more variable depending on climate, cultivar, and driver (Table S3-3).

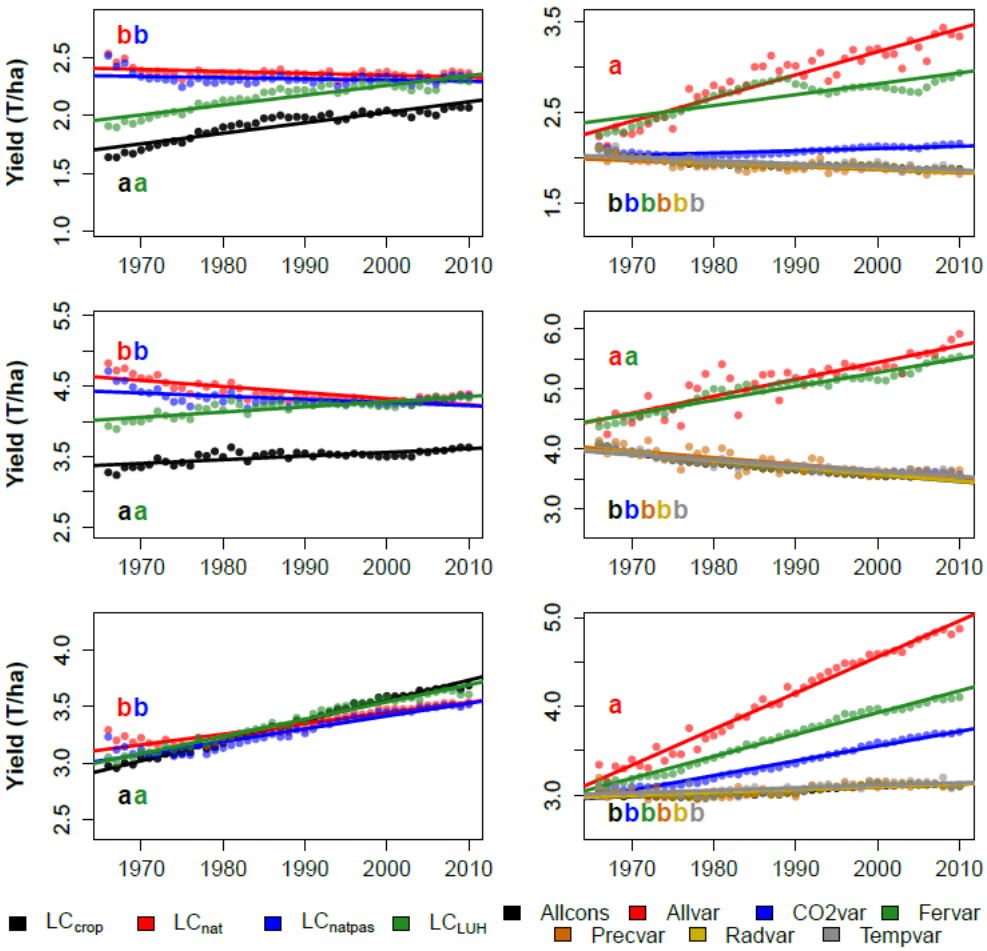

Figure 3.2. Left: time series and trends of land cover change levels (using yearly average of all drivers), right: time series and trends for driver levels (yearly average of all LCs) with CRU-NCEP. Different letters represent significant differences (95%) in slope between lines. Top: wheat, middle: maize, bottom: Rice

Slopes of all the combinations between the LCs and drivers showed clear patterns for all the crops, even for rice with CRU-NCEP, whose interaction between the two

factors was significant. It was consistentt with the response of the slopes from the main effects described above (Figures 3.2 and 3.3). CRU-NCEP produced higher slopes compared to AgMERRA. Fervar is the main contributor to the slopes of the three crops, with CRU-NCEP followed by CO2var in all the LCs for rice, and LC_{crop} and LC_{LUH} for wheat (Figure 3.3). Intercepts with CRU-NCEP were higher for Allvar and Fervar compared to the other drivers for the three crops. Rice also showed an important effect of CO2var in intercepts.

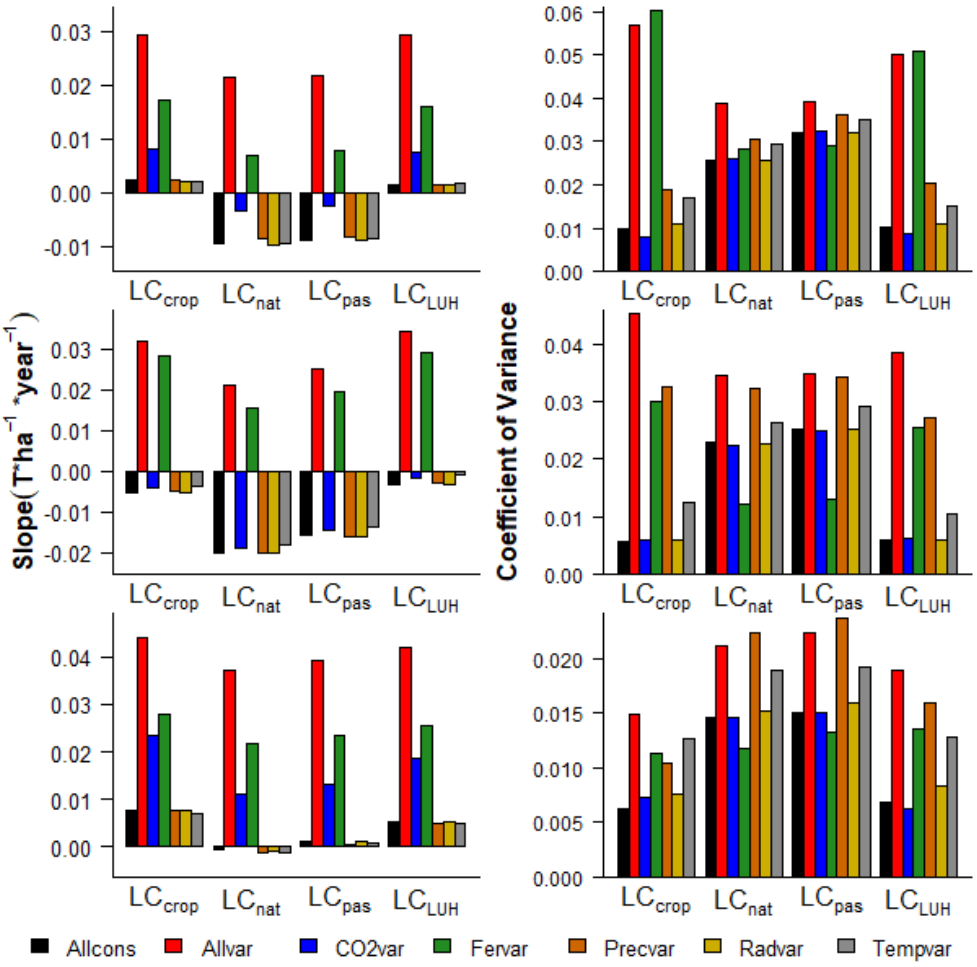

Figure 3.3. Slopes and coefficient of variance of time series simulated with CRU-NCEP as forcing climate. Combination of all levels for drivers (DRI) and land cover change (LC). Top: wheat, Middle: maize, Bottom: Rice

With AgMERRA, Fervar is also the main contributor to the slope for maize and rice, but in this case, CO2var was the main contributor for wheat and highly important in rice (Figure S3-2), likely because most of the [CO2] increase occurred over the period 1980-2010, whilst most of the N fertilisation increase occurred over the period 1960-1980. Intercepts of LC_{nat} and LC_{natpas} were higher in wheat and maize with both climates and rice only with AgMERRA. CRU-NCEP showed high variation caused by drivers on intercepts; unlike LC levels, LC_{nat} and LC_{natpas} had higher intercepts in all drivers and crops compared to LC_{crop} and LC_{LUH} in all LCs, while in AgMERRA variation was mainly caused by LCs (Figure S3-3).

Fertilisation was the main factor contributing to the variation of the simulated global yield of wheat in LC_{crop} and LC_{LUH}. Unlike LC_{nat} and LC_{natpas} where climate variables were the main factors causing yield variability (Figures 3.3 and 3.4).

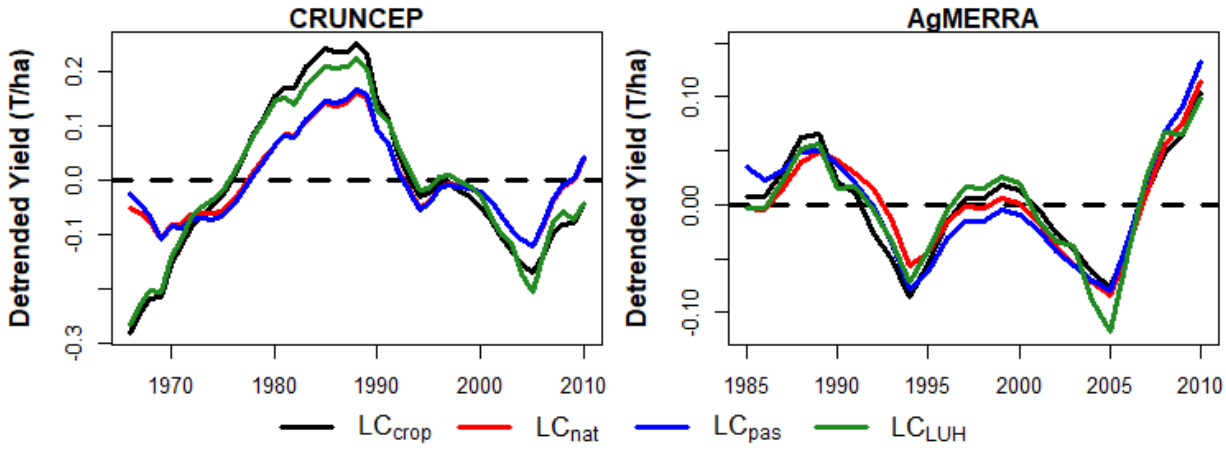

Figure 3.4. Detrended time series of wheat yield from simulations only accounting for fertilisation variation with all the evaluated land covers for CRU-NCEP (left) and AgMERRA (right)

The Levene test to compare the variances of the detrended time series by groups showed that levels of both factors, LC and Drivers, did not have equal variances of the simulated global yield of the three crops, except for LC with AgMERRA in wheat

and rice (Table 3.1). In simulations with CRU-NCEP, LC_{crop} and LC_{LUH} had higher coefficients of variation (CV) for maize and wheat for Allvar and Fervar, while LC_{nat} and LC_{natpas} had higher CV for the remaining levels of DRI. In rice, LC_{nat} and LC_{LUH} showed the highest variation for all the DRI levels (Figure 3.2). With AgMERRA, the highest variation in maize occurred for LC_{nat} and LC_{natpas} for all the DRI levels, while in maize, it happened only for Allvar and Tempvar. A similar response was found in all the LC levels in rice, and DRI caused the main variation. While with CRU-NCEP, fertilisation was the main factor causing variation, with AgMERRA, precipitation and temperature (and radiation in rice) are the main drivers causing variability, followed by fertilisation. Atmospheric CO_2 causes similar variation to Allcons for all crops and both climates.

Table 3.1. Levene test p-values for land cover change (LC) and drivers global detrended time series for wheat, maize and rice with CRU-NCEP and AgMERRA, shaded values mean no significant difference in variances between levels

	Wheat		**Maize**		**Rice**	
	CRU-NCEP	**AgMERRA**	**CRU-NCEP**	**AgMERRA**	**CRU-NCEP**	**AgMERRA**
Land cover change	0.002	0.416	<0.001	<0.001	<0.001	0.304
Drivers	<0.001	<0.001	<0.001	<0.001	<0.001	<0.001

3.4.2. Global gridded trend

Increasing trends in simulated yield occurred in most of the harvested areas for the three crops globally. However, some regions with yield stagnation and decreases were identified. For wheat, this occurred in regions of South America, Russia, and Eastern Europe. For maize, stagnation occurred in the same regions as wheat, plus some regions in Central and North America, Africa, and Southern Asia. In rice,

stagnation only occurred in regions of South America, Africa, and Eastern and Central Asia (Figure 3.5).

Improvement in yield occurred mainly in top producer countries such as China, India, USA, and Pakistan for wheat; USA, China, Argentina, and Mexico for maize; and China, India, Indonesia, Bangladesh, and Vietnam for rice (Figure 3.5).

The simulated yield was higher in 1960 (intercepts) in regions in the Americas, Russia and Europe for wheat, North America, Argentina, Russia and Europe for maize, and the Americas, Africa, Central Europe, Kazakhstan, India, and China for rice (Figure 5).

3.4.3. Trend (LPJ-GUESS vs FAO)

Global simulated yield with LPJ-GUESS showed higher values than FAO global reported yield. This overestimation tended to decrease with time causing significant differences in regression parameters of LPJ-GUESS estimated yield with higher intercepts and lower slopes compared to FAO. Maize showed the highest difference in slope where FAO data had 0.029 t ha^{-1} $year^{-1}$ higher than LPJ-GUESS simulations. while wheat and rice had a difference of 0.008 t ha^{-1} $year^{-1}$ (Figure 3.3). The correlation between detrended simulated and FAO reported global yields time series was significant with Pearson correlation coefficient $\boldsymbol{\rho}$=0.55 (*p-value*<0.001) for wheat, $\boldsymbol{\rho}$=0.50 (*p-value* <0.001) for maize, and $\boldsymbol{\rho}$=0.55 (*p-value* <0.001) for rice, demonstrating a good representation by the model of the interannual variation.

3.4.4. Soil Fertility

Comparisons between intercepts of time series from regions with high and low fertilisation, as well as the paired t-test for wheat, showed that after the transition to

cropland in 1960 from natural vegetation and pastures (LC_{nat}, LC_{natpas}), there was not significant difference between the two series. On the other side, LC_{crop} and LC_{LUH} showed significant differences in intercepts and significant paired t-test between both time series (Figure 3.5). After circa 1990, yield differences between high and low nitrogen time series tended to be similar in all the LCs, although the yield magnitudes of both time series were lower for LC_{crop} during the whole evaluated period (Figure S3-6).

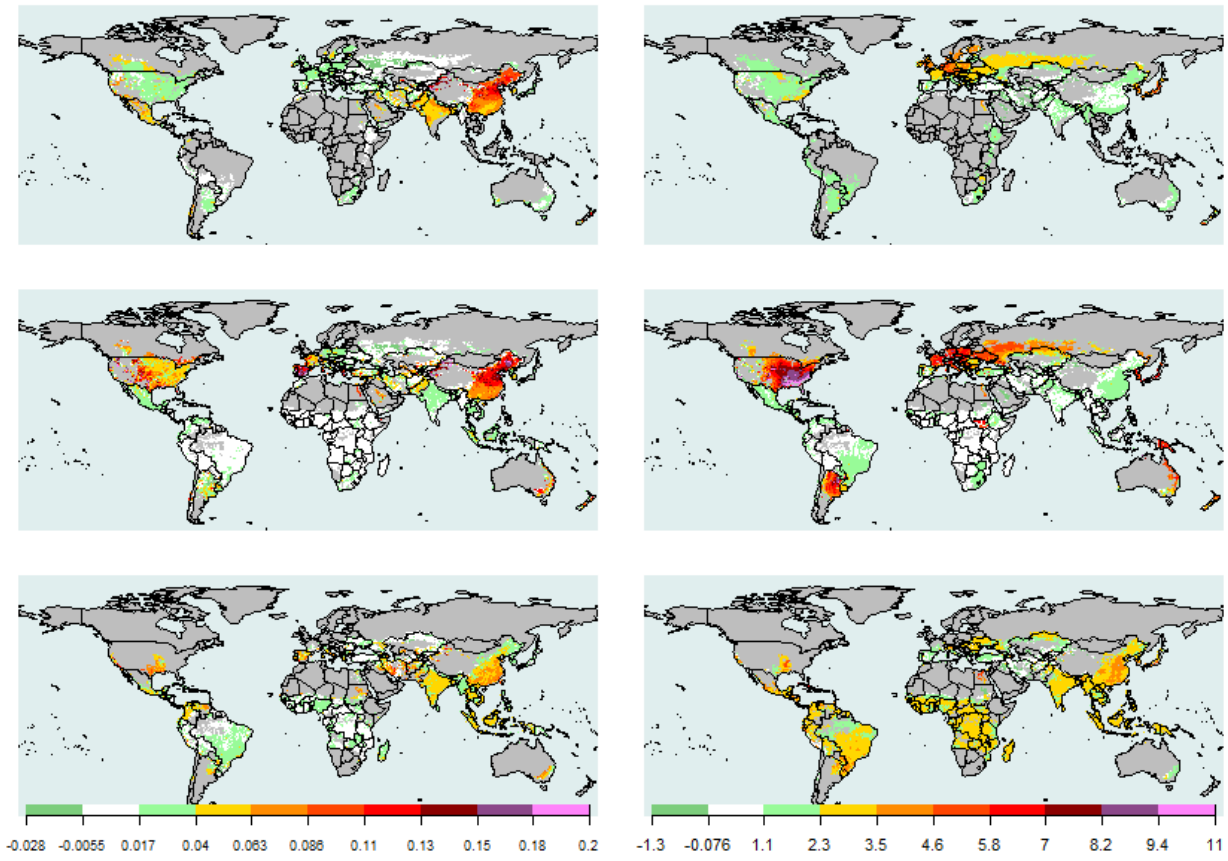

Figure 3.5. Global gridded slopes in t ha^{-1} $year^{-1}$ (left) and intercepts t ha^{-1} for 1960 (right) with LC_{crop} and Allvar and CRU-NCEP. Top: Wheat, middle: maize, and bottom: rice

For maize, all the LC levels showed a significant difference between both time series during the first simulated years based on the intercept difference and the paired t-

test, but differences between high and low nitrogen time series were higher in LC_{crop}. Also, differences became higher with time since trends are divergent in all LCs and similar to wheat LC_{crop} had lower yield magnitudes in both time series. In the case of rice, intercept differences were significant for LC_{crop} and LC_{LUH}, unlike for LC_{nat} and LC_{natpas}, but the paired t-test showed that all the LC had significant differences during the first simulation years (Figure 3.6) and LC_{crop} had the highest difference in intercepts.

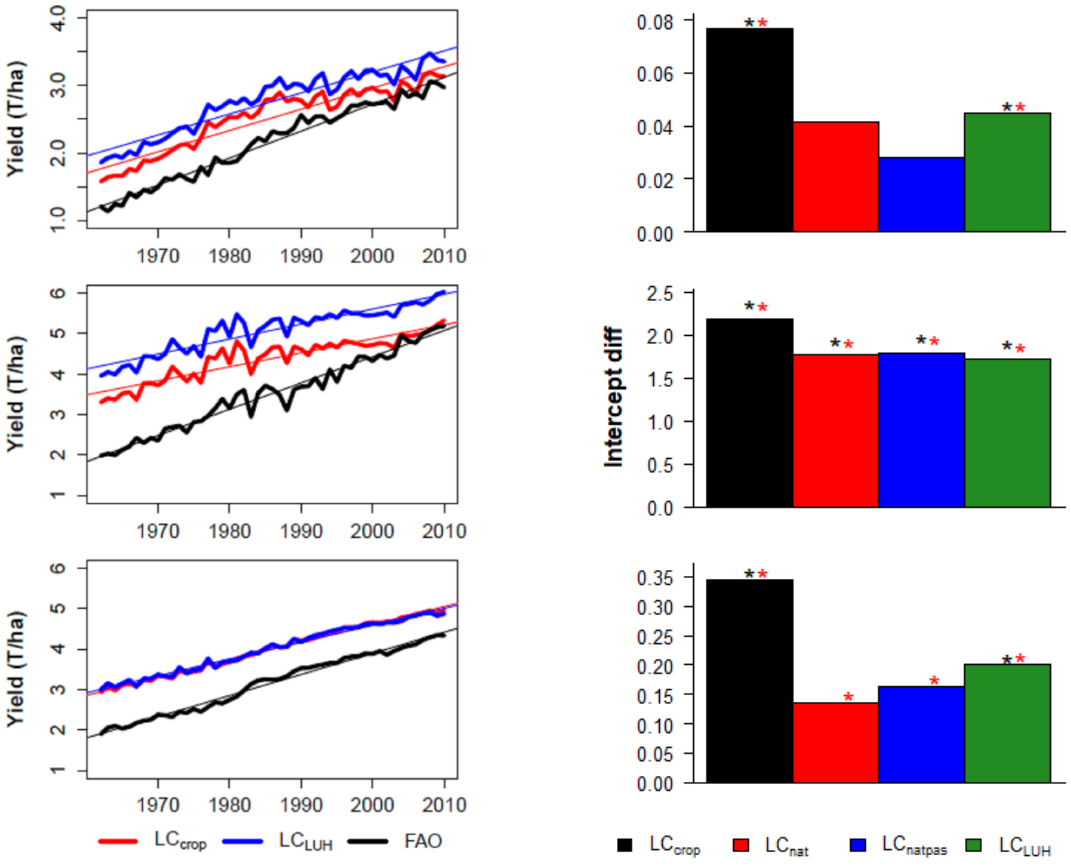

Figure 3.6. Left: Global yield time series simulated with LPJ-GUESS (Allvar and LC_{crop}) and reported by FAO. Right: Intercept of the absolute differences of adjusted lines by LC. (*) means significant difference of intercept at 95% confidence. (*) means significant difference based on the paired T-test between high and low fertilisation time series between 1961 and 1970 with all driver constant (Allcons). Top: wheat, middle: maize, bottom: Rice

3.5. DISCUSSION

Global simulated yield trends were strongly affected by the land cover history. Simulations using a previous cover of natural vegetation and pastures such as LC_{nat} and LC_{natpas} caused high yields after the transition period to cropland around 1960 and 1980, depending on the forcing climate and, consequently, later inflection points compared LC_{crop} and LC_{LUH}. This effect was clearer in Allcons, Radvar, Precvar and Tempvar because driver combinations causing strongly increasing trends like Allvar, Fervar and CO2var for wheat and rice compensate for the depletion of legacy soil N pools quicker and hence reaching an earlier inflection point (Figure 3.1). Allcons was expected to have late inflection points for all crops and climates, but it did not occur in wheat and rice in LC_{crop} and LC_{LUH} since these crops showed a slightly increasing slope (Figures 3.3 and S3-2), probably caused by cumulative fertiliser effect or another factor not considered in this study.

High yields after the transition to cropland in LC_{nat} and LC_{natpas} caused low to negative slopes since, after the inflection point, yields tended to converge to LC_{crop} values. High yields are caused by the conversion from natural vegetation to cropland, which requires killing living vegetation; most of the biomass is oxidised or removed, and about 12% goes to the litter. However, litter, soil C and soil N pools accumulated during the previous years and centuries by natural vegetation and pastures remain in the new managed land (Krause et al. 2016), increasing productivity in LC_{nat} and LC_{natpas} compared to LC_{crop} in the period following the transition. In LC_{crop} and LC_{LUH}, soil N and C stocks are reduced due to extraction of biomass during harvest and soil degradation from tillage (Guo and Gifford 2002) (Figures S3-4 and S3-5).

Fertilisation was also the main factor contributing to the variation of the simulated global yield of wheat and rice in LC_{crop} and LC_{LUH}. It is compatible with actual global yield since fertiliser usage has been one of the critical drivers of global yield since the green revolution (García-Lara and Serna-Saldivar 2019). However, the effect of higher legacy soil organic matter and soil N and C after land cover conversion to crops in LC_{nat} and LC_{natpas} suppressed yield limitation by fertiliser, decreasing variation compared to LC_{crop} and LC_{LUH} (Figures 3.3 and 3.4). In LC_{nat} and LC_{natpas}, climate variables are the main factors causing yield variability similar to the values of the variability expected by the climate in crop yields, primarily by precipitation and air temperature, in crops which are around 35% for wheat, 41% for maize and 32% for rice (Ray et al. 2015).

Differences between time series from high and low fertilisation locations during the first years of the evaluated period correspond with the mentioned effect. In LC_{nat} and LC_{natpas} yields of both time series, low and high fertiliser, are enhanced by higher legacy soil C and N pools (Olin et al. 2015a) and yield depletion in low fertiliser regions starts rapidly, causing negative trends in maize and wheat. While in high fertiliser regions, yield continues increasing during the whole evaluated period. In LC_{crop} and LC_{LUH}, on the other side, yields of both regions are low at the start of the historical simulation and during the first years, wheat yield is sensitive to the effect of the low fertilisation producing an increasing trend that spans for around 15 years when a marked yield depletion occurs abruptly. In maize a slight increase of yield occurs during the period of evaluation (Figure S3-6).

In croplands, 90% of the harvested biomass was assumed to be removed from the ecosystem mainly by crop harvest. In pastures, only 50% is assumed to be removed,

representing the fraction of biomass oxidised during grazing, whereas, in natural vegetation, removal is zero. This causes the depletion of soil C and N, in croplands after conversion until they reach a new equilibrium level, which can take centuries, depending on the climate (Pugh et al. 2015). In addition, this effect is enhanced by management activities favouring soil heterotrophic respiration, like tillage and irrigation (Godfray et al. 2010; Olin et al. 2015a; Krause et al. 2016).

Residue outtake is also an important practice in croplands. It was set to 75% in this study, while it is assumed to be zero in natural vegetation and pastures. Like harvested biomass, residue outtake causes depletion of soil C and N stocks, which retains water (effect not simulated in LPJ-GUESS) and nutrients, causing a reduction in soil fertility and plant productivity. The simulated decrease in carbon stocks, nitrogen limitation and lower plant productivity after LC conversation, as found in LC_{nat} and LC_{natpas}, is common in conversions from natural vegetation to crops, both in observations and modelling (Guo and Gifford 2002; Olin et al. 2015a; Pugh et al. 2015; Nyawira et al. 2016).

LC_{LUH} showed similar slopes to LC_{crop}, and although intercepts were higher in maize and wheat when CRU-NCEP climate was used (and not significantly different with AgMERRA), they were lower than intercepts of LC_{nat} and LC_{natpas}. Similarities between LC_{crop} and LC_{LUH} are caused by the highly productive areas of the three crops. These areas are responsible for a large fraction of global food production and have been covered by crops during several decades (Goldewijk et al. 2017; Potapov et al. 2022). Therefore, similar to LC_{crop}, by the start of the simulation these areas have depleted soil C and N stocks. Some authors report that the period between 1900 and 1930 had the most substantial extension of croplands in USA, Europe and

China while in the subsequent years, the tendency was to intensify agriculture (Ramankutty et al. 2002).

Although N content (Soil and litter) patterns of LC_{LUH} are similar to LC_{nat} and LC_{natpas}, this occurs because due to the net transitions between land covers LC_{LUH} simulations also had fractions of pasture and natural coverage in most grid cells and hence the values output are an average across all the land covers in the grid cell, rather than being representative just for cropland (Figures S3-4 and S3-5). In general, LC_{LUH} had lower N globally, but mostly in regions with a high fraction of cropland in LUH2, meaning that those areas in 1960 had already undergone substantial nutrient depletion and soil degradation processes such as in the Corn belt in USA, Eastern China, Western Europe and India (Figure 3.7). Average global values of soil N (kg ha^{-1}) only considering locations with more than 50% cropland in 1960 were 0.23 for LC_{crop}, 1.24 for LC_{nat}, 1.23 for LC_{natpas} and 1.04 for LC_{LUH}. Similarly, average values of N Litter (kg ha^{-1}) were 2.65 for LC_{crop}, 12.1 for LC_{nat}, 9.8 for LC_{natpas} and 5.94 for LC_{LUH}.

At the grid cell-scale, wheat slope differences between LC_{LUH} and LC_{crop} were close to 0 in Western and Eastern Europe, USA, Argentina and China. While the intercept differences were close to 0 in most of the harvested areas. Maize showed slope and intercept differences close to 0 in USA, Europe, and some regions of Asia, Africa and South America. Rice slope differences were close to 0 in China and USA but in China intercepts of LC_{LUH} were lower causing convergence between time series of both landcover setups. Simulations of crop yield in the regions above could use continuous cropland as land cover before the historical simulation to save time and computer resources obtaining similar yields than LC_{LUH} (Figure S3-7).

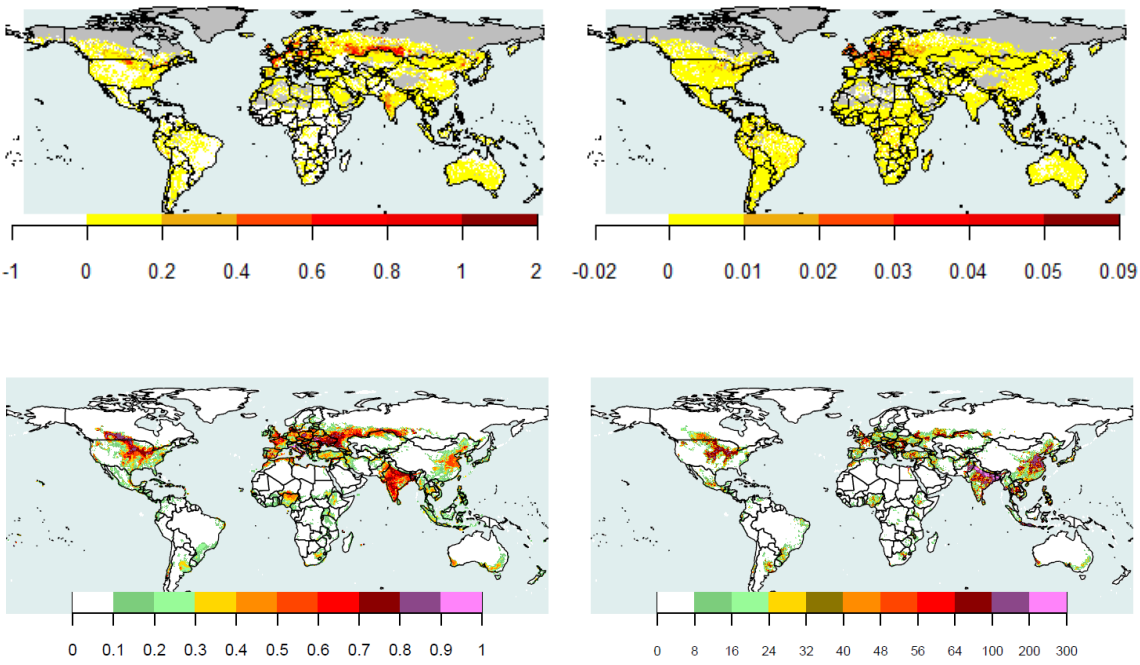

Figure 3.7. Top- Left: Difference between LC_{nat} and LC_{LUH} in soil N (left) and soil N in litter (right) for the year 1960 (kg ha^{-1}). Bottom- Left: LUH2 proportion of cropland in 1960 used in LC_{LUH}. Right: Wheat, Maize, and Rice harvested areas used for simulations in 1960 (Thousand of ha).

In all the evaluated LCs with CRU-NCEP, fertiliser was the most critical contributor to the yield increase for all the crops, followed by [CO_2] for wheat and rice. Likewise, higher atmospheric [CO_2] is expected to increase agricultural productivity in C3 photosynthetic pathway plants like wheat and rice. It has been estimated that the current rate of increase of [CO2] of 2 ppm yr^{-1} results in about about a 0.3% yr^{-1} increase in yield (Fischer and Edmeades 2010; Smith et al. 2014; Alexander et al. 2018). Maize does not show an increasing effect on yield caused by [CO_2] since it is a C4 photosynthetic pathway plant whose characteristic is to carry out the Calvin Cycle in nearly saturated conditions. Thus no direct effect of increased [CO_2] is expected (HAMIM 2005; Wang et al. 2020). An increase in maize yield due to [CO_2] is mainly related to the reported decrease in evapotranspiration and the improvement

of water use efficiency, especially in water limited locations. However, this effect has been reported in FACE experiments and simulations by doubling the [CO_2] (Deryng et al. 2016). In the present study, the effect was found to be minor, consistent with a difference of 73 ppm between 1960 and 2010.

The simulated increases in yield are compatible with the fact that between 1960 and 2010, food production per capita doubled in Asia, by a factor of 3.5 in China and 1.6 in Latin America. A general world productivity increase has occurred based on technical knowledge, access to technology and resources like irrigation, machinery, crop protection and sustainable soil practices, but mainly, fertiliser usage has increased critically after the green revolution (Godfray et al. 2010; García-Lara and Serna-Saldivar 2019). That LPJ-GUESS was able to capture most of the observed increase in yield since 1960 based on only increases in [CO_2] and N fertilisation rates suggests that these two factors are responsible for most of the observed increase, with the remaining annual increase per year being driven by other technological developments.

However, about 37% of wheat, 26% of maize and 35% of rice in global harvested areas have shown yield stagnation in the last three decades; mainly caused by climate changes and temperature increase in developed countries and socio-economic limitations in other locations like Africa (Ray et al. 2012). A high portion of these areas are located in top producer countries, while most of the yield-increasing areas during this period are located in lower producer countries. This situation affects the global yield trend and challenging food security in the growing population world (Ray et al. 2012). Stagnation of yield caused lower slopes in the simulations with AgMERRA since they only included the period of slower yield increase reported in

FAOstat (Food and Agriculture Organization of the United Nations, 2020, Figure 3.6) and explained by the impact of climate change after 1974 (Ray et al. 2012, 2019).

Intercept and slope differences between LCs were lower in rice and only significant between LC_{nat} and LC_{crop}. This has been reported in inundated environment most of the rice areas since anoxic conditions inhibit the N mineralisation, so the availability of nutrients for plants and also increase the N gaseous losses (Kader et al. 2013). In LPJ-GUESS the inundated setup decreases the N leaching and N mineralization and increases N fixation.

Whilst LPJ-GUESS tends to overestimate yield in the early period of the simulations, the overestimation decreases over time, with good correspondence between model and observations for wheat and maize in the period 2000-2010. This effect was particularly pronounced in countries with high slopes of yield increase. It is to be expected because LPJ-GUESS is parameterised to simulate yields under recent growing conditions (Camargo-Alvarez et al., 2022). Also, the high- and low-yielding spatial distribution for maize was based on yield data between 2000 and 2010, and historical distribution before that period is expected to have larger areas of low-yielding maize (Camargo-Alvarez et al. 2022).

Additionally, the model is incapable to capture several mechanisms which could decline yield like pest outbreaks, partial irrigation (the model assumes full irrigation in irrigated areas), air and water pollution, and soil degradation in addition to phosphorus, potassium and other nutrients dynamics which are not yet implemented in LPJ-GUESS and have been reported to be responsible for a yield gap of between 22% for wheat and 50% for maize in the case of phosphorus and 2% for wheat and

26% for maize in the case of potassium (Dai et al. 2013; Kvakić et al. 2021). The yield gap caused by the mentioned yield declining factors has been reduced lately due to the use of several management technologies such as mechanisation, improved nutrient and water management, integrated pest management and the use of cultivars with high potential yield and tolerance to high plant density, biotic and abiotic stresses (Duvick 2005; Darrah et al. 2019).

This increase in yield mainly occurred at the top producer countries with higher increases in yield and pulling up the simulated global yield trends (Figure 3.5). Besides the technological adaptation and intensive systems with high-income most of these countries, such as China, India, USA, and Pakistan for wheat; USA, China, Brazil and Mexico for maize; and China, India, Indonesia, Bangladesh, and Vietnam for rice, are in regions of high N fertilisation (Figure S3-8) (Duvick 2005; Darrah et al. 2019). Production in small countries has also been accelerated and enhanced by international research centres that help smallholder farmers adopt new technologies and practices (Ray et al. 2012; Yamano et al. 2016).

In rice, a systems classification is more complex than the irrigated and rainfed schemes used in the SPAM database. Rice can grow in inundated semiaquatic environments (lowlands) and dry rainfed (upland) or irrigated fields, known as aerobic (Vijayaraghavareddy et al. 2020). In this study, for simplification and due to the lack of upland-lowland distribution databases, irrigated and rainfed rice from SPAM were used as lowland and upland systems, respectively. However, this method could cause an overestimation of rice yield since some of the irrigated SPAM areas could be planted with upland rice (aerobic rice), and the highest reported yield in rice is obtained from irrigated lowland (Vijayaraghavareddy et al. 2020; Dianga et al. 2022).

Similarly, rainfed SPAM areas could be covered with lowland but non-irrigated rice, which also presents a lower yield.

Finally, another source potentially increasing global simulated yield was the estimation of the historical N application rate database using AgMIP fertiliser data as reference for the year 2000 and the relative interannual variation from Lu and Tian, (2017) to interpolate fertilisation rate and estimate the historical database from 1961 to 2010. AgMIP fertiliser database reports, in general, higher fertilisation rates than Lu and Tian database, mostly in big crop producer countries such as USA, and central and western Europe, possibly causing an overestimation of historical fertilisation rates, primarily for years before the 90s.

3.6. CONCLUSIONS

The analysis performed in this study highlights the importance of land cover history in simulations of crop production and its effect on yield historical trends for wheat, maize and rice. It also exposed the critical role of input databases, such as fertilisation, [CO_2], climate variables and their interaction with land cover history in slopes, and interannual variability of historical time series of simulated yield. This will be particularly useful for interpreting the results and dynamics of historical and future simulations and increasing the accuracy of large-scale yield simulations and the impacts of climate change and terrestrial biogeochemical cycles on food production.

Trend and interannual variability of the global yield of wheat, maize and rice were sensitive to the land cover history. Simulations assuming unmanaged land cover before transitions to cropland showed an overestimation of yields during the first period of the historical simulation. Using historical land cover databases such as

LUH2 produced a higher global yield for maize and wheat than the global yield obtained only assuming cropland before the simulations but showed similar slopes in all the drivers and for each of the three crops. This occurred because most of the production in the world is coming from highly stable cropland regions. It is therefore recommended that, the study of global or large scale crop yields, using cropland as land cover before the simulations is acceptable and will save computer and time resources and avoid extra overestimating yield. However, if the simulation is being used to assess carbon stock changes or other biogeochemical cycles, taking account of land cover history is crucial.

Simulated global yield trends were sensitive to fertilisation input database and soil fertility. Furthermore, soil N and C pools accumulated before the crop simulation increased yield significantly during several years after the land cover change from natural vegetation or pastures to cropland, this effect was particularly marked in regions with low fertilisation input. In rice, the effect of initial soil fertility conditions on the yield is less marked compared to the other crops, potentially due to the inundated management of rice in most of the harvested area. Another important contributor to increasing the global yield trend for the C3 crops wheat and rice was [CO_2], however a negligible effect of [CO_2] was found for the C4 pathway crop maize. An effect of fertilisation on the interannual yield variability was also found, which interacted with the consideration of land cover legacies. Climate, more specifically precipitation and air temperature, were also critical contributors to interannual variability, mainly in simulations where fertilisation was a less limiting factor, such as simulations of LC_{nat} and LC_{natpas}.

This study showed an overestimated global simulated yield compared to the FAO time series before and during the 90s, more significant in maize but existing in the three crops. Overestimation occurred since the model does not estimate yield limitations such as pests, partial irrigation, pollution, and soil degradation, but also due to the lack of a historical cultivar distribution database, management practices and the uncertainty in historical fertiliser databases. Development of historical databases covering these factors would likely substantially improve ability of crop models like LPJ-GUESS to simulate yield trends over time.

3.7. REFERENCES

Alexander P, Rabin S, Anthoni P, et al (2018) Adaptation of global land use and management intensity to changes in climate and atmospheric carbon dioxide. Glob Chang Biol 24:2791–2809. https://doi.org/10.1111/gcb.14110

Batjes NH (2016) Total carbon and nitrogen in the soils of the world N. Eur J Soil Sci 65:1365–2389. https://doi.org/10.1097/00002480-200007000-00002

Bayer AD, Lindeskog M, Pugh TAM, et al (2017) Uncertainties in the land-use flux resulting from land-use change reconstructions and gross land transitions. Earth Syst Dyn 8:91–111. https://doi.org/10.5194/esd-8-91-2017

Bustamante M, Robledo-Abad C, Harper R, et al (2014) Co-benefits, trade-offs, barriers and policies for greenhouse gas mitigation in the agriculture, forestry and other land use (AFOLU) sector. Glob Chang Biol 20:3270–3290. https://doi.org/10.1111/gcb.12591

Camargo-Alvarez H, Elliott RJR, Olin S, et al (2022) Modelling crop yield and harvest index: the role of carbon assimilation and allocation parameters. Model Earth Syst Environ. https://doi.org/10.1007/s40808-022-01625-x

Dai X, Ouyang Z, Li Y, Wang H (2013) Variation in yield gap induced by nitrogen, phosphorus and potassium fertilizer in north china plain. PLoS ONE 8(12): e82147. https:doi:10.1371/journal.pone.0082147

Darrah LL, McMullen MD, Zuber MS (2019) Breeding, genetics and seed corn production. In: Corn: Chemistry and Technology, 3rd Edition, 3rd edn. Elsevier Inc., pp 19–41

Deryng D, Elliott J, Folberth C, et al (2016) Regional disparities in the beneficial effects of rising CO2 concentrations on crop water productivity. Nat Clim Chang 6:786–790. https://doi.org/10.1038/nclimate2995

Dianga A-I, N. Musila R, W. Joseph K (2022) Rainfed Rice Farming Production Constrains and Prospects, the Kenyan Situation. Integr Adv Rice Res. https://doi.org/10.5772/intechopen.98389

Duvick DN (2005) Genetic progress in yield of United States maize (Zea mays L.). Maydica 50:193–202

Elliott J, Müller C, Deryng D, et al (2015) The global gridded crop model intercomparison: data and modeling protocols for phase 1 (v1.0). Geosci Model Dev 8:261–277. https://doi.org/10.5194/gmd-8-261-2015

Fischer RA, Edmeades GO (2010) Breeding and cereal yield progress. Crop Sci 50:S-85-S-98. https://doi.org/10.2135/cropsci2009.10.0564

Folberth C, Elliott J, Müller C, et al (2016) Uncertainties in global crop model frameworks: effects of cultivar distribution, crop management and soil handling on crop yield estimates. Biogeosciences Discuss 1–30. https://doi.org/10.5194/bg-2016-527

Food and Agriculture Organization of the United Nations (2020) FAOSTAT. http://www.fao.org/faostat/en. Accessed 3 Apr 2020

García-Lara S, Serna-Saldivar SO (2019) Corn history and culture. In: Corn: Chemistry and Technology, 3rd Edition. pp 1–18

Godfray HCJ, Beddington JR, Crute IR, et al (2010) Food security: The challenge of the feeding 9 billion people. Science (80-) 327:812–818. https://doi.org/10.1016/j.geoforum.2018.02.030

Goldewijk KK, Beusen A, Doelman J, Stehfest E (2017) Anthropogenic land use estimates for the Holocene - HYDE 3.2. Earth Syst Sci Data 9:927–953. https://doi.org/10.5194/essd-9-927-2017

Goldewijk KK, Ramankutty N (2004) Land cover change over the last three centuries due to human activities : The availability of new global data sets. GeoJournal 61:335–344

Guo LB, Gifford RM (2002) Soil carbon stocks and land use change: A meta analysis. Glob Chang Biol 8:345–360. https://doi.org/10.1046/j.1354-1013.2002.00486.x

HAMIM (2005) Photosynthesis of C3 and C4 Species in Response to Increased CO2 Concentration and Drought Stress. HAYATI J Biosci 12:131–138. https://doi.org/10.1016/S1978-3019(16)30340-0

Houghton RA, Nassikas AA (2017) Global and regional fluxes of carbon from land use and land cover change 1850–2015. Global Biogeochem Cycles 31:456–472. https://doi.org/10.1002/2016GB005546

Hurtt GC, Chini L, Sahajpal R, et al (2020) Harmonization of global land use change and management for the period 850-2100 (LUH2) for CMIP6

IPCC (2017) Climate Change and Land

Jackson ND, Konar M, Debaere P, Estes L (2019) Probabilistic global maps of crop-specific areas from 1961 to 2014. Environ Res Lett 14:094023. https://doi.org/10.1088/1748-9326/ab3b93

Jägermeyr J, Müller C, Ruane A, et al (2021) Climate change signal in global agriculture emerges earlier in new generation of climate and crop models. Nat Food 2:873–885. https://doi.org/https://doi.org/10.1038/s43016-021-00400-y.

Kader MA, Sleutel S, Begum SA, et al (2013) Nitrogen mineralization in sub-tropical paddy soils in relation to soil mineralogy, management, pH, carbon, nitrogen and iron contents. Eur J Soil Sci 64:47–57. https://doi.org/10.1111/ejss.12005

Kanianska R (2016) Agriculture and its Impact on Land-Use, Environment, and Ecosystem Services. In: Landscape Ecology - The influences of Land Use and Anthropogenic impacts of landscape Creation. pp 7–26

Krause A, Pugh TAM, Bayer AD, et al (2016) Impacts of land-use history on the recovery of ecosystems after agricultural abandonment. Earth Syst Dyn 7:745–766. https://doi.org/10.5194/esd-7-745-2016

Kvakić M, Pellerin S, Ciais P, Achat D, Augusto L, et al (2018) Quantifying the limitation to world cereal production due to soil phosphorus status. Global Biogeochemical Cycles 32 (1):143-157.

Lamarque JF, Bond TC, Eyring V, et al (2010) Historical (1850-2000) gridded anthropogenic and biomass burning emissions of reactive gases and aerosols: Methodology and application. Atmos Chem Phys 10:7017–7039. https://doi.org/10.5194/acp-10-7017-2010

Le Quéré C, Peters GP, Andres RJ, et al (2014) Global carbon budget 2013. Earth Syst Sci Data 6:235–263. https://doi.org/10.5194/essd-6-235-2014

Levene H (1960) Robust Tests for Equality of Variances. In: Contributions to Probability and Statistics. Stanford University Press, Palo Alto, pp 278–292

Lindeskog M, Arneth A, Bondeau A, et al (2013) Implications of accounting for land use in simulations of ecosystem carbon cycling in Africa. Earth Syst Dyn 4:385–407. https://doi.org/10.5194/esd-4-385-2013

Lu C, Tian H (2017) Global nitrogen and phosphorus fertilizer use for agriculture production in the past half century: Shifted hot spots and nutrient imbalance. Earth Syst Sci Data 9:181–192. https://doi.org/10.5194/essd-9-181-2017

Monfreda C, Ramankutty N, Foley JA (2008) Farming the planet: 2. Geographic distribution of crop areas, yields, physiological types, and net primary production in the year 2000. Global Biogeochem Cycles 22:1–19. https://doi.org/10.1029/2007GB002947

Mosier AR, Duxbury JM, Freney JR, et al (1998) Mitigating agricultural emissions of methane. Clim. Change 40:39–80

Mueller ND, Gerber JS, Johnston M, et al (2012) Closing yield gaps through nutrient and water management. Nature 490:254–257. https://doi.org/10.1038/nature11420

Müller C, Elliott J, Chryssanthacopoulos J, et al (2017) Global gridded crop model evaluation: benchmarking , skills , deficiencies and implications. Geosci Model Dev 10:1403–1422. https://doi.org/10.5194/gmd-10-1403-2017

Noszczyk T (2019) A review of approaches to land use changes modeling. Hum Ecol Risk Assess 25:1377–1405. https://doi.org/10.1080/10807039.2018.1468994

Nyawira SS, Nabel JEMS, Don A, et al (2016) Soil carbon response to land-use change: Evaluation of a global vegetation model using observational meta-analyses. Biogeosciences 13:5661–5675. https://doi.org/10.5194/bg-13-5661-2016

Olin S, Lindeskog M, Pugh TAM, et al (2015a) Soil carbon management in large-scale earth system modelling : implications for crop yields and nitrogen. Earth Syst Dyn 6:745–768. https://doi.org/10.5194/esd-6-745-2015

Olin S, Schurgers G, Lindeskog M, et al (2015b) Modelling the response of yields and tissue C : N to changes in atmospheric CO2 and N management in the main wheat regions of western Europe. Biogeosciences 12:2489–2515. https://doi.org/10.5194/bg-12-2489-2015

Potapov P, Turubanova S, Hansen MC, et al (2022) Global maps of cropland extent and change show accelerated cropland expansion in the twenty-first century. Nat Food 3:19–28. https://doi.org/10.1038/s43016-021-00429-z

Prentice IC, Webb RS, Ter-Mikhaelian MT, et al (1989) Developing A Global Vegetation Dynamics Model: Results of an IIASA Summer Workshop. Novographic, Laxenburg, Austria

Pugh TAM, Arneth A, Olin S, et al (2015) Simulated carbon emissions from land-use change are substantially enhanced by accounting for agricultural management. Environ Res Lett 10:. https://doi.org/10.1088/1748-9326/10/12/124008

R Core Team (2019) R: A language and environment for statistical computing

Ramankutty N, Foley JA, Olejniczak NJ (2002) People on the land: Changes in global population and croplands during the 20th century. Ambio 31:251–257. https://doi.org/10.1579/0044-7447-31.3.251

Ray DK, Gerber JS, Macdonald GK, West PC (2015) Climate variation explains a third of global crop yield variability. Nat Commun 6:1–9. https://doi.org/10.1038/ncomms6989

Ray DK, Ramankutty N, Mueller ND, et al (2012) Recent patterns of crop yield growth and stagnation. Nat Commun 3:1293–1297. https://doi.org/10.1038/ncomms2296

Ray DK, Sloat LL, Garcia AS, et al (2022) Crop harvest for direct food use insufficient to meet the UN's foos security goal. Nat Food. https://doi.org/10.1038/s43016-022-00504-z

Ray DK, West PC, Clark M, et al (2019) Climate change has likely already affected global food production. PLoS One 14:1–18. https://doi.org/10.1371/journal.pone.0217148

Schaefer H (2019) On the Causes and Consequences of Recent Trends in Atmospheric Methane. Curr Clim Chang Reports 5:259–274. https://doi.org/10.1007/s40641-019-00140-z

Smith B (2001) LPJ-GUESS – an ecosystem modelling framework. Dep Phys Geogr Ecosyst Anal INES, Sölvegatan 12:22362

Smith B, Prentice IC, Climate MTS (2001) Representation of vegetation dynamics in the modelling of terrestrial ecosystems : comparing two contrasting approaches within European climate space. Glob Ecol Biogepgraphy 10:621–637

Smith B, Wårlind D, Arneth A, et al (2014) Implications of incorporating N cycling and N limitations on primary production in an individual-based dynamic vegetation model. Biogeosciences 11:2027–2054. https://doi.org/10.5194/bg-11-2027-2014

United Nations (2019) World population prospects 2019, Online Edi

Vermeulen SJ, Aggarwal PK, Ainslie A, et al (2012) Options for support to agriculture and food security under climate change. Environ Sci Policy 15:136–144. https://doi.org/10.1016/j.envsci.2011.09.003

Vijayaraghavareddy P, Xinyou Y, Struik PC, et al (2020) Responses of Lowland, Upland and Aerobic Rice Genotypes to Water Limitation During Different Phases. Rice Sci 27:345–354. https://doi.org/10.1016/j.rsci.2020.05.009

Waha K, Van Bussel LGJ, Müller C, Bondeau A (2012) Climate-driven simulation of global crop sowing dates. Glob Ecol Biogeogr 21:247–259. https://doi.org/10.1111/j.1466-8238.2011.00678.x

Wang F, Gao J, Yong JWH, et al (2020) Higher Atmospheric CO2 Levels Favor C3 Plants Over C4 Plants in Utilizing Ammonium as a Nitrogen Source. Front Plant Sci 11:1–16. https://doi.org/10.3389/fpls.2020.537443

Wramneby A, Smith B, Zaehle S, Sykes MT (2008) Parameter uncertainties in the modelling of vegetation dynamics-Effects on tree community structure and

ecosystem functioning in European forest biomes. Ecol Modell 216:277–290. https://doi.org/10.1016/j.ecolmodel.2008.04.013

Yamano T, Arouna A, Labarta RA, et al (2016) Adoption and impacts of international rice research technologies. Glob Food Sec 8:1–8. https://doi.org/10.1016/j.gfs.2016.01.002

3.8. SUPPLEMENTARY MATERIAL

3.8.1. S3-1. Rice calibration

Rice was calibrated following the methodology presented in Camargo-Alvarez et al., (2022). Eigth parameters were constrained based on four reference datasets. One candidate setup (combination of parameters) was selected from each reference dataset as presented in Table S3-1.1 and the best setup was selected based on a production-weighted mean absolute error for yield calculated at the country and gridcell scale. Yield and harvest index obtained with the selected setup produced the yield and harvest indes described in Figures S3-1.1 and S3-1.2.

Table S3-1.1. Selected setups according to reference dataset for rice and original setups in LPJ-GUESS. (-Av) represents the setups based on the parameters mean of the ten best setups. The shaded row represents the selected setup after global evaluation

Crop	Dataset	Sret	SLA	C:Nmin	C:Nrange	Nret	Cret	kN	Ndred
Rice	**Ray**	1	45	5	2.78	0.40	0.40	0.30	2.72
Rice	**FAO**	1	50	5	2.78	0.40	0.40	0.30	0
Rice	**Ray-Av**	0.9	47.5	5	3.07	0.37	0.37	0.29	23.03
Rice	**FAO-Av**	1	46.5	5	3.21	0.37	0.39	0.28	0.82
Rice	**Original**	**1**	**45**	**7**	**5**	**0.1**	**0.1**	**0.27**	**0**

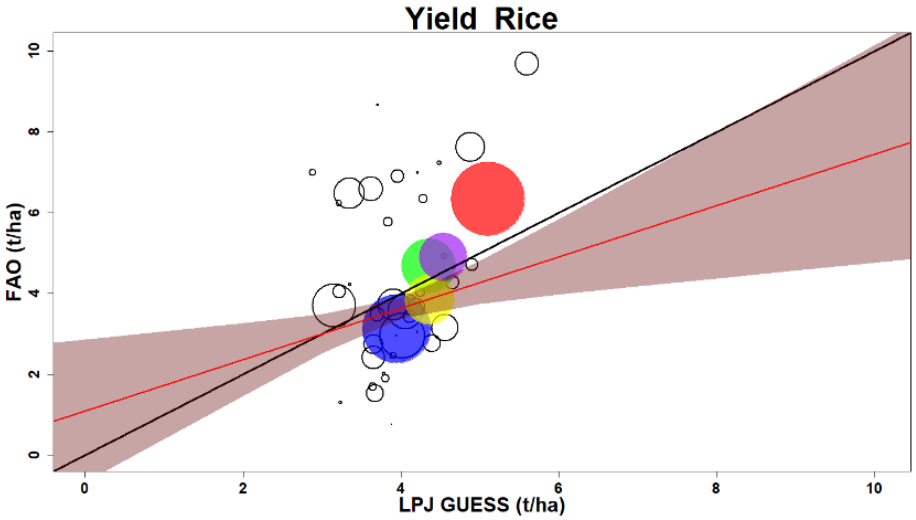

Figure S3-1.1. By country comparison between simulated yields with LPJ-GUESS and reported by FAO averaged values (2001-2010) for rice. Circle size is proportional to production reported by FAO during the same period. Coloured dots show the five top producers in the world. In order: Red (China), Blue (India), Green (Indonesia), Yellow (Bangladesh) and Purple (Vietnam). Red lines represent the adjusted linear regression between simulated and observed yields. Shaded areas show the 95% confidence interval, and black lines represent the 1:1 line

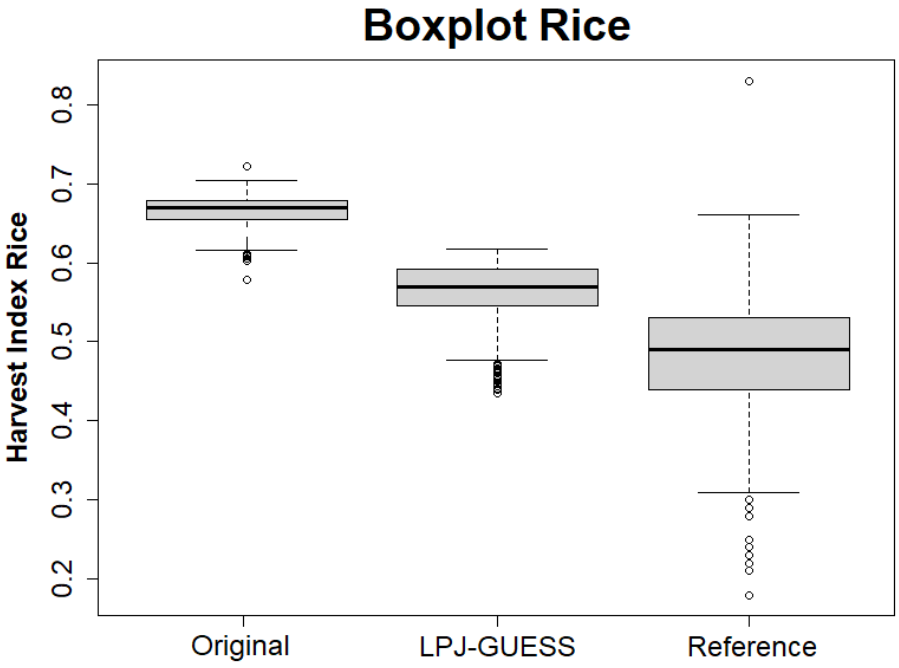

Figure S3-1.2. Boxplot for HI from the compiled database and simulated HI using the original model and the newly selected setup for rice

3.8.2. Additional results

Table S3-1. Ancova p-values for the evaluated effects on global simulated yield of the mentioned crops. LC (land cover change). Shaded values are non-significant at the 95% confidence

	Wheat		Maize		Rice	
Effect	**CRU-NCEP**	**AgMERRA**	**CRU-NCEP**	**AgMERRA**	**CRU-NCEP**	**AgMERRA**
LC	<0.001	<0.001	<0.001	<0.001	<0.001	<0.001
Drivers	<0.001	<0.001	<0.001	<0.001	<0.001	<0.001
Time*LC	<0.001	<0.001	<0.001	<0.001	<0.001	<0.001
Time*Drivers	<0.001	<0.001	<0.001	<0.001	<0.001	<0.001
LC*Drivers	0.201	0.994	0.99	0.99	<0.001	0.985
Time*LC*Drivers	0.844	1.000	0.941	0.99	<0.001	0.99

Table S3-2. Linear regression p-values for the Land use evaluated effects on global simulated yield of the mentioned crops. LC (land cover change). Shaded values are non-significant at the 95% confidence

	Wheat		Maize		Rice	
Effect	**CRU-NCEP**	**AgMERRA**	**CRU-NCEP**	**AgMERRA**	**CRU-NCEP**	**AgMERRA**
Int LCcrop	<0.001	<0.001	<0.001	<0.001	<0.001	<0.001
Int LCnat-LCcrop	<0.001	<0.001	<0.001	<0.001	0.003	0.001
Int LCnatpas-LCcrop	<0.001	<0.001	<0.001	<0.001	0.115	0.004
Int LCLUH-LCcrop	0.001	0.460	<0.001	0.651	0.240	0.172
Slope LCcrop	<0.001	0.005	0.060	0.180	<0.001	<0.001
Slope LCnat-LCcrop	<0.001	<0.001	<0.001	<0.001	0.001	0.009
Slope LCnatpas-LCcrop	<0.001	<0.001	0.014	<0.001	0.009	0.028
Slope LCLUH-LCcrop	0.811	0.606	0.586	0.705	0.293	0.853

Table S3-3. Linear regression p-values for the evaluated effects on global simulated yield of the mentioned crops. LC (land cover change). Shaded values are non-significant at the 95% confidence

	Wheat		Maize		Rice	
Effect	**CRU-NCEP**	**AgMERRA**	**CRU-NCEP**	**AgMERRA**	**CRU-NCEP**	**AgMERRA**
Int Allvar	<0.001	<0.001	<0.001	<0.001	<0.001	<0.001
Int Allcons-Allvar	0.022	0.007	0.002	0.506	0.312	0.017
Int CO2var-Allvar	0.005	0.013	0.002	0.468	0.024	0.007
Int Fervar-Allvar	<0.001	0.053	0.739	0.096	0.493	0.421
Int Precvar-Allvar	0.004	0.394	0.016	0.001	0.014	<0.001
Int Radvar-Allvar	0.026	0.422	0.003	0.096	0.114	0.093

Int Tempvar-Allvar	0.031	0.006	0.001	0.079	<0.001	<0.001
Slope Allvar	<0.001	0.005	<0.001	<0.001	<0.001	<0.001
Slope Allcons-Allvar	<0.001	<0.001	<0.001	<0.001	<0.001	<0.001
Slope CO2var-Allvar	<0.001	0.656	<0.001	<0.001	<0.001	<0.001
Slope Fervar-Allvar	<0.001	0.002	0.115	0.057	<0.001	<0.001
Slope Precvar-Allvar	<0.001	<0.001	<0.001	<0.001	<0.001	<0.001
Slope Radvar-Allvar	<0.001	<0.001	<0.001	<0.001	<0.001	<0.001
Slope Tempvar-Allvar	<0.001	<0.001	<0.001	<0.001	<0.001	<0.001

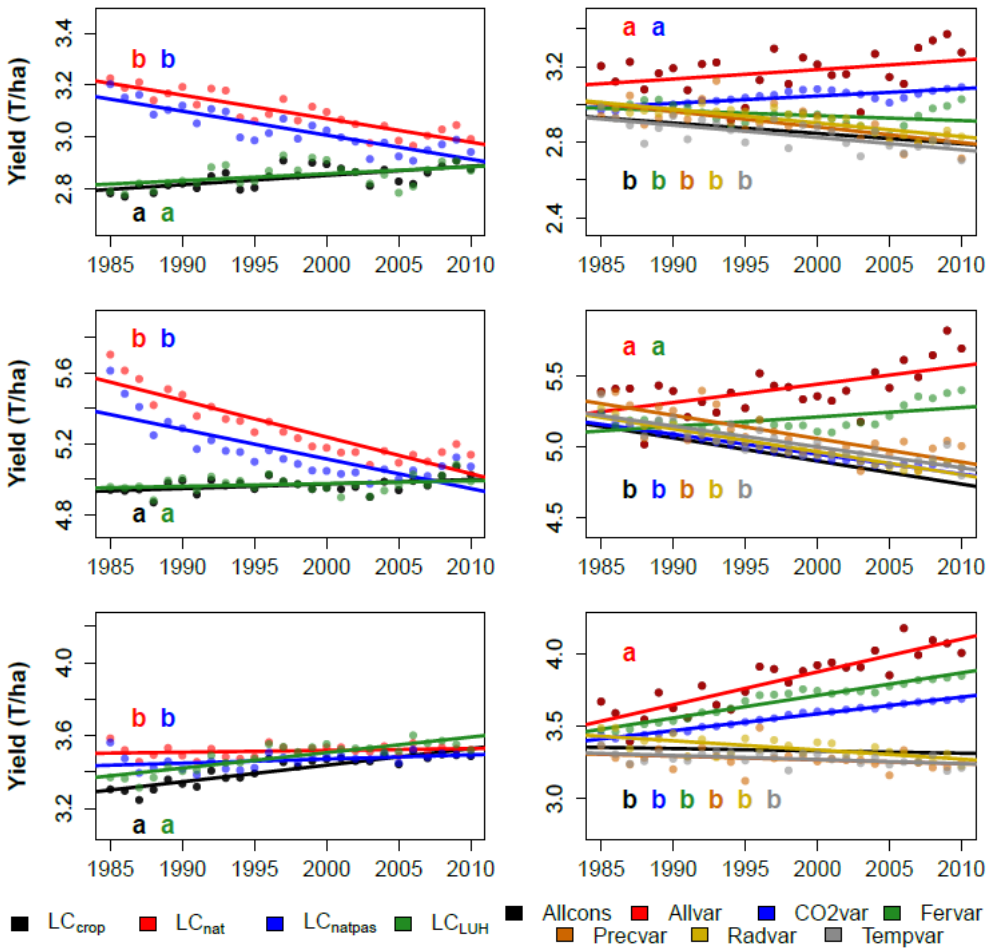

Figure S3-1. Adjusted trends for time series of global simulated yield with AgMERRA. Left: land cover change levels (yearly average of all driver levels) and right: driver levels (yearly average of all LC levels). Top: wheat, middle: maize, bottom: Rice

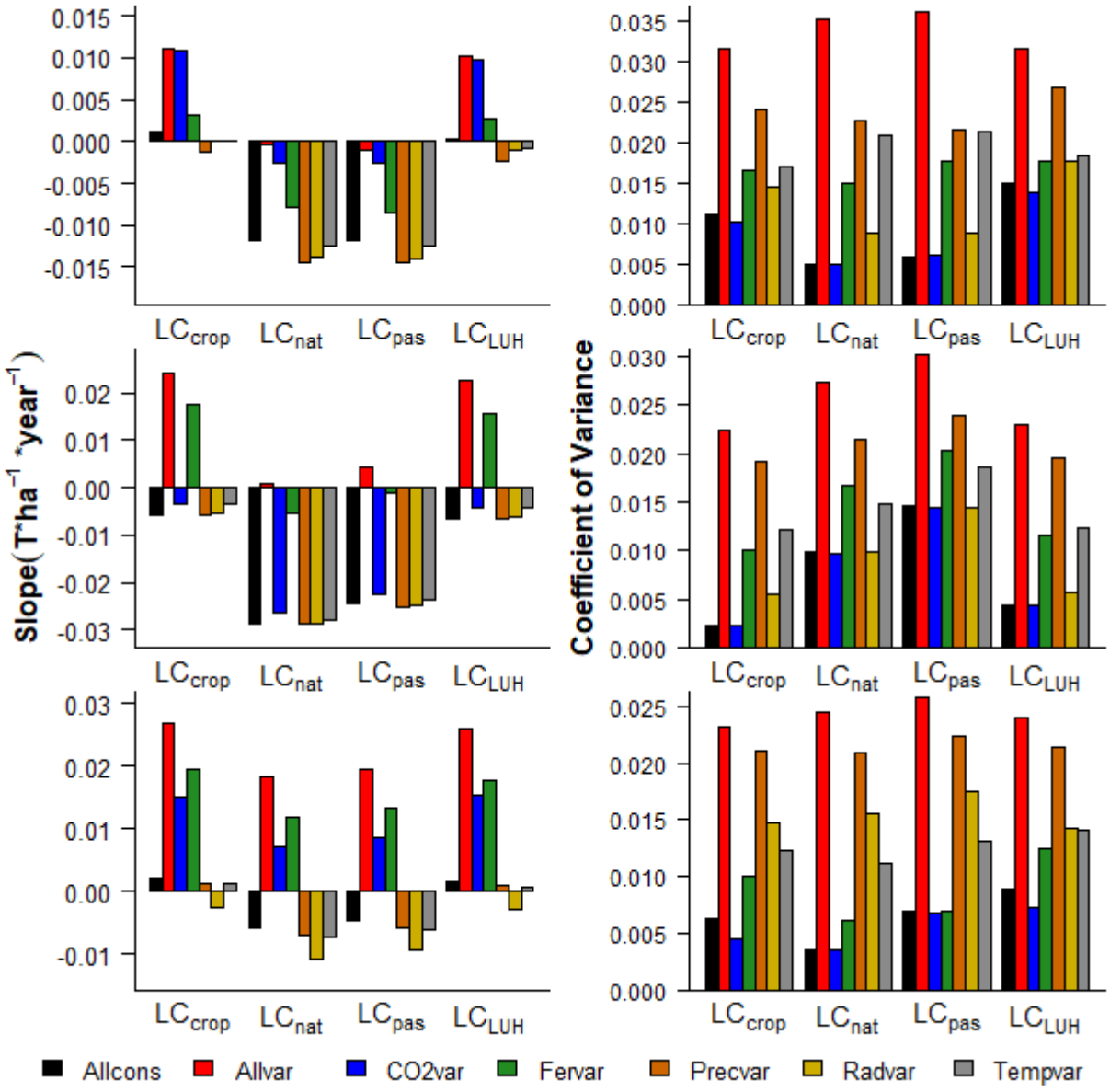

Figure S3-2. Slopes and coefficient of variation of time series simulated with AgMERRA as forcing climate. Combination of all levels for drivers (DRI) and land cover change (LC). Top: wheat, Middle: maize, Bottom: Rice

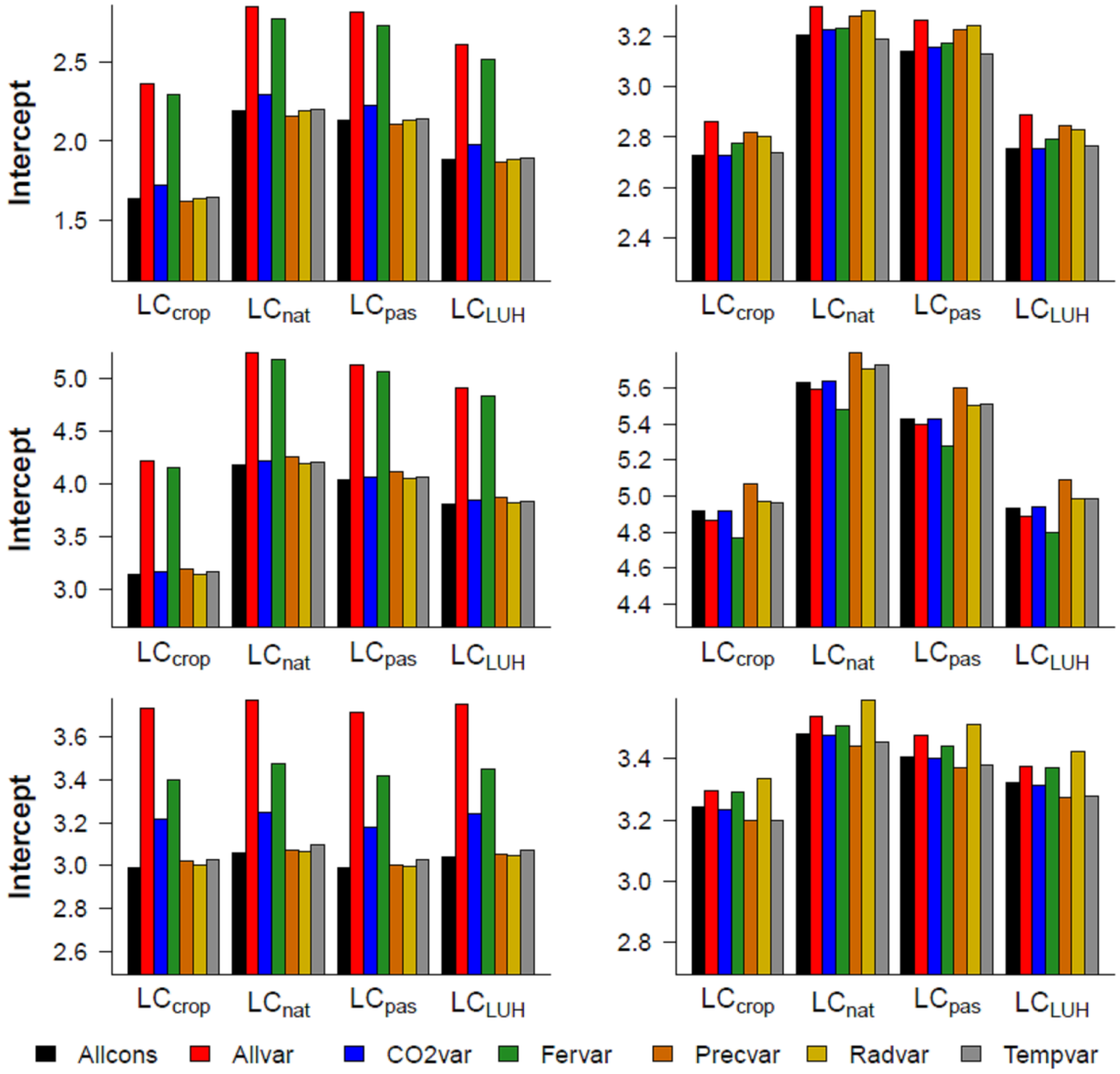

Figure S3-3. Intercepts of time series caused by the combination of all levels for drivers (DRI) and land cover change (LC). Top: wheat, Middle: maize, Bottom: Rice. Left: CRU-NCEP, right: AgMERRA

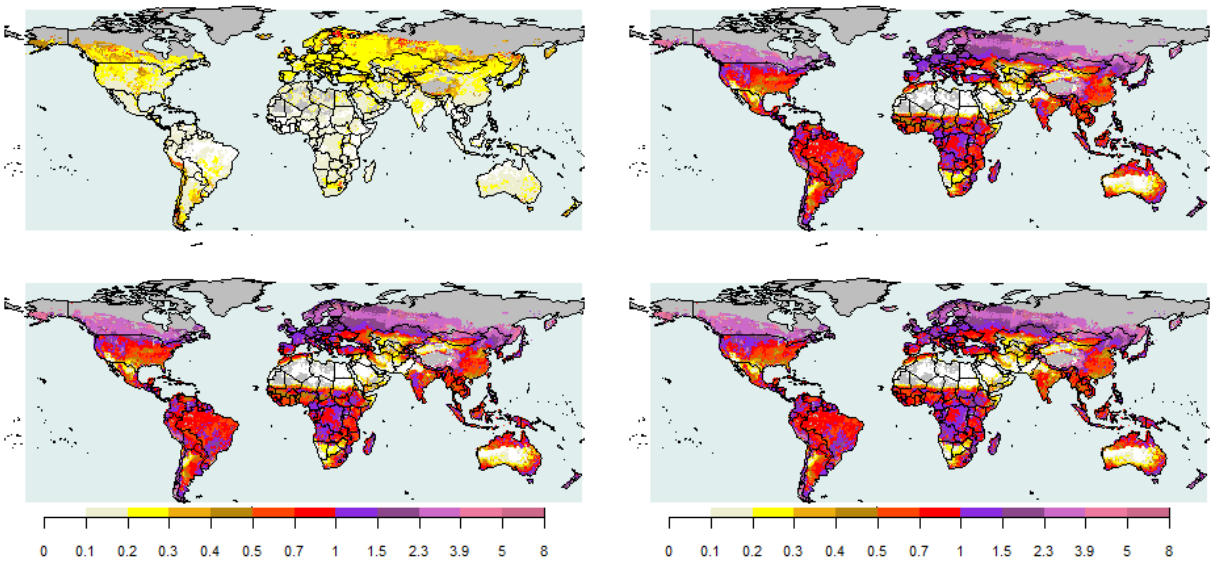

Figure S3-4. Soil Nitrogen (kg ha^{-1}) in 1960 for each LC level. Top-left: LC_{crop}, top-right: LC_{nat}, bottom-right: LC_{natpas}, bottom-left: LC_{LUH}

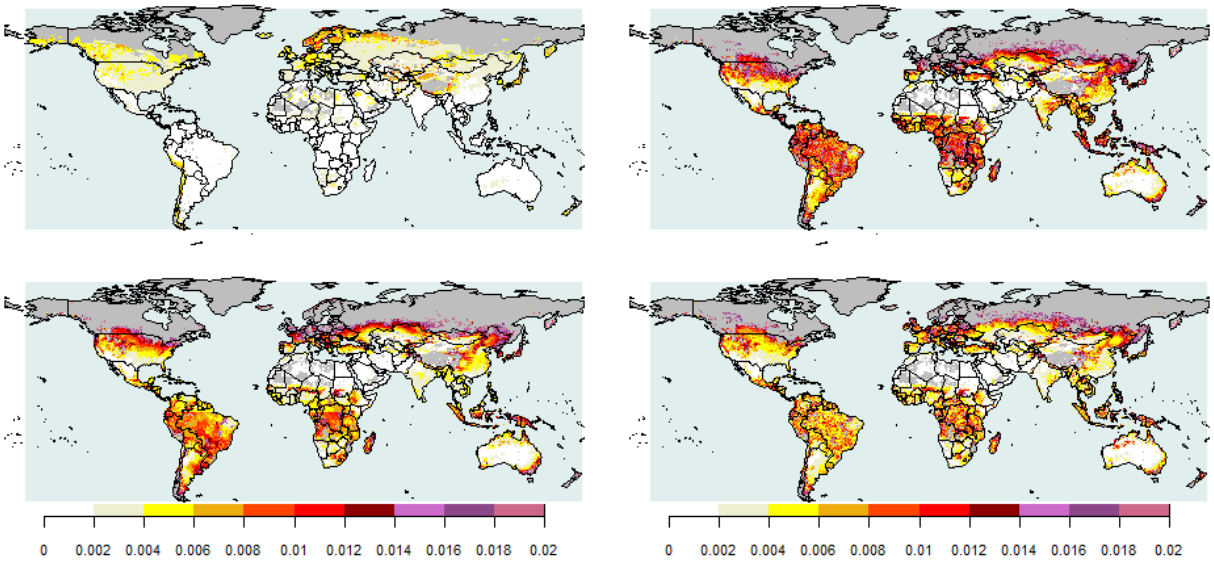

Figure S3-5. Litter Nitrogen (kg ha^{-1}) in 1960 for each LC level. Top-left: LC_{crop}, top-right: LC_{nat}, bottom-right: LC_{natpas}, bottom-left: LC_{LUH}

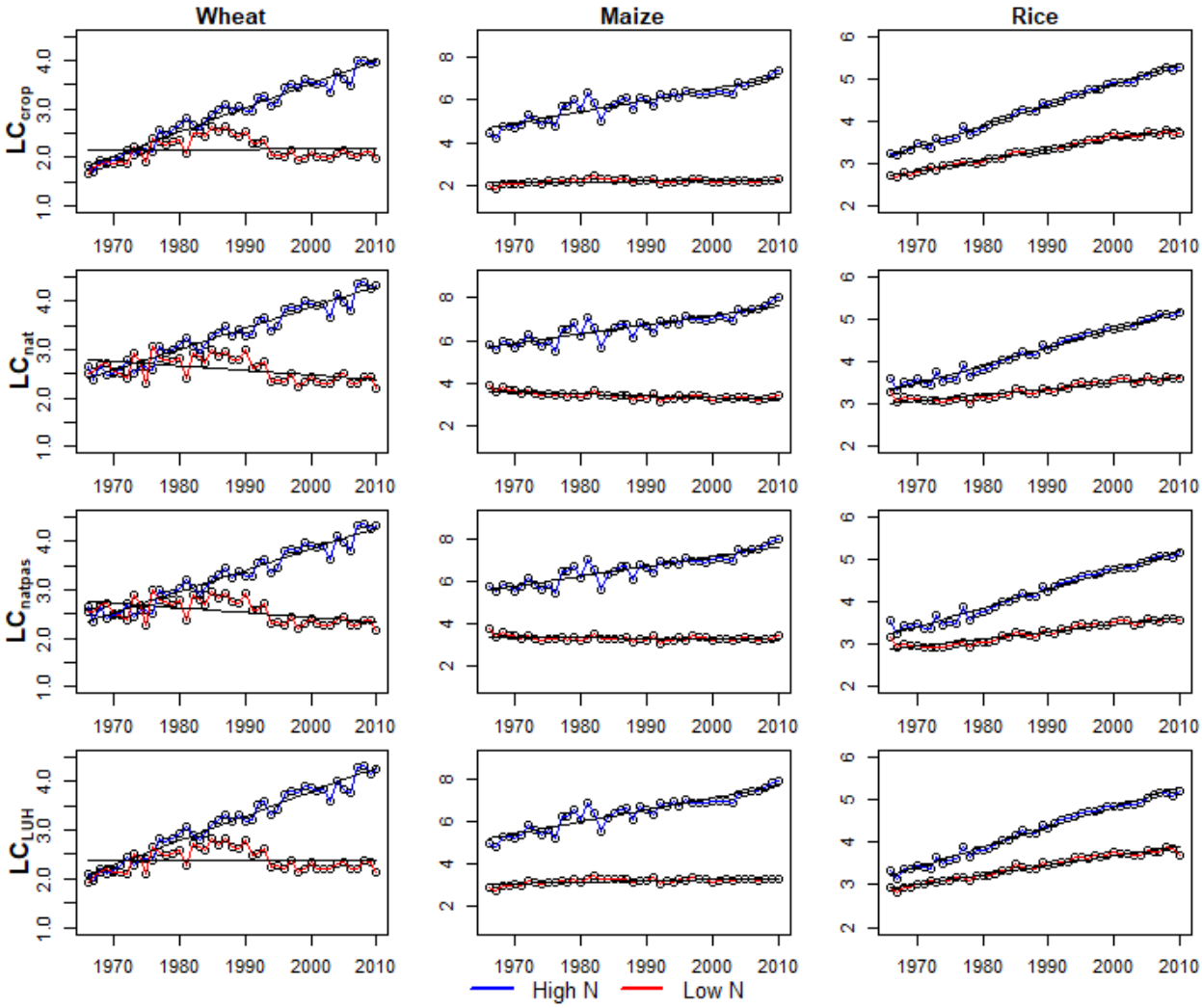

Figure S3-6. Time series and adjusted lines of yield in high and low fertilisation regions for the four land cover changes and the three crops with all drivers time variable and CRU-NCEP

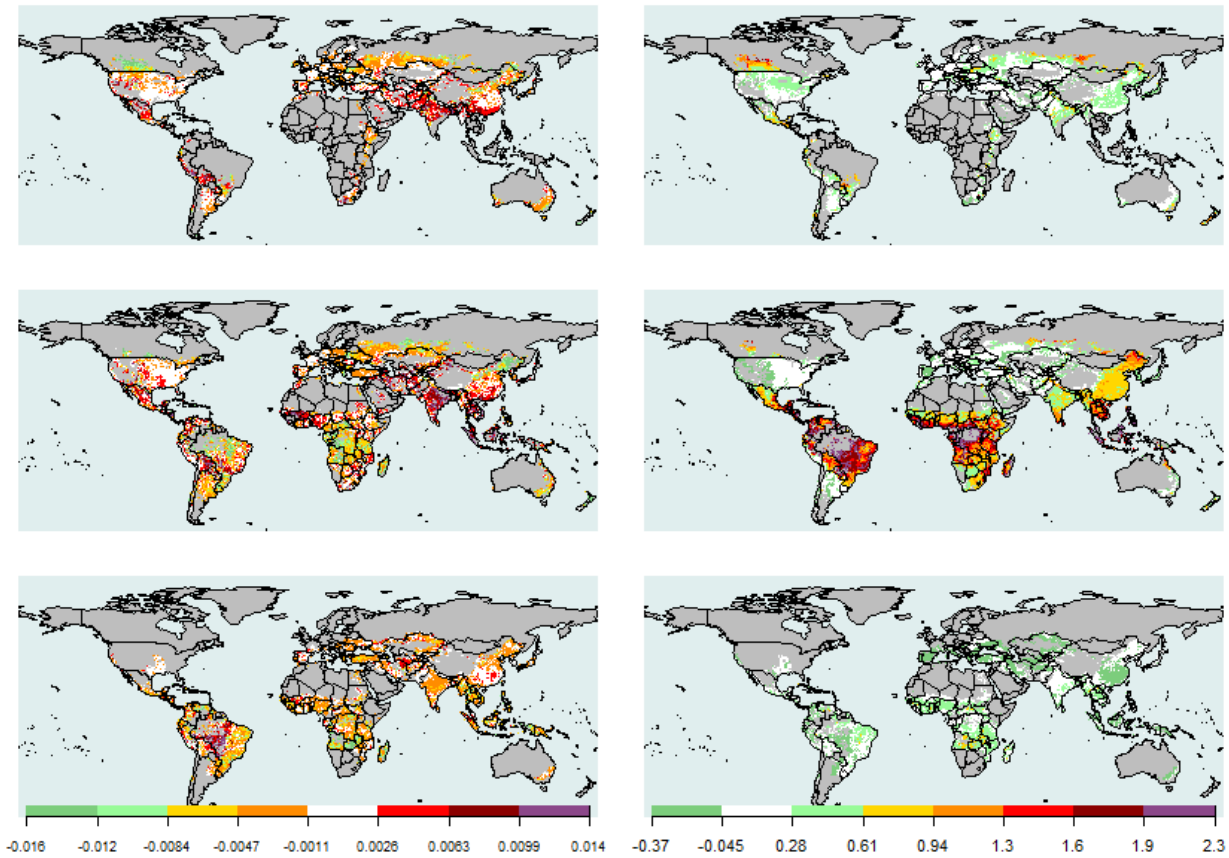

Figure S3-7. Differences (LC_{LUH} – LC_{crop}) in slope (left) in t ha^{-1} yr^{-1} and intercept (right) in t ha^{-1} at grid cell scale with Allvar and CRU-NCEPfor Top: wheat, Middle: maize, Bottom: Rice

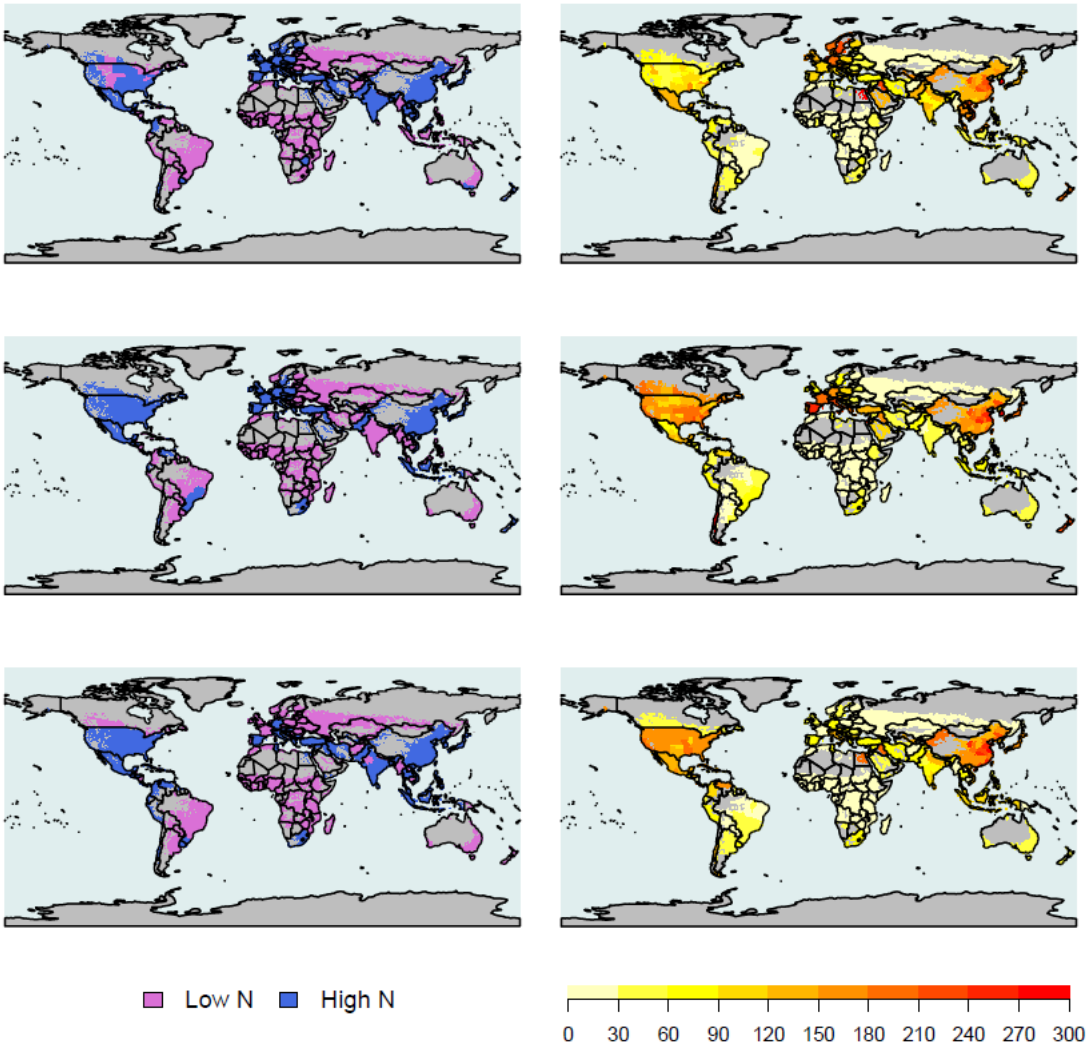

Figure S3-8. Nitrogen fertilisation for year 2000 for top: wheat, middle: maize, bottom: rice. Right: regions with high and low N fertilisation, Left: N fertilisation rate (kg ha^{-1})

CHAPTER FOUR: GROUND-LEVEL OZONE POLLUTION EFFECT IN GLOBAL CROP MODELLING: THE CASE OF WHEAT

4.1. Abstract

Ground-level ozone (O_3) is a highly damaging air pollutant that significantly impacts plant productivity. This study evaluates the implementation and performance of the O_3 damage module in LPJ-GUESS, a dynamic global vegetation model, in simulating the impact of O_3 stress on wheat and assesses its interaction with CO_2 and drought. The research aims to provide insights into the impact of ground-level O_3 on crop productivity under the influence of multiple environmental factors. An O_3 stress module was integrated into LPJ-GUESS, following a two stage process. The first step calculates the dry deposition of O_3 from the free atmosphere, while the second step calculates the accumulated Phytotoxic Ozone Dose above a threshold flux of 6 nmol m-2 s-1 (POD_6) during the plant sensitivity period. The POD_6 causes leaf senescence which affects plant productivity. The project involved calibrating the rate of damage caused by POD_6 and the lower and upper limits of the period of O_3 sensitivity by minimizing the difference between simulated yield, harvest index (HI), and POD_6 of wheat with observed data. Additional analyses included evaluating the calibrated module against experimentally observed data, examining model sensitivity to time resolution in input O_3 data, and conducting a factorial experiment to assess the effect of O_3 concentrations interacting with different CO_2 concentrations and drought. Results demonstrated that the model can reproduce the damaging effect of tropospheric O_3 on yield and HI, although there was an overestimation of yield and HI when O_3 concentrations were low, and the opposite occurred when concentrations were high. The factorial experiment also indicated that high concentrations of CO_2 can compensate for the damaging effect of O_3, especially in rainfed wheat, where the yield loss is less significant with increasing O_3 levels. The results can help policymakers to make informed decisions regarding crop

management strategies to mitigate the negative impact of air pollution on crop productivity.

Keywords: Senescence, winter wheat, spring wheat, stomatal conductance, phenology

4.2. INTRODUCTION

Ground-level or tropospheric ozone (O_3) is recognised as one of the most deleterious air pollutant that affects plant productivity. Ozone is highly oxidising and its damaging effect on plant productivity can occur via several interlinked pathways (Ainsworth et al. 2012b; Schauberger et al. 2019). Direct damage occurs when O_3 is taken up into plant tissues through stomata, causing oxidative damage and early senescence in cells, as well as decreasing the activity of the enzyme Rubisco. This effect can substantially affect carbon assimilation when scaled up from cells to leaves and canopy. Indirectly, O_3 induces the plant to reduce stomatal conductance to prevent damage, which in turn decreases transpiration, Carbon dioxide (CO_2) intake and, consequently, the photosynthesis rate. Mechanisms related to transpiration, such as nutrient uptake, are also affected. Additionally, investing assimilated carbon in mechanisms for repairing and limiting oxidative damage reduces net carbon assimilation (Broberg and Pleijel 2015; Emberson et al. 2018; Schauberger et al. 2019).

Ground-level [O_3] shows high spatio-temporal variation because it is produced by a solar radiation dependant chemical reaction of methane (CH_4), volatile organic compounds (VOCs), NO_x and carbon monoxide (CO), pollutants that can move far from the emission point; in addition, O_3 is highly reactive with short lifetimes (Ehhalt and Prather 2001; Ainsworth et al. 2012a). Therefore, ground [O_3] peaks occur

during summer which are also related to high-pressure systems, heatwaves, and droughts (Lin et al. 2020). This variation makes it challenging to formulate plant exposure indices to O_3 since damage is directly influenced by the stomatal O_3 flux which is influenced by several environmental factors such as solar radiation, air temperature, vapor pressure deficit, CO_2 concentration and soil water content in the root area (Aunan et al. 2000; Schauberger et al. 2019; Pleijel et al. 2022).

Early research included exposure indices like the mean concentration 7 hr (0900-1600) calculated over the growing period (M7), the sum over hourly [O_3] for hours when [O_3] is above 60 ppb (SUM06) or the AOT40, which is the difference between [O_3] and 40 ppb for hours when [O_3] is above 40 ppb. SUM06 and AOT40 are typically calculated over a 3-month period (Aunan et al. 2000; Huixiang et al. 2005). However, those indices only account for air concentrations and do not account for the effect of the environment on plant sensitivity (Pleijel et al. 2022). As a solution, the Phytotoxic Ozone Dose (POD), was developed, accounting for the stomatal uptake and ignoring the non-stomatal O_3 deposition (Franz et al. 2017). POD_y is the accumulated stomatal O_3 flux (mmol O_3 m^{-2} PLA) above a threshold of *y* (nmol m^{-2} s^{-1}) (Büker et al. 2015). POD_y has shown better performance than other indices based on concentrations (Mills et al. 2018; Pleijel et al. 2022).

Several studies have estimated (using process-based modelling) and quantified the effect of O_3 in crops, mainly wheat. A global yield loss of 9% was estimated for wheat for the period 2010-2012 (Mills et al. 2018), as well as 5.4% for rainfed and 15.1% for irrigated wheat between 2008-2010 (Schauberger et al. 2019). Similarly, a 9% increase was found by Pleijel (2011) when wheat growth occurred under filtered air and a yield loss of 8.4% was reported from a meta-analysis for wheat (Pleijel et al. 2018). A meta-analysis from 81 publications world-wide published between 1980

and 2007 reported a mean yield loss of 11% for six major crops (potato, barley, wheat, rice, bean and soybean) under ambient [O_3], 7 or 12h calculated, which was on average 31-49 ppb (Feng and Kobayashi 2009). Also, a linear decrease of yield at a rate of 0.4% per increase of [O_3] by one ppb was reported for wheat (Broberg and Pleijel 2015). Additionally, plant sensitivity to O_3 varies between species and cultivars, a yield decrease of 0.26% per ppb of O_3 (M7-based) was found for tolerant cultivars and 0.54% for intermediate cultivars of wheat in Mexico (Guarin et al. 2019a).

Projected rise of atmospheric [CO_2] during the next century is expected to compensate the damaging effect of high [O_3] due to the increase in net carbon assimilation since higher [CO_2] enhance photosynthesis in C3 plants decreasing the limitation of the carboxylation by Rubisco. Besides, photorespiration is also reduced at high [CO_2] due to the reduction of the oxygenase activity, since oxygen and CO_2 compete for reaction sites. Elevated CO_2 also causes stomatal closure, reducing conductance, lower transpiration and higher water use efficiency (Fangmeier et al. 1999; Broberg and Pleijel 2015). However, in fava beans, it has been found that the O_3 negative effect is higher than the positive CO_2 effect (Otieno et al. 2022). In wheat, an antagonistic, additive effect between O_3 and CO_2 has been found with different magnitudes of yield losses depending on the cultivar sensitivity to O_3 (Mishra et al. 2013; Guarin et al. 2019b; Hansen et al. 2019).

In North America and Western Europe, the control of emissions of NOx and VOCs has led to reductions of [O_3]. However, the global background O_3 precursors is increasing, particularly nitrogen oxides, due to human activities like crop fertilisation (Ashmore 2005). Although photochemistry of O_3 makes difficult to measure large scale changes in troposphere, it is clear that pre-industrial levels were lower in the

19th century than today and a global average increase of 13 ppb was estimated (Ehhalt and Prather 2001). By the end of this century, [O_3] is estimated to increase as much as 18% in the Northern Hemisphere under the highest Radiative Concentration Pathway RCP8.5 (Young et al. 2013; Otu-Larbi et al. 2020). Similarly, under the fossil-intensive scenario (A1F1) of SRES a global increase of [O_3] of about 30 ppb is projected during this century (Ehhalt and Prather 2001).

This study was focused on wheat since it represents around 20% of the globally consumed calories and most of the used cultivars in the world are sensitive to O_3 (Guarin et al. 2019a). Besides, several studies have demonstrated the reduction of quantity and quality of wheat production caused by ground-level ozone, risking the global food security (Pleijel et al. 1998; Fischer 2019; Guarin et al. 2019a). The increasing importance of tropospheric O_3 pollution and depletion that it causes on crop production makes it critical to implement its effect in the crop system models such as LPJ-GUESS to improve the representation of actual yields, increasing the reliability of the food system studies and to complement further research about O_3 pollution in crops. This study introduces the representation in global gridded crop models of stomatal flux indexes such as POD_6 to evaluate the ozone exposure in plants.

4.2.1. LPJ-GUESS.

The Lund-Postdam-Jena General Ecosystem Simulator (LPJ-GUESS) is a model that simulates dynamic vegetation response to climate, atmospheric CO_2 and nitrogen (N) dynamics (Lindeskog et al. 2013; Smith et al. 2014; Olin et al. 2015b) and includes an implementation of managed land cover for crops and managed pastures (Lindeskog et al. 2013; Olin et al. 2015a). Crops in LPJ-GUESS are simulated as Crop Functional Types (CFT) that differ in parameters and response to

climate and management. Management options include irrigation (inundation in the case of rice), fertilisation, tillage, and inter-growing season grass cover (Olin et al. 2015b).

The main processes simulated daily to represent crops are soil hydrology, photosynthesis, canopy conductance, respiration, phenology, plant N demand, and carbon allocation (Smith et al. 2001; Olin et al. 2015b). Stomatal conductance in LPJ-GUESS is regulated by water status, under water deficit, stomatal closure reduces water loss but also decreases intercellular [CO_2] in the leaves and, in turn, photosynthesis (Ahlström et al. 2012). Similarly, down-regulation of stomatal conductance occurs under high [CO_2] and low boundary layer humidity (Smith et al. 2014). The explicit simulation of stomatal conductance regulation in LPJ-GUESS allows the implementation of O_3 module based on POD index. Therefore, this project aims to describe and evaluate the implementation and performance of the O_3 module in LPJ-GUESS in the simulation of wheat at the global level and to assess its interaction with CO_2 and drought.

4.3. METHODS

4.3.1. Model setup

LPJ-GUESS v4.1, Subversion revision 11524, was used for this study. Simulations were conducted for spring and winter wheat at selected location cells (0.5° x 0.5°). Sowing and harvest dates were calculated automatically for each gridcell based on the prevailing climate, as described in Lindeskog et al. (2013), following Waha et al. (2012). One growing season per year was simulated for each cultivar in each location. Both rainfed and fully-irrigated conditions were simulated for each gridcell. Management options included tillage and N application, inter-growing-season grass was turned off. All simulations were performed with the AgMERRA climate forcing

dataset (Ruane et al. 2015) and a 500 years period, known as the spinup, to approach equilibrium in the accumulation of vegetation, soil and litter carbon and nitrogen, starting from bare soil (Smith 2001; Wramneby et al. 2008). This period uses fixed [CO_2] and N inputs and detrended climate. N input was provided based on the atmospheric N deposition dataset from Lamarque *et al*., (2010). The N fertilisation database was estimated for the period between 1961 and 2010 by interpolating the global gridded dataset of circa 2000 fertilisation data at a resolution of 0.5° x 0.5° from the AgMIP Gridded Crop Modelling Initiative (Mueller et al. 2012; Elliott et al. 2015a) based on the relative variations reported in the fertilisation dataset from Lu and Tian, (2017). The gridded data of texture, pH and organic matter in soils was used from Batjes (2016).

4.3.2. Ozone stress effect on leaf senescence

The O_3 stress module includes two different steps. In the first, a scheme for dry deposition of O_3 from the free atmosphere is introduced. This scheme transforms [O_3] from some height above the canopy to the canopy [O_3] and allows obtaining canopy [O_3] from [O_3] input obtained from the lowest level of chemical transport models (CTM), generally 45 m above the surface (Franz et al. 2017; Emberson et al. 2018). In the second step, the accumulated Phytotoxic Ozone Dose above a threshold flux of Y nmol m^{-2} s^{-1} (POD_y) during the plant sensitivity period is calculated and the leaf senescence induced by the estimated POD_y (Figure 4.1).

The implemented deposition scheme developed by Franz et al. (2018) transforms atmospheric [O_3] ([O_{3_atm}]) to canopy [O_3] ([O_{3_ca}], nmol m^{-3}) based on the aerodynamical resistance (R_a), the canopy boundary layer resistance (R_b) and the compound surface resistance (R_c) which is the sum of the stomatal and non-stomatal

resistances (canopy air space, leaf surface and ground resistances) following the Equation 4 - 1.

$$[O_{3\_ca}] = [O_{3\_atm}]\left(1 - \frac{R_a}{R_a+R_b+R_c}\right) \quad \text{Equation 4 - 1}$$

The leaf stomatal conductance of water vapour (g_s) was calculated by dividing the stomatal canopy conductance for water (G_s), which is calculated daily within LPJ-GUESS, by the effective LAI (LAI_e) using the big-leaf model of canopy stomatal conductance. LAI_e is defined as actual LAI for LAI ≤ 2, LAI/2 for LAI ≥ 4, and 2 for others (Ding et al. 2014). Then, g_s is scaled to O_3 (g_{O3}, m s^{-1}), multiplying g_s by 0.662, the conversion factor for molecular diffusivity from water vapour to O_3. The stomatal flux of O_3 (F_{O3}, nmol m^{-2} s^{-1}) is obtained by the product of the g_{O3} and $[O_{3\_ca}]$ (Pleijel et al. 2007; Franz et al. 2018; Peng et al. 2019). Daily POD_y (mmol m^{-2}) is the accumulated F_{O3} above a *Y* threshold during the day. The threshold *Y* represents the maximum plant capacity to detoxify itself with antioxidants such as ascorbate. For wheat, this value has been reported to be 6 nmol m^{-2} s^{-1} (Pleijel et al. 2007; Peng et al. 2019).

LPJ-GUESS simulates daily stomatal conductance; however, the hourly stomatal conductance is estimated in the O_3 stress module using a cosine function (Equation 4 - 2) to simulate the diurnal variation and peaks of stomatal conductance which usually occur around midday depending on the temperature as reported for maize (Berkelhammer et al. 2020). This approach allows to capture positive F_{O3} and POD_6 values during peak stomatal conductance hours. Otherwise, using the daily average of g_{O3} and F_{O3} could lead to substantial underestimation of POD_6 (Equations 4 - 2 to 4 - 5).

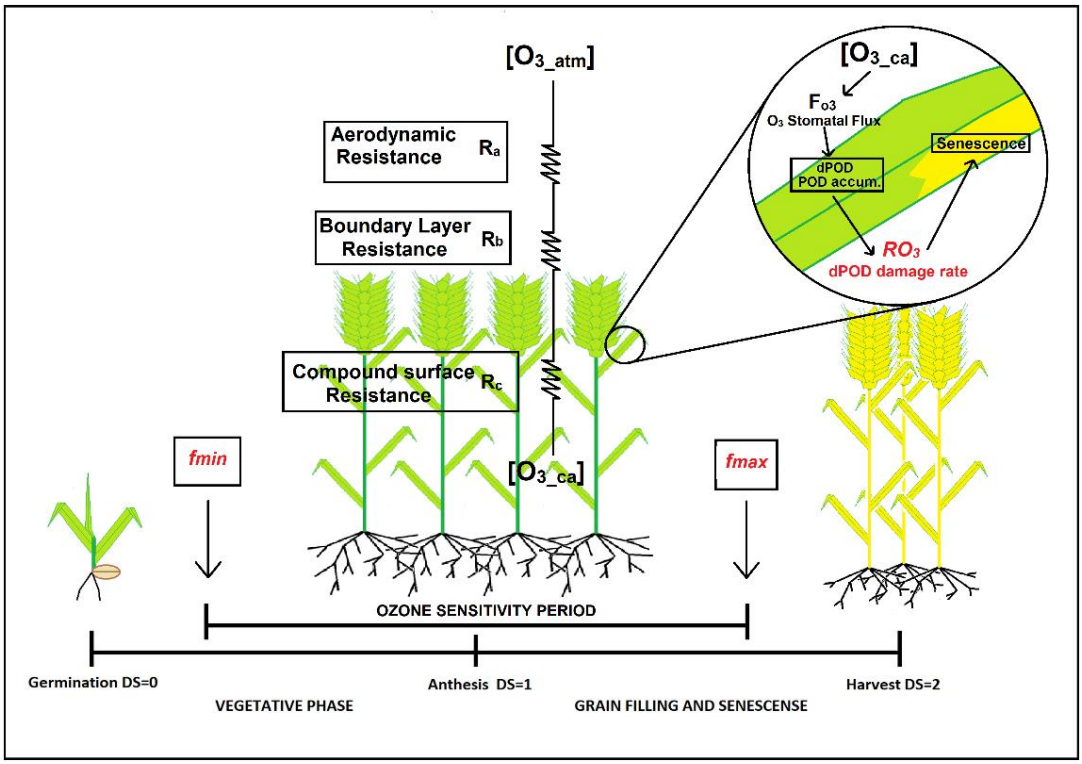

Figure 4.1. Diagram of the relationship between ozone deposition, parameters *fmin*, *fmax* and *RO3* and Developmental stage (DS)

$$g_{o3(i)} = g_{o3}\left(1 + \cos\left(\frac{i*2*\pi}{DL} + \pi\right)\right) \quad \text{Equation 4 - 2}$$

$$F_{O3(i)} = g_{o3(i)} * [O3_{ca}] \quad \text{Equation 4 - 3}$$

$$dPOD_y = \sum_{i=1}^{DL} \max(F_{O3(i)} - y, 0) * \frac{3600}{10^6} \quad \text{Equation 4 - 4}$$

$$POD_y = \sum dPOD_y \quad \text{Equation 4 - 5}$$

Where *i* is the hour of the day starting from daybreak, *DL* is the daylength in hours, $dPOD_y$ is the daily accumulation of POD_y above a threshold of y = 6 nmol m^{-2} s^{-1}.

Crop senescence in LPJ-GUESS is primarily induced based on crop maturity or with nitrogen stress when the available N in leaves declines below necessary levels to maintain the current Leaf Area Index (LAI) (Yin et al. 2000; Smith et al. 2001; Gregersen et al. 2013; Olin et al. 2015b). The new implementation of the O_3 module

adds a new factor accelerating senescence, since it is the main mechanism causing O_3 damage effect in plants, which directly affects the LAI. The effect of $dPOD_6$ in senescence varies depending on the accumulated POD_6; when the accumulated POD_6 is low, around 1.5 mmol m^{-2}, the senescent fraction of leaves is negligible, but it increases as long as the POD_6 accumulates following a quadratic function (Equation 4 - 6). This relationship was found in a data compilation performed by Pleijel, H. in 2018 (unpublished, Figure S4-1). In the LPJ-GUESS model, senescence caused by O_3 is calculated at the daily time step by multiplying $dPOD_6$ by the instantaneous rate of change of the effect of $dPOD_6$, the derivative of the quadratic effect (Equation 4 - 7), which is a linear function of the accumulated POD_6 (Equation 4 - 8).

$$\mathrm{Leaf_{green}} = \mathrm{a} * \mathrm{POD_6}^2 + \mathrm{b} * \mathrm{POD_6} + \mathrm{c} \qquad \text{Equation 4 - 6}$$

$$\frac{\mathrm{dLeaf_{green}}}{\mathrm{dPOD_6}} = 2\mathrm{a} * \mathrm{POD_6} + \mathrm{b} \quad \text{Equation 4 - 7}$$

$$2\mathrm{a} = \mathrm{RO_3}$$

$$\mathrm{Leaf_{dead_{(j)}}} = (\mathrm{b} + \mathrm{RO_3} * \mathrm{POD_{6_{(j)}}}) * \mathrm{dPOD_{6(j)}} \qquad \text{Equation 4 - 8}$$

where j is the day, $Leaf_{green}$ and $Leaf_{dead}$ are the fraction of green and dead leaves, respectively. RO_3 is the linear rate of change of the effect of $dPOD_6$ on senescence.

Ozone-related leaf senescence and the period of accumulation of POD_6, when wheat is sensitive to O_3 is directly related to the phenological stage, which in turn is mainly related to temperature (Del Pozo et al. 2008). For wheat, the period between 200 degree days (°C days) before anthesis and 700 °C days after anthesis using a base temperature of 0 °C has been reported for O_3 accumulation (Pleijel et al. 2007). However, different base temperatures have been used to model phenology in spring

wheat, like 2.6 °C (Seefeldt et al. 2002) and 5.4 °C (Del Pozo et al. 2008). In LPJ-GUESS, the crop development stage is simulated as a function of temperature, vernalisation and photoperiod based on Wang and Engel (1998). The development stage (DS) is represented by a number between 0 and 2, anthesis is characterized by a value of 1, values below 1 represent the vegetative phase and values above 1 represent the reproductive phase (Olin et al. 2015b). The period for which POD_6 is accumulated (*fmin* to *fmax* in Figure 4.1) was calibrated in this study.

4.3.3. Calibration

For calibration, three locations were selected where the effect of O_3 on POD_6, relative yield and relative HI was evaluated on wheat: Tervuren, Belgium, with experiments in 1994, 1995 and 1996 (Bender et al. 1999; Fangmeier et al. 1999) where concentrations of charcoal filtered and non-filtered chamber concentrations were evaluated; Gothenburg, Sweden, with experiments in 1987, 1988, 1994, 1997, and 1999 (Pleijel et al. 1991, 1997, 2006; Gelang et al. 2001), and Jokioinen, Finland, with experiments in 1992 and 1993 (Ojanperä et al. 1998). Charcoal-filtered, non-filtered, and ozone-enriched chamber concentrations were evaluated in the last two locations.

Simulations of three variables, yield, harvest index (HI) and POD_6 of wheat, were performed with LPJ-GUESS combining different levels of three parameters from the O_3 implementation (Table 4.1). The rate RO_3, defined in Equation 4 - 6 with ten levels. The lower (*fmin*) and upper (*fmax*) limits of the period of O_3 sensitivity were also calibrated using seven levels for each and three approaches to calculate them: 1) Expressed as the minimum and maximum DS (between 0 and 2), 2) accumulation of °C days using a base temperature of 0 °C, and 3) accumulation of °C days using a base temperature of 5 °C. The combination of the parameter levels produced 490

simulations (10x7x7) for each of the three sensitivity-period methods, for a total of 1470 simulations.

A linear interpolation was performed for each experiment (location and year) to estimate the yield and HI when POD_6 = 0 as the linear regression intercept between POD_6 and yield. This value was used as a reference for no O_3 effect. The relative values for yield were subsequently estimated for all the concentrations as the fraction of simulated yields to the reference. The relative HI was calculated following the same process.

Table 4.1. Simulated levels for all the calibrated parameters and phenology methods used

Parameter	Method	Units	Simulated Levels
RO_3	All	mmol m^{-2}	0.01, 0.02, 0.03, 0.04, 0.05, 0.06, 0.07, 0.08, 0.09, 0,1
fmin	DS	unitless	0.1, 0.2, 0.3, 0.4, 0.5, 0.6, 0.7
	dd0	°C days	200, 300, 400, 500, 600, 700, 800
	dd5	°C days	100, 150, 200, 250, 300, 350, 400
fmax	DS	unitless	1.4, 1.5, 1.6, 1.7, 1.8, 1.9, 2.0
	dd0	°C days	1000, 1100, 1200, 1300, 1400, 1500, 1600
	dd5	°C days	800, 850, 900, 950, 1000, 1050, 1100

Simulated and observed relative yield, HI values, and POD_6 were min-max normalised over all the observed and simulated data (Equation 4 - 9), this method transforms linearly the original variable to values between 0 and 1 keeping the relationships among the original values (Han et al. 2012). A total of 28 data points were used for comparison from each simulation combining location, years and different [O_3]. Then, the root mean square error (RMSE) between observed and simulated normalised variables was calculated per simulation (Equation 4 - 10). The simulations were constrained to those with maximum simulated POD_6 between 5 and 7.5 mmol m^{-2}, this range is the 80^{th} quantile of observed POD_6 of 4.9 mmol m^{-2} and the maximum observed POD_6 of 6.74 mmol m^{-2}, allowing some elasticity. The constriction avoided simulations with over- or underestimation of POD_6, even if yield

and HI are well represented. Finally, the Euclidean distance of the tridimensional vector created by the RMSE values from the three variables was minimised to identify the simulations that best reproduce the observed data (Equation 4 - 11).

$$N = \frac{var - \min(var)}{\max(var) - \min(var)} \quad \text{Equation 4 - 9}$$

$$RMSE = \sqrt{\frac{\sum(N_{obs} - N_{sim})^2}{n}} \quad \text{Equation 4 - 10}$$

$$Distance = \sqrt{RMSE_{Yield}{}^2 + RMSE_{HI}{}^2 + RMSE_{POD}{}^2} \quad \text{Equation 4 - 11}$$

Where *var* is the variable (yield, HI or POD_6). *N* represent the normalised variable, N_{obs} and N_{sim}, the normalised observed or simulated and *n* is the number of values compared per simulation. *Distance* is the Euclidean distance from the RMSE of the three variables and used for minimisation, referred to as *distance* in the following.

The best ten combinations of parameters with the lowest *distance* from the 1470 simulations were selected and the simulation with the highest Pearson linear correlation between observed and simulated yield was used as the secondary criteria to differentiate between these best ten.

4.3.4. Evaluation

Comparison between simulations from LPJ-GUESS and observed data from O_3 enrichment experiments were used to evaluate the new O_3 module. These experiments evaluate different ambient, charcoal filtered and open-top chamber O_3 effects on HI and wheat yield. The POD_6 was not evaluated since simulations with AgMERRA climate span until 2010 and before that year, reports of POD_6 were very limited in the literature and the index was not well developed.

A total of 13 experiments from 8 publications in 7 different locations were used to evaluate the module (Table S4-1). From there, 40 and 20 treatments of O_3 were simulated for yield and HI, respectively. The simulations were performed assuming the reported average [O_3] in the publications as constant during the daylight time in the growing season. For each experiment, the relative yield and HI were calculated as described in the calibration section for observed and simulated values, but regressions were between [O_3] and yield since POD_6 was not reported in the publications.

Linear comparisons between observed and simulated values were carried out by an analysis of covariance (ANCOVA). This method evaluates the interaction of observed and simulated values and [O_3] to compare slopes.

4.3.5. Time Scale differences

To evaluate the sensitivity of POD_6 estimation by LPJ-GUESS to the temporal resolution of [O_3] data, hourly [O_3] data was collected from three different O_3 experiments with a total of ten treatments conducted on wheat in Belgium during 1994, including two treatments, charcoal-filtered and non-filtered (Fangmeier et al. 1999); Sweden in 1994 with four treatments non-filtered and three levels of O_3 enrichment (Pleijel et al. 2014) and Sweden in 1997 with four treatments charcoal filtered, non-filtered, and two levels of O_3 enrichment (Gelang et al. 2001).

The collected data were used to simulate POD_6 directly using data at hourly resolution, as well as the mean daily, weekly, monthly and growing season [O_3] data. The root mean square error was calculated for all the time scales, as shown in Equation 4 - 10. Besides, a comparison between the fitted lines for daily and seasonal mean data was performed using an analysis of covariance (ANCOVA).

4.3.6. Ozone, CO_2 and drought effect on yield

A factorial experiment with LPJ-GUESS simulations was performed where spring and winter wheat was simulated in 2003 under irrigated and rainfed management. Eleven levels of atmospheric CO_2 in ppm (350, 375.8, 400, 450, 500, 550, 600, 650, 700, 750, 800) and tropospheric O_3 in ppb (0, 10, 20, 30, 40, 50, 60, 70, 80, 90, 100) were combined for a total of 121 simulations in the three locations used for calibration Belgium (4°15' E, 50°45' N), Sweden (12°15' E, 57°45' N) and Finland (23°15' E, 60°45' N). The year was selected because it had a high portion of days during the growing season when plants endured water stress under rainfed management and showed a clear difference in yield with irrigated management.

The simulation with 0 ppb of O_3, 375.8 ppm of CO_2 (actual concentration for 2003), and irrigation was used as a reference. All the simulated yields were divided by the reference separately for spring and winter wheat to standardise to a relative yield. Isopleths of relative yield by CO_2 and [O_3] were performed by location and management. Harvest index, POD_6, actual evapotranspiration and stomatal conductance were also simulated.

4.4. RESULTS

4.4.1. Calibration

The implementation of the O_3 module in the model allowed the simulation of the deleterious effect on leaves and the early senescence caused by tropospheric O_3. The calibration of the parameters showed that, for all three phenology approaches, the parameter *RO_3* caused most of the variation in yield and HI, followed by *fmin*. In general, the combinations of parameters causing a lower damaging effect of O_3, such as low values of *RO_3*, late *fmin* and early *fmax*, showed higher *distance* meaning poor model performance. Medium and low values of *RO_3* in some cases

compensate for the lack of damaging effect with a wider POD_6 accumulation period, early start and late end of the O_3 sensitivity. These parameter combinations caused low *distance* because of the good fit of yield and HI but caused significant overestimation of POD_6. To control this effect, simulations were constricted those with maximum POD_6 between 5 and 7.5 mmol m^{-2} which showed that the lowest values of *distance* occurred with high RO_3 values and a moderate O_3 sensitivity period (Figure 4.2. S4-2, S4-3).

The method to calculate the period of sensitivity to O_3 based on DS consistently had the lowest *distance* compared to dd0 and dd5. All the quartiles of the *distance* and the mean *distance* were lower with DS (Figure 4.2. S4-2, S4-3). This implies that DS is more appropriate and accurately estimates yield, HI and POD_6. Five of the best ten simulations selected were from the DS approach, three from the dd5 and two from the dd0.

From the best ten simulations, the highest Pearson correlation coefficient ($\boldsymbol{\rho}$ = 0.66) between observed and simulated yield was found in the combination of parameters: RO_3 = 0.09, *fmin*= 0.5 and *fmax*= 1.5 using the DS scale. This parameter setup simulated a similar decrease in relative yield and harvest index as POD_6 increases. However, simulated POD_6 is underestimated when observed POD_6 is between 0 and 4 mmol m^{-2}, causing an underestimation of relative yield and harvest index loss mainly with $[O_3]$ below 40 ppb (Figure 4.3).

4.4.2. Evaluation

The evaluation comparison between observed and simulated relative yield showed a higher intercept (1.14) and a lower slope (higher yield loss) for simulated values (-0.0080) compared to observed values with an intercept of 0.92 and a slope of -

0.0044 differences are significant with a confidence of 95% (p=0.0022 and p=0.006, respectively).

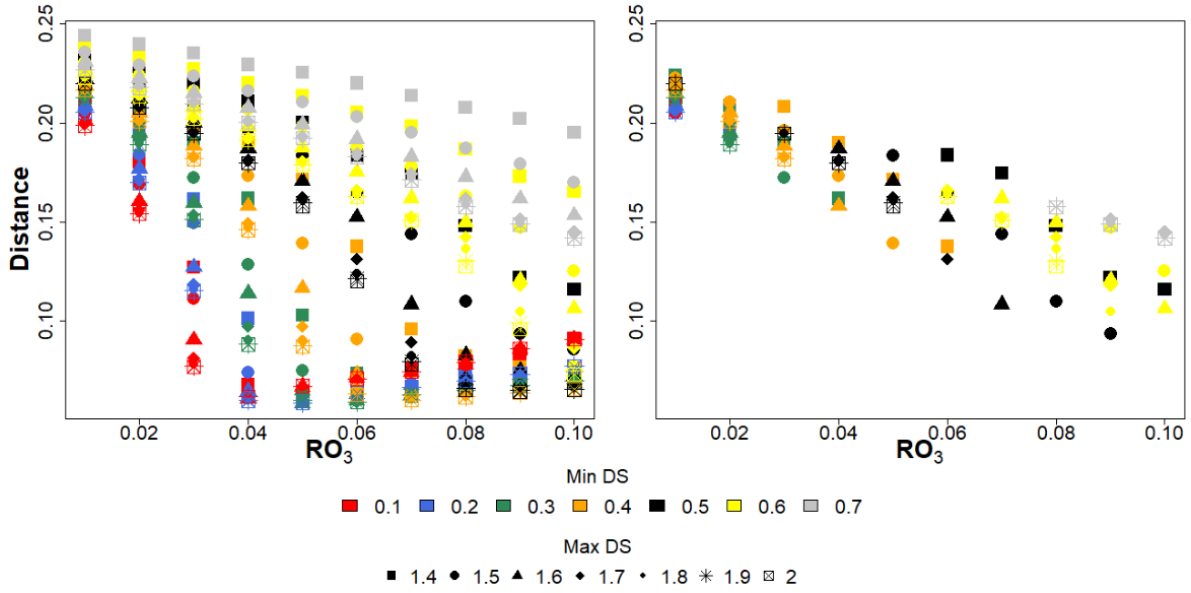

Figure 4.2. Euclidean distance of simulations using DS phenology approach, Left: All the evaluated parameter values and Right: Simulations with maximum POD6 between 5 and 7.5 mmol m-2

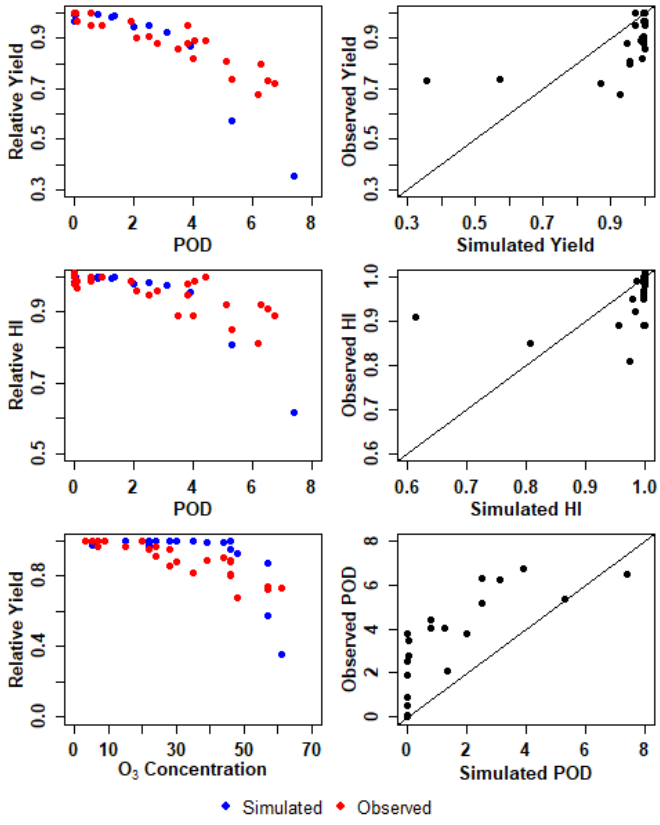

Figure 4.3. Left:Relative Yield and HI vs POD6 (mmol m-2) and O_3 concentration (ppb). Right: Simulated vs Observed POD, and relative yield and HI with the selected parameters for LPJ-GUESS

In HI, the opposite response was found; an intercept of 1.01 was found for both observed and simulated data, but the slope was higher for simulated (-0.0015), indicating slower HI loss compared to observed (0.0027). Equally, this difference was not significant, with a confidence of 95% (p=0.305).

This difference in relative yield is mainly caused by the model underestimating the loss effect in some simulations below an [O_3] of 60 ppb and an overestimation when [O_3] is higher than 90 ppb. In HI, the same underestimation of the HI loss below 60 ppb causes this response (Figure 4.4).

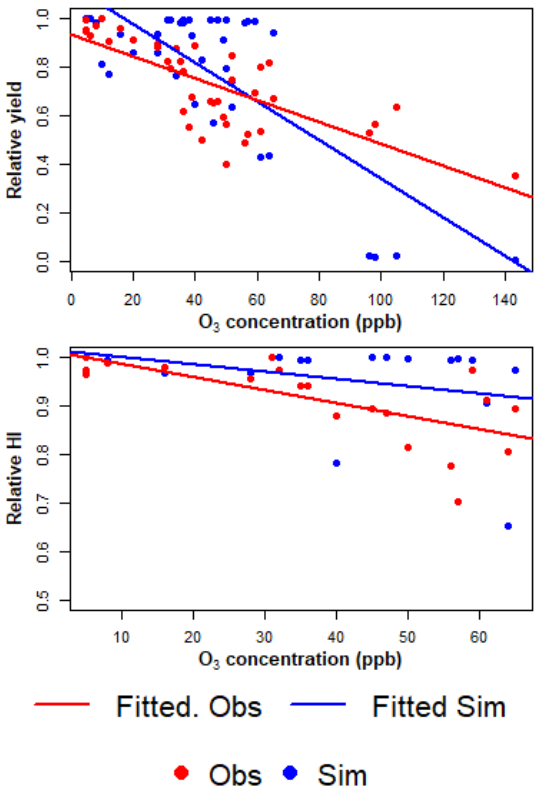

Figure 4.4. Observed and simulated relative yield and harvest index vs O_3 concentrations from locations used for evaluation

4.4.3. Time Scale differences

The model was highly sensitive to the time scale of the [O_3] data input. The main difference occurred between hourly data and the rest of the scales, but in general, at a higher time resolution, the estimated POD_6 is higher, as shown in Figure 4.5.

In that sense, the hourly [O_3] data caused a significant overestimation of POD_6, while the other scales caused a general underestimation. Therefore, the hourly [O_3] data had the highest RMSE of 1.91, while the daily input [O_3] data had the lowest RMSE of 1.52, indicating that the daily resolution better represents the observed POD_6. Seasonal mean [O_3] data has the worst underrepresentation of POD_6 with an RMSE of 1.82, while weekly and monthly scales had medium values, 1.69 and 1.80, respectively.

Although there was no significant difference between intercepts and slopes fitted from estimated POD_6 based on daily and seasonal [O_3] data, a higher slope was found from daily data (intercept = -0.112, slope = 0.793) compared to seasonal data (intercept = -0.24, slope = 0.72). In summary, the findings suggest that the time resolution affects the estimation of POD_6 and daily [O_3] input data may be the most appropriate for accurately estimating the POD_6 in wheat crops in LPJ-GUESS.

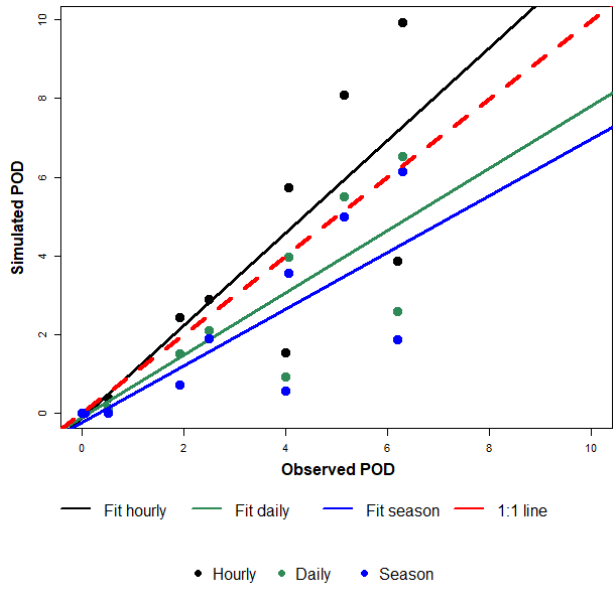

Figure 4.5. Simulated vs Observed POD_6 (mmol m^{-2}) based on hourly, daily and mean season [O_3] data

4.4.4. Ozone, CO_2 and drought effects on yield

The relative yield showed differences in the response surface between the three locations. However, a general trend was observed, in which the relative yield was not significantly affected by the increase in [O_3] below 30-40 ppb. Conversely, a marked reduction in relative yield was observed under higher [O_3], decreasing relative yield below 0.2 when [O_3] is above 80 ppb in all the locations. Both cultivars exhibited a similar response pattern, although the magnitudes differed, as shown in Figures 4.6 and S4-4. This response included a higher yield loss under irrigated management due to the increase of O_3 conductance, compared to rainfed management.

On the other hand, the relative yield was sensitive to [CO_2], with an increase of up to 0.5 of the reference yield observed in Belgium for irrigated winter wheat. The high CO_2 concentrations were able to compensate for the yield loss caused by the rise in O_3 levels. In rainfed wheat, CO_2 concentrations of around 500-600 ppm were enough to maintain the actual relative yield ([CO_2] =375.8 ppm and [O_3] = 0 ppb) when [O_3] rose even above 80 ppb. A similar compensation was found in the irrigated

management wheat, but higher CO_2 concentrations were required to maintain the reference yield when [O_3] was above 80 ppb, as illustrated in Figures 4.6 and S4.4.

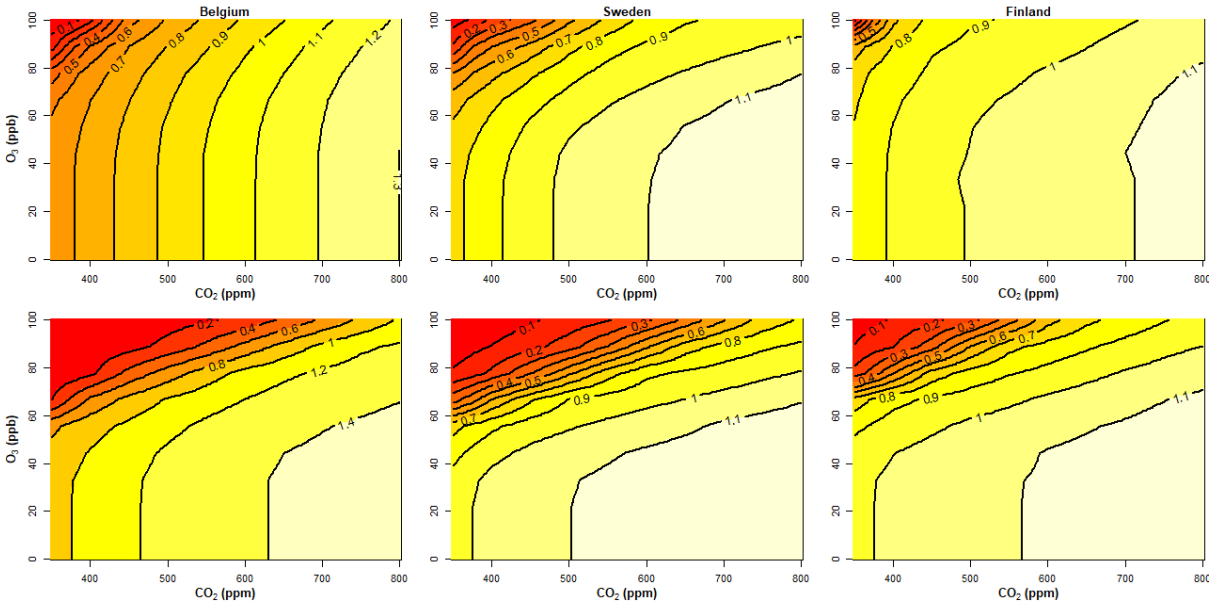

Figure 4.6. Isopleths of relative winter wheat yield to reference (O_3 of 0 ppb and actual CO_2) for year 2003 for three locations. Top: Rainfed, Bottom: Irrigated

4.5. DISCUSSION

4.5.1. Effect of O_3 in simulated crops

The main mechanism driving yield loss from O_3 is not entirely understood. Distinguishing experimentally between the decrease of photosynthesis and the induction of early senescence presents a challenge. Recent research has found that the O_3 effect on the photosynthetic rate is only observed after accelerated senescence is induced (Osborne et al. 2019). Similarly, Emberson et al. (2018) found that most of the effects of O_3 on crops can be explained by the early induction of senescence. The latter study also found that the four main effects of O_3 needed to be considered in modelling were: 1) higher O_3 sensitivity in the reproductive phase, 2) acceleration of leaf senescence associated with the loss in photosynthetic capacity, 3) reduction in harvest index, and 4) an increase in seed protein concentration. The O_3 module implemented in LPJ-GUESS simulates damage

through accelerated senescence and assesses the first three effects in this study. The last effect was not evaluated in this study. However, due to the mechanistic nature of LPJ-GUESS, the increase in simulated seed protein could be occur even if it was not directly modeled. Further research, with more model development, will allow for the examination of this effect.

Although ground-level O_3 has been shown to have harmful effects on plants, it has not been broadly incorporated into crop models. Previous implementations include a modulating factor for stomatal conductance based on water stress which affects the O_3 flux through the stoma in WOFOST (Cappelli et al. 2016), the O_3 concentration-based index M7 in DSSAT (Guarin et al. 2019b) and a more complex module considering environmental effect in stomatal conductance and O_3 intake was developed for LPJmL (Schauberger et al. 2019). One of the advantages of the developed O_3 module in LPJ-GUESS is the use of the POD_6, which allows the simulation of the O_3 effect on plant productivity based on environmental factors that determine stomatal uptake rather than just [O_3] (Peng et al. 2019; Pleijel et al. 2022). This approach causes variability in the simulated O_3 effect between evaluated locations and years, even with the same [O_3]. Some studies have found that this variability is overlooked in simulations with indexes like the M7 and AOT40, while POD_6 indexes are better at predicting O_3 damage in wheat (Osborne et al. 2019).

Experimental evidence has shown a period of high O_3 sensitivity in wheat which begins before anthesis and continues until the end of grain filling (Pleijel et al. 2007). This period ranges from development stage 0.5 to 1.5 in this study, while other reports use thermal time (base temperature =0 °C) between 200-270 °C days before anthesis and 600-700 °C days after anthesis (Pleijel et al. 2007; Feng et al. 2012; LRTARP 2017).

The calibrated period presented in this study seems to be centred around anthesis more than the reproductive period, as described in the other studies. However, DS allows the representation of different plant responses to environmental factors such as temperature in different phases and does not have a linear relationship with time (Olin et al. 2015b). For example, the cardinal temperatures for wheat growth differ between the pre-anthesis and post-anthesis periods, with the latter shifted 5 °C higher (Wang and Engel 1998). This means that the phenological development of 0.5 on the DS scale before anthesis requires fewer days than after anthesis with equal mean air temperature in both periods. A similar response is caused by daylength and nitrogen stress.

The average number of days to reach from DS = 0.5 to DS = 1.0 between 2001-2003 for the three locations used in the factorial experiment (section 3.4) was 30 days, and from DS = 1 to DS = 1.5, is 37 days. The experiments from Wang and Engel (1998) in North Germany for wheat reported that the period between anthesis and the end of the grain-filling requires 15 days under optimum environmental conditions and observed, on average, 20 days between the beginning of anthesis and medium milk stage, when the grain weight and size has already been reached. In Sweden, the grain-filling period in six experiments was reported to be 44 days (Pleijel et al. 2000).

The only direct link between the POD_6 accumulation and the senescence damage caused by O_3 in the implemented LPJ-GUESS module is the parameter describing the rate of senescence caused by POD_6 (RO_3) on a daily basis. The consequent effect on carbon assimilation, allocation and yield are part of the proper dynamics and processes represented in the model. This mechanistic approach differs from the empirical relationships between POD_6, or any other O_3 exposure index, and relative

yield, grain mass and protein yield used in several crop models (Grünhage et al. 2012; LRTARP 2017).

4.5.2. Model Evaluation

While the implemented module in LPJ-GUESS was capable of simulating yield and HI loss due to O_3 effects, the evaluation revealed discrepancies between simulated and observed data. The primary reason for underestimating the O_3 effect when [O_3] are low is the scale of the input [O_3] data. During the model evaluation, the mean [O_3] of the whole growing season, reported in the experiments, was used as constant in the simulations, causing an underestimation of POD_6, as shown in figure 4.5. Increasing the time resolution of [O_3] data from the growing season to a daily basis reduces the POD_6 underestimation increasing the yield loss. However, that improvement is not sufficient to completely fix the problem. One advantage of the POD_6 index compared to concentration indexes is the ability to capture the peaks of [O_3] during the daytime (Guarin et al. 2019b). Ozone concentrations typically reach maximum values around noontime and decrease after the late afternoon with clear differences at different seasons (Beig et al. 2007; Feng et al. 2007; M. Pugh et al. 2010). This daily pattern of [O_3] and variation also occurs in experimental chambers. Data from Belgium in 1994 from a charcoal-filtered chamber (Fangmeier et al. 1999) showed an 11-hour (8:00 – 18:00) mean [O_3] of 6.02 ppb. However, peaks reached as high as 25 ppb in some hours (Figure 4.7). Therefore, the use of hourly [O_3] data could increase the POD_6 avoiding underestimation; however, the availability of hourly data is a challenge.

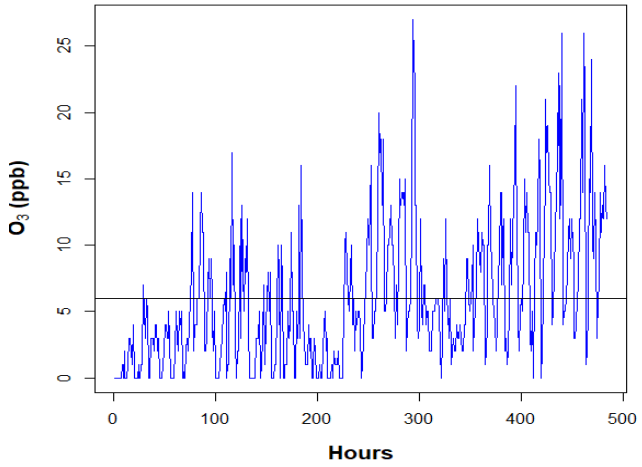

Figure 4.7. Hourly ozone concentration in Belgium 1994 (8:00 – 18:00). Horizontal line represents the season mean value

The model overestimated the POD_6 and damage under extremely high seasonal mean [O_3] reported in the literature for model evaluation (Table S4-1), such as 105 ppb (Feng et al. 2007) or 98 and 143 ppm (Zheng et al. 2013). This response could occur because these concentrations at prolonged exposure are unrealistic. In most agricultural landscapes, moderate background [O_3] is found with occasional peaks (Osborne et al. 2019). Considering that these average values are for only 8 hours, it is probable that the reported [O_3] is caused by several hours of moderate values with extremely high peaks increasing the mean value. If the peak coincides with a time of relatively low stomatal conductance, then the POD_6 would be relatively low. Thus, similarly to the POD_6 underestimation due to the low mean [O_3], the use or estimation of hourly or sub-daily more realistic [O_3] data may decrease POD_6 and yield loss.

Furthermore, extended exposure to O_3 will lead to stomatal closure, controlling the O_3 influx to leaves but also affecting the uptake of CO_2 and carbon assimilation (Sitch et al. 2007; Vainonen and Kangasjärvi 2015). Also, [O_3] peaks occur mainly in the afternoon and are related to high temperatures and vapour pressure deficit,

conditions that normally cause stomatal closure (Beig et al. 2007; Feng et al. 2007). Those two mechanisms relating [O_3] and stomatal conductance cause the relative increase in POD_6 to be lower than the [O_3] relative increase at high [O_3] (Pleijel et al. 2022) while the new implemented module represents a linear relationship between [O_3] and POD_6.

4.5.3. Combined effects of O_3, CO_2 and drought

The combination of irrigated management, low [CO_2] and high [O_3] led to the most significant simulated yield loss in this study. This result was expected as water stress is accompanied by decreased stomatal conductance, limiting the O_3 influx to the leaves (Feng et al. 2008; Guarin et al. 2019b). In wheat, plants with water between 60 and 75% of the soil water capacity showed the highest stomatal conductance and consequently the highest yield loss by O_3, while plants at 35% of soil water capacity experienced a yield loss by O_3 close to zero (Khan and Soja 2003). In the current study, the irrigated management showed higher stomatal conductance in all the locations (Figure 4.8).

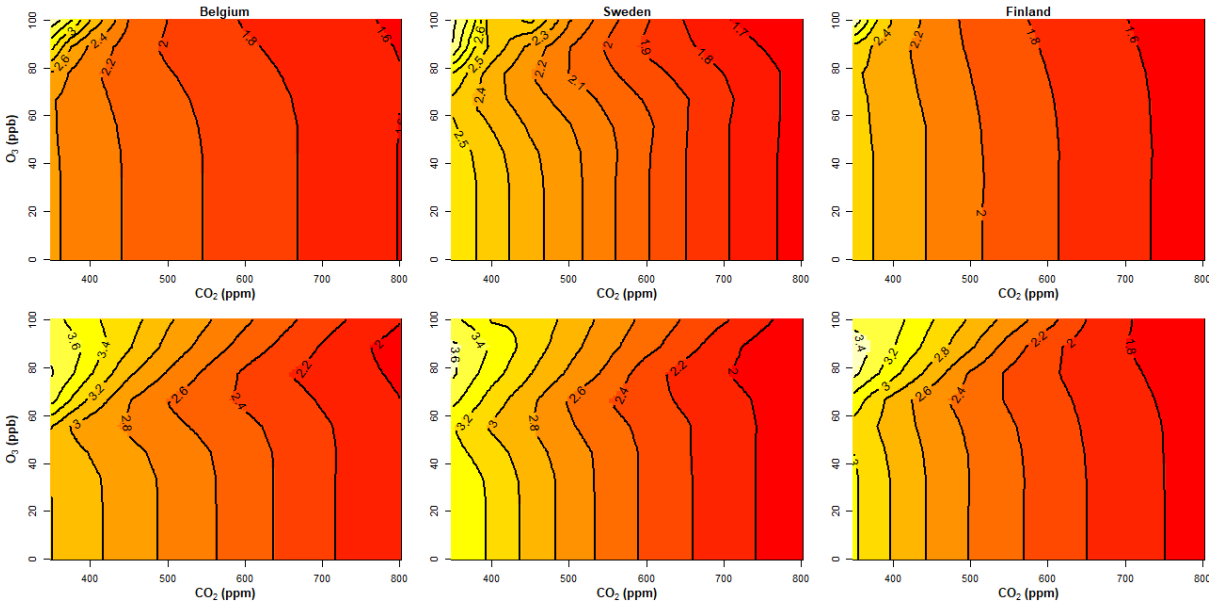

Figure 4.8. Isopleths of stomatal conductance (mm) of winter wheat for 2003 at three locations. Top: Rainfed, Bottom: Irrigated

Similarly to stomatal conductance, higher evapotranspiration was found from the irrigated management compared to rainfed. However, evapotranspiration decreased as [O_3] or [CO_2] rose in both managements (Figure S4-5). This response supports experimental data where high CO_2 levels reduce stomatal conductance and evapotranspiration (Feng et al. 2008; Mishra et al. 2013; Broberg and Pleijel 2015). This antagonistic effect between O_3 and CO_2 plus the CO_2 fertilisation (Broberg et al. 2019; Schauberger et al. 2019) compensates for the damaging effect of O_3 in simulated yields.

At high [O_3] above ~ 70 ppb and low [CO_2], simulated stomatal conductance increased; the underlying mechanism in the model representation causing that response is not well understood but it has been observed in previous research where high [O_3] can damage the stomatal functioning and slow the closure response (Broberg and Pleijel 2015; Masutomi et al. 2019). Even though LPJ-GUESS does not represent this effect explicitly, it could be a plant response to compensate for the loss of leaf area caused by O_3, by increasing the photosynthesis of living leaves. Additionally, compensation is enhanced considering that the senescent leaf tissue in LPJ-GUESS is assumed to continue attached to the plant affecting light transmission and keeping the same extinction coefficient.

4.5.4. Future research

Future research could improve the implementation of the effect of tropospheric ozone in plants, for instance, the representation of a maximum daily POD_6 thresholds or the increase of stomatal closure as a function of [O_3], avoiding overestimation at extremely high extended [O_3]. The threshold of ozone flux into the leaves at extremely high extended [O_3] based on stomata closure for protection has been reported previously in wheat plants (Pleijel et al. 2022). Likewise, estimating

hourly ozone concentrations to capture the ozone peaks could enhance the model simulation of POD values and, consequently, plant damage mainly under low O_3 concentrations. Further research should also evaluate the effect of the ozone concentration at larger or global scales and the evaluation of simulated global yield data affected by ozone compared with historical data. Finally, it is critical the extension and parameterisation to other sensitive crops such as potato, barley, rice, bean and soybean (Feng et al. 2008) and maize, which has been reportedly identified as a crop with low sensitivity to ozone. However, recent research has shown maize significant global losses due to ozone pollution (McGrath et al. 2015; Peng et al. 2020).

4.6. CONCLUSION

A new module representing the effects of tropospheric ozone on wheat production were implemented in LPJ-GUESS by adding the stomatal flux index Phytotoxic Ozone Dose above a threshold flux of 6 nmol m^{-2} s^{-1} (POD_6) and a calibrated function linking (POD_6) to the accelerated senescence, which, in turn, leads to productivity loss. The period of sensitivity to ozone was also calibrated to allow the module implementation to recreate the observed yield and harvest index loss rates caused by ozone in wheat. Future efforts could improve the model by estimating hourly [O_3] independently of the input time resolution and limiting the damage at extremely high [O_3].

The module can also reproduce the expected interaction between ozone, CO_2 and drought in yield and stomatal conductance, making it an important tool for researching air pollution in agriculture and food security. Further development can extend the module to other crops but it was calibrated for wheat since it is a major crop worldwide and ground-level ozone has been demonstrated to reduce wheat

production affecting global food security. Strategic research on mitigation and adaptation to the effects of ozone in an environmentally sustainable manner is critical for farmers and policymakers to reduce pollution impacts and the thread of production losses. Therefore, the ozone module implemented in LPJ-GUESS and its ability to recreate the damaging ozone effect on yield and harvest index can be a powerful tool for research and decision support to meet the future global demand for food. Besides, the research has implications for developing more robust and accurate crop models considering the complex interactions between crop production, ozone and environmental factors.

4.7. REFERENCES

Ahlström A, Miller PA, Smith B (2012) Too early to infer a global NPP decline since 2000. Geophys Res Lett 39:1–6. https://doi.org/10.1029/2012GL052336

Ainsworth EA, Sitch S, Collins WJ, Emberson LD (2012a) The effects of tropospheric ozone on net primary productivity and implications for climate change. Annu Rev Plant Biol 63:637–631

Ainsworth EA, Yendrek CR, Sitch S, et al (2012b) The Effects of Tropospheric Ozone on Net Primary Productivity and Implications for Climate Change ∗. Annu Rev Plant Biol 63:637–663. https://doi.org/10.1146/annurev-arplant-042110-103829

Ashmore MR (2005) Assessing the future global impacts of ozone on vegetation. Plant Cell Environ 949–964

Aunan K, Berntsen TK, Seip HM (2000) Surface Ozone in China and Its Possible Impact on Agricultural Crop Yields. Ambio 29:294–301

Batjes NH (2016) Total carbon and nitrogen in the soils of the world N. Eur J Soil Sci 65:1365–2389. https://doi.org/10.1097/00002480-200007000-00002

Beig G, Gunthe S, Jadhav DB (2007) Simultaneous measurements of ozone and its precursors on a diurnal scale at a semi urban site in India. J Atmos Chem 57:239–253. https://doi.org/10.1007/s10874-007-9068-8

Bender J, Hertstein U, Black CR (1999) Growth and yield responses of spring wheat to increasing carbon dioxide, ozone and physiological stresses: A statistical analysis of “ESPACE-wheat” results. Eur J Agron 10:185–195. https://doi.org/10.1016/S1161-0301(99)00009-X

Berkelhammer M, Alsip B, Matamala R, et al (2020) Seasonal Evolution of Canopy Stomatal Conductance for a Prairie and Maize Field in the Midwestern United States

from Continuous Carbonyl Sulfide Fluxes. Geophys Res Lett 47:1–12. https://doi.org/10.1029/2019GL085652

Broberg M, Pleijel H (2015) Effects of elevated ozone and carbon dioxide on wheat crop yield-Meta-analysis and exposure-response relationships

Büker P, Feng Z, Uddling J, et al (2015) New flux based dose-response relationships for ozone for European forest tree species. Environ Pollut 206:163–174. https://doi.org/10.1016/j.envpol.2015.06.033

Cappelli G, Confalonieri R, Van M, et al (2016) Modelling inclusion, testing and benchmarking of the impacts of ozone pollution on crop yields at regional level Module development and testing and benchmarking with the WOFOST generic crop model

Del Pozo AH, García-Huidobro J, Novoa R, Villaseca S (2008) Relationship of Base Temperature to Development of Spring Wheat. Exp Agric 23:21. https://doi.org/10.1017/S0014479700001095

Ding R, Kang S, Du T, et al (2014) Scaling up stomatal conductance from leaf to canopy using a dual-leaf model for estimating crop evapotranspiration. PLoS One 9:1–12. https://doi.org/10.1371/journal.pone.0095584

Ehhalt D, Prather M (2001) Atmospheric Chemistry and Greenhouse Gases. Clim Chang 2001 Sci Basis 239–287

Elliott J, Müller C, Deryng D, et al (2015) The global gridded crop model intercomparison: data and modeling protocols for phase 1 (v1.0). Geosci Model Dev 8:261–277. https://doi.org/10.5194/gmd-8-261-2015

Emberson LD, Pleijel H, Ainsworth EA, et al (2018) Ozone effects on crops and consideration in crop models. Eur J Agron 100:19–34. https://doi.org/10.1016/j.eja.2018.06.002

Fangmeier A, De Temmerman L, Mortensen L, et al (1999) Effects on nutrients and on grain quality in spring wheat crops grown under elevated CO2 concentrations and stress conditions in the European, multiple-site experiment “ESPACE-wheat.” Eur J Agron 10:215–229. https://doi.org/10.1016/S1161-0301(99)00012-X

Feng Z, Kobayashi K (2009) Assessing the impacts of current and future concentrations of surface ozone on crop yield with meta-analysis. Atmos Environ 43:1510–1519. https://doi.org/10.1016/j.atmosenv.2008.11.033

Feng Z, Kobayashi K, Ainsworth EA (2008) Impact of elevated ozone concentration on growth, physiology, and yield of wheat (Triticum aestivum L.): A meta-analysis. Glob Chang Biol 14:2696–2708. https://doi.org/10.1111/j.1365-2486.2008.01673.x

Feng Z, Tang H, Uddling J, et al (2012) A stomatal ozone flux-response relationship to assess ozone-induced yield loss of winter wheat in subtropical China. Environ Pollut 164:16–23. https://doi.org/10.1016/j.envpol.2012.01.014

Feng ZZ, Yao FF, Chen Z, et al (2007) Response of gas exchange and yield components of field-grown Triticum aestivum L. to elevated ozone in China. Photosynthetica 45:441–446. https://doi.org/10.1007/s11099-007-0073-6

Fischer T (2019) Wheat yield losses in India due to ozone and aerosol pollution and their alleviation: A critical review. Outlook Agric 48:181–189. https://doi.org/10.1177/0030727019868484

Franz M, Alonso R, Arneth A, et al (2018) Evaluation of simulated ozone effects in forest ecosystems against biomass damage estimates from fumigation experiments. Biogeosciences 15:6941–6957

Franz M, Simpson D, Arneth A, Zaehle S (2017) Development and evaluation of an ozone deposition scheme for coupling to a terrestrial biosphere model. Biogeosciences 14:45–71. https://doi.org/10.5194/bg-14-45-2017

Gelang J, Selldén G, Younis S, Pleijel H (2001) Effects of ozone on biomass, non-structural carbohydrates and nitrogen in spring wheat with artificially manipulated source/sink ratio. Environ Exp Bot 46:155–169. https://doi.org/10.1016/S0098-8472(01)00092-2

Gregersen PL, Culetic A, Boschian L, Krupinska K (2013) Plant senescence and crop productivity. Plant Mol Biol 82:603–622. https://doi.org/10.1007/s11103-013-0013-8

Grünhage L, Pleijel H, Mills G, et al (2012) Updated stomatal flux and flux-effect models for wheat for quantifying effects of ozone on grain yield, grain mass and protein yield. Environ Pollut 165:147–157. https://doi.org/10.1016/j.envpol.2012.02.026

Guarin JR, Emberson L, Simpson D, et al (2019a) Impacts of tropospheric ozone and climate change on Mexico wheat production. Clim Change 155:157–174. https://doi.org/10.1007/s10584-019-02451-4

Guarin JR, Kassie B, Mashaheet AM, et al (2019b) Modeling the effects of tropospheric ozone on wheat growth and yield. Eur J Agron 105:13–23. https://doi.org/10.1016/j.eja.2019.02.004

Han J, Kamber M, Pei J (2012) Data Preprocessing. In: Data Mining: Concepts and Techniques. Morgan Kaufmann Publishers, San Francisco, pp 83–124

Hansen EMØ, Hauggaard-Nielsen H, Launay M, et al (2019) The impact of ozone exposure, temperature and CO2 on the growth and yield of three spring wheat varieties. Environ Exp Bot 168:103868. https://doi.org/10.1016/j.envexpbot.2019.103868

Huixiang W, Kiang CS, Xiaoyan T, et al (2005) Surface ozone : A likely threat to crops in Yangtze delta of China. Atmos Environ 39:3843–3850. https://doi.org/10.1016/j.atmosenv.2005.02.057

Khan S, Soja G (2003) Yield responses of wheat to zone exposure as modified by drought-induced differences in ozone uptake. Water Air Soil Pollut 147:299–315. https://doi.org/10.1023/A:1024577429129

Lamarque JF, Bond TC, Eyring V, et al (2010) Historical (1850-2000) gridded anthropogenic and biomass burning emissions of reactive gases and aerosols: Methodology and application. Atmos Chem Phys 10:7017–7039. https://doi.org/10.5194/acp-10-7017-2010

Lin M, Horowitz LW, Xie Y, et al (2020) Vegetation feedbacks during drought exacerbate ozone air pollution extremes in Europe. Nat Clim Chang 10:444–451. https://doi.org/10.1038/s41558-020-0743-y

Lindeskog M, Arneth A, Bondeau A, et al (2013) Implications of accounting for land use in simulations of ecosystem carbon cycling in Africa. Earth Syst Dyn 4:385–407. https://doi.org/10.5194/esd-4-385-2013

LRTARP (2017) Manual on Methodologies and Criteria for Modelling and Mapping Critical Loads & Levels and Air Pollution Effects, Risks and Trends (Chapter 3): Mapping critical levels for vegetation. https://icpvegetation.ceh.ac.uk/sites/default/files/FinalnewChapter3v4Oct2017_000.pdf. Accessed 20 Mar 2023

Lu C, Tian H (2017) Global nitrogen and phosphorus fertilizer use for agriculture production in the past half century: Shifted hot spots and nutrient imbalance. Earth Syst Sci Data 9:181–192. https://doi.org/10.5194/essd-9-181-2017

M. Pugh TA, MacKenzie AR, Hewitt CN, et al (2010) Simulating atmospheric composition over a South-East Asian tropical rainforest: Performance of a chemistry box model. Atmos Chem Phys 10:279–298. https://doi.org/10.5194/acp-10-279-2010

Masutomi Y, Kinose Y, Takimoto T, et al (2019) Ozone changes the linear relationship between photosynthesis and stomatal conductance and decreases water use efficiency in rice. Sci Total Environ 655:1009–1016. https://doi.org/10.1016/j.scitotenv.2018.11.132

Mills G, Sharps K, Simpson D, et al (2018) Ozone pollution will compromise efforts to increase global wheat production. Glob Chang Biol 24:3560–3574. https://doi.org/10.1111/gcb.14157

Mishra AK, Rai R, Agrawal SB (2013) Differential response of dwarf and tall tropical wheat cultivars to elevated ozone with and without carbon dioxide enrichment: Growth, yield and grain quality. F Crop Res 145:21–32. https://doi.org/10.1016/j.fcr.2013.02.007

Mueller ND, Gerber JS, Johnston M, et al (2012) Closing yield gaps through nutrient and water management. Nature 490:254–257. https://doi.org/10.1038/nature11420

Ojanperä K, Pätsikkä E, Yläranta T (1998) Effects of low ozone exposure of spring wheat on net CO2 uptake, Rubisco, leaf senescence and grain filling. New Phytol 138:451–460. https://doi.org/10.1046/j.1469-8137.1998.00120.x

Olin S, Lindeskog M, Pugh TAM, et al (2015a) Soil carbon management in large-scale earth system modelling : implications for crop yields and nitrogen. Earth Syst Dyn 6:745–768. https://doi.org/10.5194/esd-6-745-2015

Olin S, Schurgers G, Lindeskog M, et al (2015b) Modelling the response of yields and tissue C : N to changes in atmospheric CO2 and N management in the main wheat regions of western Europe. Biogeosciences 12:2489–2515. https://doi.org/10.5194/bg-12-2489-2015

Osborne S, Pandey D, Mills G, et al (2019) New insights into leaf physiological responses to ozone for use in crop Modelling. Plants 8:. https://doi.org/10.3390/plants8040084

Otieno M, Peters MK, Duque L, Steffan-Dewenter I (2022) Interactive effects of ozone and carbon dioxide on plant-pollinator interactions and yields in a legume crop. Environ Adv 9:100285. https://doi.org/10.1016/j.envadv.2022.100285

Otu-Larbi F, Conte A, Fares S, et al (2020) Current and future impacts of drought and ozone stress on Northern Hemisphere forests. Glob Chang Biol 26:6218–6234. https://doi.org/10.1111/gcb.15339

Peng J, Shang B, Xu Y, et al (2019) Ozone exposure- and flux-yield response relationships for maize. Environ Pollut 252:1–7. https://doi.org/10.1016/j.envpol.2019.05.088

Pleijel H (2011) Reduced ozone by air filtration consistently improved grain yield in wheat. Environ Pollut 159:897–902. https://doi.org/10.1016/j.envpol.2010.12.020

Pleijel H, Broberg MC, Uddling J, Mills G (2018) Current surface ozone concentrations significantly decrease wheat growth, yield and quality. Sci Total Environ 613–614:687–692. https://doi.org/10.1016/j.scitotenv.2017.09.111

Pleijel H, Danielsson H, Broberg MC (2022) Benefits of the Phytotoxic Ozone Dose (POD) index in dose-response functions for wheat yield loss. Atmos Environ 268:118797. https://doi.org/10.1016/j.atmosenv.2021.118797

Pleijel H, Danielsson H, Emberson L, et al (2007) Ozone risk assessment for agricultural crops in Europe: Further development of stomatal flux and flux-response relationships for European wheat and potato. Atmos Environ 41:3022–3040. https://doi.org/10.1016/j.atmosenv.2006.12.002

Pleijel H, Danielsson H, Gelang J, et al (1998) Growth stage dependence of the grain yield response to ozone in spring wheat (Triticum aestivum L.). Agric Ecosyst Environ 70:61–68. https://doi.org/10.1016/S0167-8809(97)00167-9

Pleijel H, Danielsson H, Karlsson GP, et al (2000) An ozone flux-response relationship for wheat. Environ Pollut 109:453–462. https://doi.org/10.1016/S0269-7491(00)00048-8

Pleijel H, Danielsson H, Simpson D, Mills G (2014) Have ozone effects on carbon sequestration been overestimated? A new biomass response function for wheat. Biogeosciences 11:4521–4528. https://doi.org/10.5194/bg-11-4521-2014

Pleijel H, Eriksen AB, Danielsson H, et al (2006) Differential ozone sensitivity in an old and a modern Swedish wheat cultivar - Grain yield and quality, leaf chlorophyll and stomatal conductance. Environ Exp Bot 56:63–71. https://doi.org/10.1016/j.envexpbot.2005.01.004

Pleijel H, Ojanpera K, Mortensen L (1997) Effects of tropospheric ozone on the yield and grain protein content of spring wheat (Triticum aestivum L.) in the nordic countries. Soil plant Sci 47:20–25

Pleijel H, Skärby L, Wallin G, Selldén G (1991) Yield and grain quality of spring wheat (Triticum aestivum L., cv. Drabant) exposed to different concentrations of ozone in open-top chambers. Environ Pollut 69:151–168. https://doi.org/10.1016/0269-7491(91)90140-R

Ruane AC, Goldberg R, Chryssanthacopoulos J (2015) Climate forcing datasets for agricultural modeling: Merged products for gap-filling and historical climate series estimation. Agric For Meteorol 200:233–248. https://doi.org/10.1016/j.agrformet.2014.09.016

Schauberger B, Rolinski S, Schapho S, Müller C (2019) Global historical soybean and wheat yield loss estimates from ozone pollution considering water and temperature as modifying effects. Agric For Meteorol 265:1–15. https://doi.org/10.1016/j.agrformet.2018.11.004

Seefeldt SS, Kidwell KK, Waller JE (2002) Base growth temperatures, germination rates and growth response of contemporary spring wheat (Triticum aestivum L.) cultivars from the US Pacific Northwest. F Crop Res 75:47–52. https://doi.org/10.1016/S0378-4290(02)00007-2

Sitch S, Cox PM, Collins WJ, Huntingford C (2007) Indirect radiative forcing of climate change through ozone effects on the land-carbon sink. Nature 448:. https://doi.org/10.1038/nature06059

Smith B (2001) LPJ-GUESS – an ecosystem modelling framework. Dep Phys Geogr Ecosyst Anal INES, Sölvegatan 12:22362

Smith B, Prentice IC, Climate MTS (2001) Representation of vegetation dynamics in the modelling of terrestrial ecosystems : comparing two contrasting approaches within European climate space. Glob Ecol Biogepgraphy 10:621–637

Smith B, Wårlind D, Arneth A, et al (2014) Implications of incorporating N cycling and N limitations on primary production in an individual-based dynamic vegetation model. Biogeosciences 11:2027–2054. https://doi.org/10.5194/bg-11-2027-2014

Vainonen JP, Kangasjärvi J (2015) Plant signalling in acute ozone exposure. Plant Cell Environ 38:240–252. https://doi.org/10.1111/pce.12273

Waha K, Van Bussel LGJ, Müller C, Bondeau A (2012) Climate-driven simulation of global crop sowing dates. Glob Ecol Biogeogr 21:247–259. https://doi.org/10.1111/j.1466-8238.2011.00678.x

Wang E, Engel T (1998) Simulation of phenological development of wheat crops. Agric Syst 58:1–24. https://doi.org/10.1016/S0308-521X(98)00028-6

Wramneby A, Smith B, Zaehle S, Sykes MT (2008) Parameter uncertainties in the modelling of vegetation dynamics-Effects on tree community structure and ecosystem functioning in European forest biomes. Ecol Modell 216:277–290. https://doi.org/10.1016/j.ecolmodel.2008.04.013

Yin X, Schapendonk AHCM, Kropff MJ, et al (2000) A generic equation for nitrogen-limited leaf area index and its application in crop growth models for predicting leaf senescence. Ann Bot 85:579–585. https://doi.org/10.1006/anbo.1999.1104

Young PJ, Archibald AT, Bowman KW, et al (2013) Pre-industrial to end 21st century projections of tropospheric ozone from the Atmospheric Chemistry and Climate Model Intercomparison Project (ACCMIP). Atmos Chem Phys 13:2063–2090. https://doi.org/10.5194/acp-13-2063-2013

Zheng F, Wang X, Zhang W, et al (2013) Effects of elevated O3 exposure on nutrient elements and quality of winter wheat and rice grain in Yangtze River Delta, China. Environ Pollut 179:19–26. https://doi.org/10.1016/j.envpol.2013.03.051

4.8. SUPPLEMENTARY MATERIAL

Table S4-1. References for the model evaluation of Yield and HI. OA: Open ambient, NF: Non filtered, NF+O3: non filtered ozone enriched, CF: Charcoal filtered

Reference	Lon	Lat	Year	Treatment	O_3	O_3 Exposure (hours)	Yield	Units Yield	HI
Fangmeier et al 1996	8.75	50.75	1994	OA	40	Daylight	2.75	g plant^{-1}	0.47
Fangmeier et al 1996	8.75	50.75	1994	NF+O3	64	Daylight	2.54	g plant^{-1}	0.43
Sarkar and Agrawal 2010	83.25	25.75	2008	CF	5	12	585	g m^{-2}	0.49
Sarkar and Agrawal 2010	83.25	25.75	2008	NF	45	12	408	g m^{-2}	0.45
Sarkar and Agrawal 2010	83.25	25.75	2008	NF+O3	50	12	350	g m^{-2}	0.41
Sarkar and Agrawal 2010	83.25	25.75	2008	NF+O3	56	12	300	g m^{-2}	0.39
Sarkar and Agrawal 2010	83.25	25.75	2009	CF	5	12	578	g m^{-2}	0.48
Sarkar and Agrawal 2010	83.25	25.75	2009	NF	47	12	399	g m^{-2}	0.44
Sarkar and Agrawal 2010	83.25	25.75	2009	NF+O3	57	12	318	g m^{-2}	0.35
Feng et al 2007	121.25	31.75	2006	CF	10	8	1.75	g plant^{-1}	
Feng et al 2007	121.25	31.75	2006	NF	52	8	1.31	g plant^{-1}	
Feng et al 2007	121.25	31.75	2006	CF+O3	105	8	1.12	g plant^{-1}	
Zheng et al 2013	121.25	31.75	2007	CF	12	8	1.6	g plant^{-1}	
Zheng et al 2013	121.25	31.75	2007	NF	34	8	1.55	g plant^{-1}	
Zheng et al 2013	121.25	31.75	2007	CF+O3	52	8	1.5	g plant^{-1}	
Zheng et al 2013	121.25	31.75	2007	CF+O4	98	8	1	g plant^{-1}	
Zheng et al 2013	121.25	31.75	2008	CF	20	8	1.55	g plant^{-1}	
Zheng et al 2013	121.25	31.75	2008	NF	28	8	1.5	g plant^{-1}	
Zheng et al 2013	121.25	31.75	2008	CF+O3	96	8	0.9	g plant^{-1}	
Zheng et al 2013	121.25	31.75	2008	CF+O4	143	8	0.6	g plant^{-1}	
Mortensen and Engvild 1995	12.25	55.75	1991	CF	16	8	3.7	g plant^{-1}	0.43
Mortensen and Engvild 1995	12.25	55.75	1991	NF	28	8	3.3	g plant^{-1}	0.42
Mortensen and Engvild 1995	12.25	55.75	1991	NF+O3	61	8	2.7	g plant^{-1}	0.40
Tomer et al 2015	77.25	28.75	2009	CF	5	7	527	g m^{-2}	0.41
Tomer et al 2015	77.25	28.75	2009	OA	32	7	421	g m^{-2}	0.40
Tomer et al 2015	77.25	28.75	2009	NF	31	7	439	g m^{-2}	0.41
Tomer et al 2015	77.25	28.75	2009	NF+O3	59	7	369	g m^{-2}	0.40
Tomer et al 2015	77.25	28.75	2010	CF	8	7	499	g m^{-2}	0.42
Tomer et al 2015	77.25	28.75	2010	OA	36	7	404	g m^{-2}	0.40
Tomer et al 2015	77.25	28.75	2010	NF	35	7	423	g m^{-2}	0.40
Tomer et al 2015	77.25	28.75	2010	NF+O3	65	7	345	g m^{-2}	0.38
Wahid et el 1995	74.25	31.25	1985	CF	6	6	25.8	g plant^{-1}	
Wahid et el 1995	74.25	31.25	1985	NF	36	6	13.75	g plant^{-1}	

Wahid et al 1995	74.25	31.25	1985	NF	38	6	12.31	g plant^{-1}	
Zhu et al 2011	119.75	32.75	2007	NF	46	12	0.86	kg m^{-2}	
Zhu et al 2011	119.75	32.75	2007	NF+O3	61	12	0.71	kg m^{-2}	
Zhu et al 2011	119.75	32.75	2008	NF	42	12	0.99	kg m^{-2}	
Zhu et al 2011	119.75	32.75	2008	NF+O3	50	12	0.8	kg m^{-2}	
Zhu et al 2011	119.75	32.75	2009	NF	39	12	0.65	kg m^{-2}	
Zhu et al 2011	119.75	32.75	2009	NF+O3	49	12	0.57	kg m^{-2}	

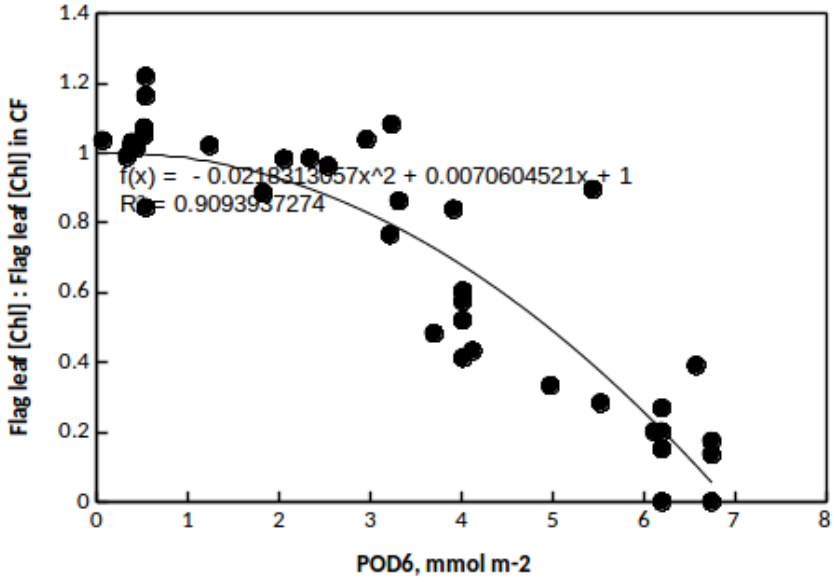

Figure S4-1. Relationship Between POD_6 and leaf senescence compiled by Pleijel, 2018 (unpublished)

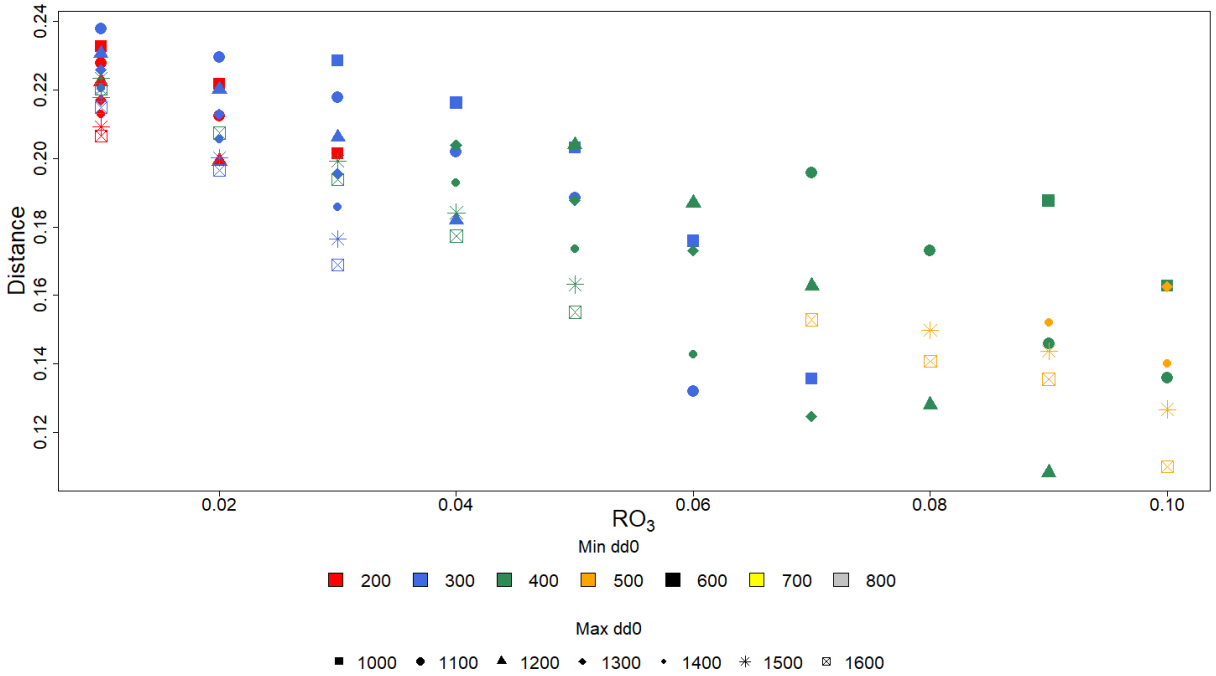

Figure S4-2. Euclidean distance of simulations using dd0 phenology approach with maximum POD_6 between 5 and 7.5 mmol m^{-2}

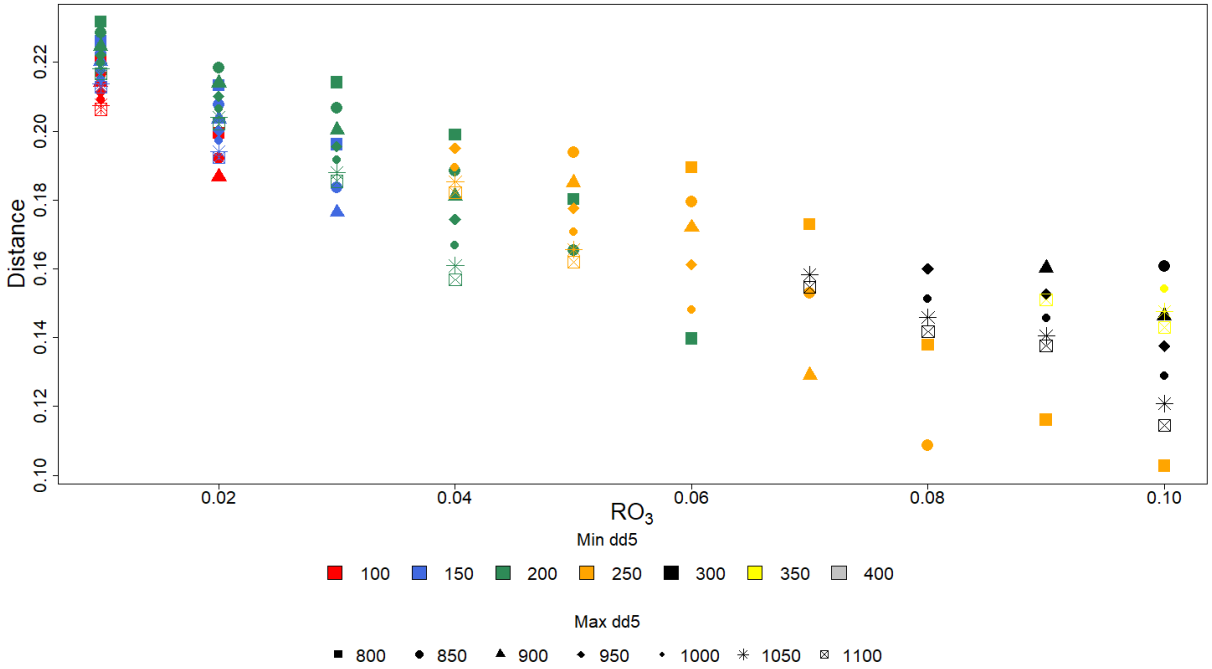

Figure S4-3. Euclidean distance of simulations using dd5 phenology approach with maximum POD_6 between 5 and 7.5 mmol m^{-2}

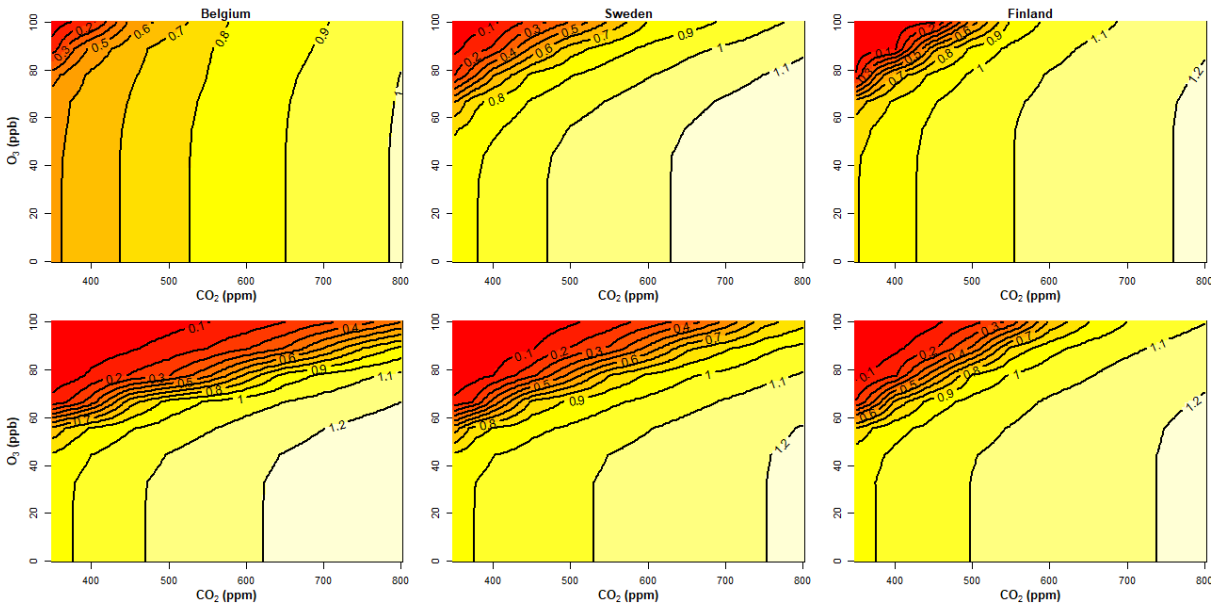

Figure S4-4. Isopleths of relative spring wheat yield to reference (O_3 of 0 ppb and actual CO_2, irrigated) for year 2003 for three locations. Top: Rainfed, Bottom: Irrigated

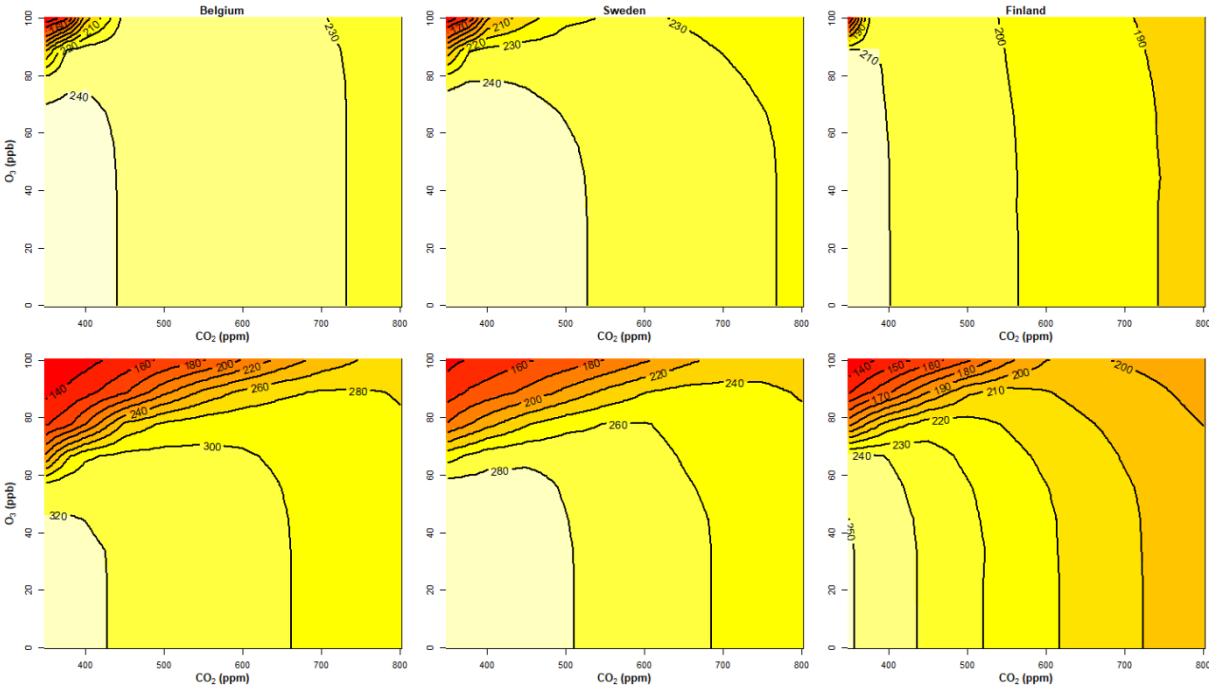

Figure S4-5. Isopleths of actual evapotranspiration (mm/year) of winter wheat for year 2003 at the three locations. Top: Rainfed, Bottom: Irrigated

CHAPTER FIVE: CONCLUSIONS

5.1. Summary and synthesis

Previous developments of the LPJ-GUESS model enhanced its capability to represent the carbon cycle and vegetation state globally by incorporating agroecosystems and managed land. These incorporations included the explicit representation of crop processes and yields and also enabled the application of the model in food system studies. Overall, this thesis aimed to improve the ability of LPJ-GUESS to simulate yields on a regional to global scale through three studies directed at aspects of large uncertainty for global simulations. Increasing the reliability of model simulations and outputs will benefit future model applications in food production systems, crop production projections, food security impact and sustainability.

The first study of this thesis focused on carbon assimilation and allocation processes within wheat and maize. As hypothesised, there was an improvement in the estimation of yield and harvest index globally compared to the original setup used in LPJ-GUESS, which tended to strongly overestimate the harvest index compared to the evaluation dataset collected in this thesis. The study highlighted the importance of simulating crops in LPJ-GUESS, considering the performance of internal crop processes besides yield. Accordingly, the minimum leaf carbon to nitrogen (C:N) ratio and the range in which leaf C:N ratio was allowed to vary were the main parameters affecting the simulated carbon assimilation, gross primary production (GPP), and yield. These parameters regulate the nitrogen content in leaf tissue during the growing season. The harvest index, on the other hand, is most strongly influenced by the retranslocation of labile carbon from the stem to grain after anthesis. This parameter caused high variation in the harvest index, as they directly influenced the

ratio of carbon in grains and vegetative organs. The exclusion of labile carbon retranslocation to grains was found to be the most crucial parameter that had the effect of decreasing the harvest index without significantly affecting yield.

The retranslocation rate of nitrogen and carbon from leaf to grain during senescence also impacted the harvest index significantly. This occurs because the carbon assimilation rate and the period with active photosynthesis are highly affected by the retranslocation rate of nitrogen and carbon and nitrogen demand reduction after anthesis. Lower rates of carbon and nitrogen retranslocation from leaves, coupled with a slower nitrogen uptake reduction after anthesis, result in a more extended period of productive green tissue and higher assimilation during grain filling. This impacts gross primary production (GPP), yield, and harvest index.

Two cultivars were developed for maize; high-yielding and low-yielding. These cultivars differed in their C:N ratio parameters and the nitrogen and carbon retranslocation rates. The high-yielding cultivar had a lower minimum and range of leaf C:N ratios representing a higher leaf nitrogen concentration. It had a higher capacity for carbon assimilation due to the extended period of green tissue, with low carbon and nitrogen retranslocation rates compared to the low-yielding maize. The newly parameterised cultivars substantially improved the ability of LPJ-GUESS to capture the geographic variation in yields globally over the period 2000-2010.

The second part of the thesis highlighted and confirmed the hypothesis about how land cover change legacies strongly influence historical yield trends of wheat, maize and rice. However, it showed that a historical land cover database, such as the Land Use Harmonization 2 (LUH2;Hurtt et al. 2020), had similar trends in the simulated

global yield to those obtained only assuming cropland before the simulations. This suggests that the assumption of crop cover before the historical simulation is satisfactory when simulating large-scale or global crop yields and not another land cover is studied. The constant crop assumption has the benefit of saving computer and time resources. Soil nitrogen and carbon pools accumulated before the crop simulation increased yield significantly for several years after the land cover change from natural vegetation or pastures to cropland. The relative increase in yield was particularly marked in regions with low fertiliser input. In rice, the effect of initial soil fertility conditions on the yield is less marked than in the other crops, potentially due to the inundated management of rice in most of the harvested area.

Similarly to the legacy of soil fertility from different land covers, this study revealed that fertilisation and atmospheric CO_2 mixing ratio (in C3 crops like wheat and rice) are the most important drivers contributing to simulated global yield increasing trends. A negligible effect of CO_2 was found for the C4 pathway crop maize. All the global simulated yields with different assumptions showed an overestimation compared to the FAO time series in the three crops before and during the 1990s, but mainly in maize. This probably occurred because the model does not consider pests, partial irrigation, pollution, soil degradation and other yield limitations. Also, the historical fertiliser and cultivar distribution databases add uncertainty to the model outputs. The improvement of the spatial but also temporal resolution of these two databases would likely represent progress in simulating yield trends over time. This study is particularly informative for interpreting coming large-scale crop simulations of yield and other agricultural outputs in LPJ-GUESS and other crop models.

The final stage of the thesis focused on the implementation and analysis of the tropospheric ozone on wheat production. As described in the hypothesis, the implementation allowed to capture losses in yield and harvest index caused by ozone. Wheat is the world most cultivated crop of which, production can be significantly affected by ground-level ozone, threatening global food security. To study this issue, a mechanistic ozone module was integrated into LPJ-GUESS. The module is based on the Phytotoxic Ozone Dose (POD), a stomatal ozone index that affects the accelerated senescence of wheat, ultimately leading to crop productivity loss. Through this implementation, the model could reproduce yield and harvest index losses in wheat caused by increasing ozone concentrations. In addition, the module can replicate the expected interaction between high ozone levels causing yield loss and high CO_2 levels enhancing yield. The damaging effect of ozone was more pronounced under irrigated management where stomatal conductance, and thus POD, tended to remain higher. The model could also replicate the stomatal conductance closure caused by high CO_2 and drought, which is the main cause of the reductions in ozone damage under such conditions. As a result, this tool has the potential to become a powerful resource for research on air pollution in agriculture and food security.

5.2. Limitations

The first limitation is inherent to crop modelling and the challenge to represent all the factors that can affect crop yields, such as biotic stresses, under irrigation and soil degradation in the case of LPJ-GUESS. These factors can be undetected at large-scale simulations, making the direct comparison between simulated outputs and observed values challenging.

Additionally, the inner limitations of the LPJ-GUESS due to its model structure, assumptions and processes affected this research and were not addressed here. For example, the few calibrated crops and cultivars available in LPJ-GUESS limit the potential to simulate crop production, mainly at a large scale which aggregates more diversity. Also, the model simulates one season per year, while two seasons are present in crop production in some locations. This is compensated by considering both seasons in the harvested area; however, it affects the study of other outputs due to the dynamic nature of the model. Similarly, the model has the ability to include management options like tillage, residue or interannual crops, but these options are applied globally and not spatial or temporal distributed.

The availability of gridded time series input datasets represented another limitation. Historical datasets of harvested areas are available, but segregation between rainfed and irrigated is unavailable. In the absence of this information, fractions of the harvested area under irrigation for the period 2000 - 2010 were applied to the whole time series based on the relative changes reported in the HYDE (Goldewijk et al. 2017). Since the general trend in irrigation fraction increased over time, an overestimation of irrigated areas for the period before 2000 is expected. Standard fertiliser datasets are unavailable for several crops, and the standardised data from the AgMIP initiative only applies to circa 2000.

Similarly to the irrigation interpolation before 2000 could cause an overestimation. There is also a general lack of cultivar distribution databases, and the estimation with distribution assumptions is required to supply them as performed in this research, where observed yield at the country level from FAO allowed to distribute both maize cultivars globally for the period 2000 -2010. This cultivar distribution also represents

an uncertainty of the estimations, possibly biased to overestimate high-yielding cultivar areas before 2000.

Finally, one of the most important limitations was the lack of hourly or daily ozone mixing ratio data to simulate the ozone effect on wheat in the calibration and evaluation in Chapter 4. Only the average daylight ozone mixing ratio per season was used to simulate the ozone effect, ignoring high ozone variability and peaks during the day and the season. Depending on the treatment, this caused overestimation of the simulated PODs and, consequently, of crop damage when mean ozone mixing ratios were high and underestimated POD and crop damage when mean ozone mixing ratios were low. So, in general, this result tended to increase the negative trend of the effect of ozone on yield.

5.3. **Future work**

The enhancements made to the LPJ-GUESS model in this thesis have significant implications for future research into the impact of various environmental factors, management practices and growing conditions on the global crop yield of three essential crops: maize, wheat, and rice. However, modelling requires continuous improvement and development, and the three research chapters described in this thesis also opened some new questions, research opportunities and necessities that were not addressed but can be complemented in future work.

In Chapter 2, contrasting values between both cultivars of maize showed the need to improve the cultivar distribution of the current cultivars and, if possible, to diversify the number of cultivars since maize is one of the most diverse crops in the world. At the same time, the enhancement of cultivar representation implies further parameter constraint and calibration to ensure a reliable representation of reality, mainly at large

scales. This would require the characterisation of different representative cultivars and the estimation of distribution databases.

Some parameters, such as the minimum and range of C:N or the N and C retranslocation rates, can continue being constrained to more precise ranges for each cultivar. Similarly, ***Sret,*** a parameter representing the inclusion (1) or absence (0) of labile carbon from stem to grains during senescence, could be constrained to fraction values between 0 and 1 for a better description of the retranslocation process.

In Chapter 3, the main conclusion showed that the most productive areas in the world could be simulated assuming cropland cover before the historical simulations. Evaluation of the effect of land use datasets in different models that, like LPJ-GUESS, simulate land use history would help to understand at what level the model structure caused the response found in this chapter. This will show how to effectively deal with land use history, mainly in models that do not simulate it but rather initialise their soil nutrient concentrations. In that case, the initial input dataset of soil fertility could be simulated with LPJ-GUESS. Additionally, this chapter showed the urgent need to standardise and characterise the uncertainty of fertilisation gridded time series for crop simulation due to the high contribution of this factor on simulated global yield trends

In Chapter 4, two mechanisms were not implemented and could improve the simulation of the effect of ozone in plants. First, the inclusion of a maximum threshold of ozone above which the plant will close stomata for protection, but also because magnitudes of temperature and vapour pressure deficit related to ozone peaks normally cause stomatal closure. Likewise, estimating hourly ozone mixing ratios to

capture the ozone peaks could enhance the model simulation of POD values and, consequently, plant damage. Thie work presented in this chapter additionally requires further research about the effect of the ozone concentration at larger or global scales and the evaluation of simulated global yield data affected by ozone compared with historical data. Extension and parameterisation for other sensitive crops such as potato, barley, rice, bean and soybean (Feng et al. 2008) are also needed to represent global agricultural production fully. One important crop to analyse is maize since it has been reportedly identified as a crop with low sensitivity to ozone. However, recent research has shown maize significant global losses due to ozone pollution (McGrath et al. 2015; Peng et al. 2020).

5.4. **Synthesis**

Following the aims described in Chapter 1 for the three research chapters, LPJ-GUESS was improved in this thesis, enhancing its capability to replicate yields, crop productivity processes, and the harmful effects on yield and harvest index simulated by the ozone module. Additionally, the response of simulated global crop production to land use and environmental drivers data was described allowing to understand their contribution and limitations as decision suport for model setup in future model applications and developments. Enhancement of model simulations by the addition of the ozone module in the model structure was not directly tested but the capability to decrease yields and HI based on troporpheric ozone pollution implies a model improvement. Anyway, the effect of ozone module on global yields still requires a deeper evaluation.

These improvements have significant implications for developing more comprehensive and precise crop simulations that account for the complex

interactions between crop production, environmental and management factors, and ozone and contribute to potentially more accurate global and large-scale yield simulations, to better understand the impacts of climate change and terrestrial biogeochemical cycles on food production.

The thesis emphasized the importance of simulating crop processes considering internal performance rather than only yield in LPJ-GUESS. It examined three types of uncertainty that the model has to address and are finally reflected In model outputs, such as parameter uncertainty (Chapter 2), input uncertainty (Chapter 3) and structural uncertainty (Chapter 4). These types of uncertainty mainly highlighted the significant influence of input datasets of climate, land use change, soil fertility, fertilisation, atmospheric CO_2 mixing ratio, and ozone on crop yield simulation and their potential threat to global food security. Further improvement in the spatial and temporal resolution of databases such as fertilisers and cultivar diversity and distribution could improve the accuracy of future model applications. The LPJ-GUESS model, with the integrated mechanistic ozone module, has significant potential for studying air pollution in agriculture and food security.

Although there are limitations to the model, this thesis has provided valuable insights into large-scale crop simulations and their impact on food systems, crop production projections, food security, and sustainability. Overall, this thesis's outcomes contribute to advancing the knowledge and understanding of global crop production and its impact on the environment and food systems. Additionally, improved LPJ-GUESS represent a valuable tool for strategic research on mitigating and adapting to the effects of ozone in an environmentally sustainable manner. This kind of research is critical for researchers and policymakers to reduce pollution impacts and

production losses and can serve as a powerful tool for research and decision support, essential for meeting future global food demands.

5.5. REFERENCES

Feng Z, Kobayashi K, Ainsworth EA (2008) Impact of elevated ozone concentration on growth, physiology, and yield of wheat (Triticum aestivum L.): A meta-analysis. Glob Chang Biol 14:2696–2708. https://doi.org/10.1111/j.1365-2486.2008.01673.x

Goldewijk KK, Beusen A, Doelman J, Stehfest E (2017) Anthropogenic land use estimates for the Holocene - HYDE 3.2. Earth Syst Sci Data 9:927–953. https://doi.org/10.5194/essd-9-927-2017

Hurtt GC, Chini L, Sahajpal R, et al (2020) Harmonization of global land use change and management for the period 850-2100 (LUH2) for CMIP6

McGrath JM, Betzelberger AM, Wang S, et al (2015) An analysis of ozone damage to historical maize and soybean yields in the United States. Proc Natl Acad Sci 112:14390–14395. https://doi.org/10.1073/pnas.1509777112

Peng J, Shang B, Xu Y, et al (2020) Effects of ozone on maize (Zea mays L.) photosynthetic physiology, biomass and yield components based on exposure- and flux-response relationships. Environ Pollut 256:113466. https://doi.org/10.1016/j.envpol.2019.113466

APPENDIX: PEER-REVIEWED PUBLICATED AND PRESENTED CHAPTERS

Modeling Earth Systems and Environment
https://doi.org/10.1007/s40808-022-01625-x

ORIGINAL ARTICLE

Modelling crop yield and harvest index: the role of carbon assimilation and allocation parameters

Hector Camargo-Alvarez[1] · Robert J. R. Elliott[2] · Stefan Olin[4] · Xuhui Wang[5] · Chenzhi Wang[5] · Deepak K. Ray[6] · Thomas A. M. Pugh[1,3,4]

Received: 26 May 2022 / Accepted: 1 December 2022

Abstract

Crop yield improvement during the last decades has relied on increasing the ratio of the economic organ to the total aboveground biomass, known as the harvest index (HI). In most crop models, HI is set as a parameter; this empirical approach does not consider that HI not only depends on plant genotype, but is also affected by the environment. An alternative is to simulate allocation mechanistically, as in the LPJ-GUESS crop model, which simulates HI based on daily growing conditions and the crop development stage. Simulated HI is critical for agricultural research due to its economic importance, but it also can validate the robust representation of production processes. However, there is a challenge to constrain parameter values globally for the allocation processes. Therefore, this paper aims to evaluate the sensitivity of yield and HI of wheat and maize simulated with LPJ-GUESS to eight production allocation-related parameters and identify the most suitable parameter values for global simulations. The nitrogen demand reduction after anthesis, the minimum leaf carbon to nitrogen ratio (C:N) and the range of leaf C:N strongly affected carbon assimilation and yield, while the retranslocation of labile stem carbon to grains and the retranslocation rate of nitrogen and carbon from vegetative organs to grains after anthesis mainly influenced HI. A global database of observed HI for both crops was compiled for reference to constrain simulations before calibrating parameters for yield against reference data. Two high- and low-yielding maize cultivars emerged from the calibration, whilst spring and winter cultivars were found appropriate for wheat. The calibrated version of LPJ-GUESS improved the simulation of yield and HI at the global scale for both crops, providing a basis for future studies exploring crop production under different climate and management scenarios.

Keywords Retranslocation · N concentration · Parameter sensitivity · Calibration · LPJ-GUESS

Introduction

The world population is projected to reach about 9.7 billion by the middle of the century, according to the medium variant of the World Population Prospect (United Nations 2019). The increased population, combined with a higher calorie demand per capita, will pose a significant challenge to ensure that food production can meet the increasing food demand (Godfray et al. 2010; Vermeulen et al. 2012). This challenge is further complicated by expected reductions in crop production caused by climate change and other environmental issues (Ray et al. 2019; Ortiz-Bobea et al. 2021; Soleymani 2022). Therefore, a sustainable solution requires understanding the complexity of agricultural systems and their interaction with other biogeochemical dynamics (Cramer et al. 1999; Sitch et al. 2003; Lindeskog et al. 2013). A class of global gridded crop

✉ Hector Camargo-Alvarez
hac809@student.bham.ac.uk

1 School of Geography, Earth and Environmental Science, University of Birmingham, Edgbaston, Birmingham B15 2TT, UK

2 Department of Economics, University of Birmingham, Edgbaston, Birmingham B15 2TT, UK

3 Birmingham Institute of Forest Research, University of Birmingham, Edgbaston, Birmingham B15 2TT, UK

4 Department of Physical Geography and Ecosystem Science, Lund University, 223 62 Lund, Sweden

5 Sino-French Institute for Earth System Science, College of Urban and Environmental Sciences, Peking University, Beijing 100871, China

6 Institute on the Environment (IonE), University of Minnesota, Saint Paul, MN 55108, USA

? Help / FAQ
Home
Search
Schedule by Day
Browse Program
Sessions and Events
Index Terms
Suggested Itineraries
Pod Reservation System 2022
Meeting Resources

GC23A-05 - Influence of Land Use Change, Climate and Management on Historical Simulated Yields of Wheat, Maize and Rice

Tuesday, 13 December 2022
14:46 - 14:57
McCormick Place - S503ab (South, Level 5)

Abstract

During the last century, the global cropland area has increased by about 67% to compensate for the increasing population and demand for food, fibre and energy. This continuous land use change (LUC) may affect the global food production. Considering LUC in dynamic vegetation global models, like LPG-GUESS, has improved the simulation of vegetation cover and carbon cycling. Still, current crop simulations with LPJ-GUESS account for a previous spinup period of 500 years, assuming cropland globally. Therefore, this research aims to evaluate the global effect of land use history on global crop yield for wheat, maize and rice and its interaction with drivers such as climate, atmospheric CO_2, and soil fertilization. A total of 56 global simulations were performed by combining three different factors. (1) Four different setups for global LUC: spinup with cropland cover, spinup with natural vegetation cover, spinup of natural vegetation and land use change to pastures in 1920, and application of LUC database from the land use harmonization (LUH2) during spinup and simulation. (2) Seven levels where only one driver was variable during the simulation: atmospheric CO_2, precipitation, radiation, temperature and fertilization; in addition to two levels with all drivers variable and all drivers constant. (3) Two different climate forcings: CRUNCEP, whose simulations span from 1960 to 2010 and AgMERRA, whose simulations span from 1980 to 2010. Both climate forcing datasets showed a similar response in trend and interannual variability of yield, while spinup with natural vegetation and pastures caused a higher nitrogen pool, increasing global yield at the beginning of the simulations. All the LUC levels reached similar yield magnitudes at the end of the simulation period except the cropland spinup, which showed a lower yield than the other LUC setups. Fertilization was the main driver of increasing yield during the simulation period, while the contribution of atmospheric CO_2 was lower. Interannual variability is mainly caused by fertilization and precipitation, while temperature contributes to a lesser extent. The results highlight the importance of accurate LUC and fertilizer databases inputs to increase the fitness of simulated global food production, climate change impacts and terrestrial biogeochemical cycles.

First Author

C
Hector Camargo
University of Birmingham

Authors

P
Thomas Pugh
Lund University

E
Robert Elliott
University of Birmingham

O
Stefan Olin
Lund University